NUREG/CR-4384
EGG-2416
March 1986

Break Spectrum Analyses for Small Break Loss of Coolant Accidents in a RESAR-3S Plant

C. D. Fletcher
C. M. Kullberg

F O R M A L R E P O R T

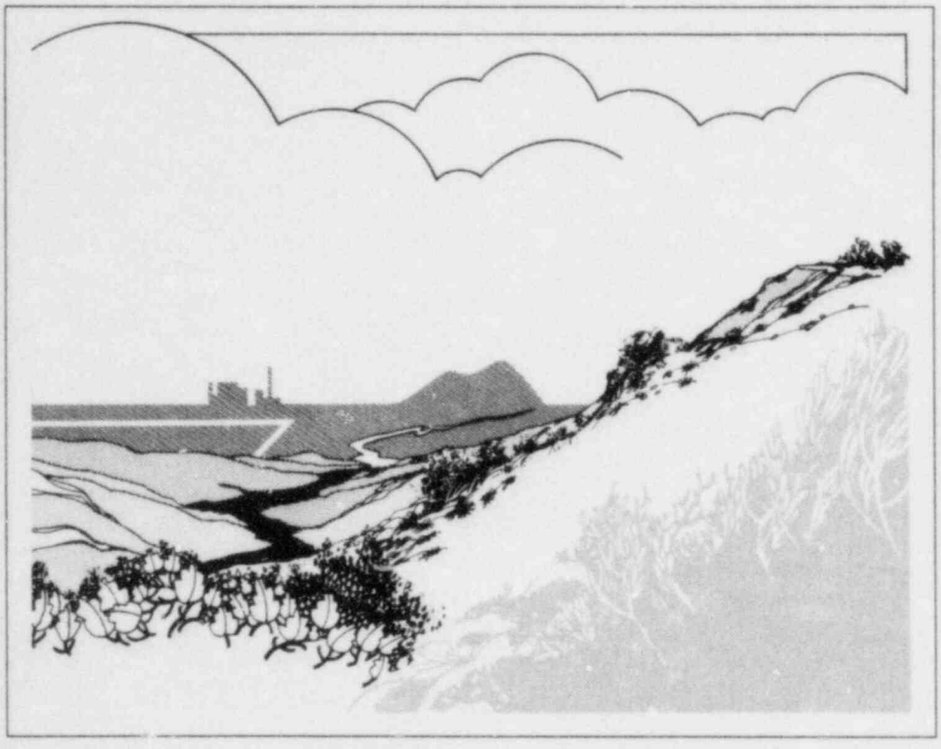

EG&G Idaho

Work performed under DOE Contract No. DE-AC07-76ID01570 for the ***U.S. Nuclear Regulatory Commission***

Idaho National Engineering Laboratory

Managed by the U.S. Department of Energy

8604230131 860331
PDR NUREG
CR-4384 R PDR

Available from

Superintendent of Documents
U.S. Government Printing Office
Post Office Box 37082
Washington, D.C. 20013-7982

and

National Technical Information Service
Springfield, VA 22161

NOTICE

This report was prepared as an account of work sponsored by an agency of the United States Government. Neither the United States Government nor any agency thereof, nor any of their employees, makes any warranty, expressed or implied, or assumes any legal liability or responsibility for any third party's use, or the results of such use, of any information, apparatus, product or process disclosed in this report, or represents that its use by such third party would not infringe privately owned rights.

NUREG/CR-4384
EGG-2416
Distribution Category: R4

BREAK SPECTRUM ANALYSES FOR SMALL BREAK LOSS OF COOLANT ACCIDENTS IN A RESAR-3S PLANT

Published
March 1986

C. D. Fletcher
C. M. Kullberg

Idaho National Engineering Laboratory
EG&G Idaho, Inc.
Idaho Falls, Idaho 83415

Prepared for the
U.S. Nuclear Regulatory Commission
Washington, D.C. 20555
Under DOE Contract No. DE-AC07-76ID01570
FIN No. A6047

ABSTRACT

A series of thermal-hydraulic analyses were performed to investigate phenomena occurring during small break loss-of-coolant-accident (LOCA) sequences in a RESAR-3S pressurized water reactor. The analysis included simulations of plant behavior using the TRAC-PF1 and RELAP5/MOD2 computer codes. Series of calculations were performed using both codes for different break sizes. The analyses presented here also served an audit function in that the results shown here were used by the U.S. Nuclear Regulatory Commission (NRC) as an independent confirmation of similar analyses performed by Westinghouse Electric Company using another computer code.

SUMMARY

A series of thermal-hydraulic analyses were performed, using the TRAC-PF1 and RELAP5/MOD2 computer codes, to investigate phenomena occurring during small break loss-of-coolant-accident (LOCA) sequences in a RESAR-3S pressurized water reactor.

Plant models were assembled to represent the plant with Model F steam generators using both computer codes, and with Model D steam generators using the RELAP5/MOD2 code. An additional RELAP5/MOD2 model was assembled to investigate the effect of reducing the steam generator model size.

Three calculations, with cold leg break diameters of 2, 3, and 4 in., were performed using the TRAC-PF1 Model F steam generator model. Fourteen RELAP5/MOD2 calculations were performed. With Model F steam generators, RELAP5 calculations were performed for break diameters of 1.5, 2, 3, 4, 5, 6, and 7 in. With Model D steam generators, RELAP5 calculations were performed for break diameters of 2, 3, 4, 5, 6, and 7 in. Another RELAP5 calculation was performed using coarsely-nodalized Model D steam generators for a 2-in. break diameter.

The primary calculational results of interest were the peak cladding temperatures attained for each break size. These results were used by the NRC to audit the results of similar calculations performed by Westinghouse Electric Company using another computer code. Cladding temperature excursions were observed in two time periods: before and after clearing of the liquid in the loop seals. However, temperature excursions were not necessarily observed in both periods for each break size.

Calculated results, for the same break sizes, using the TRAC and RELAP5 codes were comparable in most respects. However, depression of the core level was not sufficient to cause a cladding temperature excursion with TRAC, but was sufficient using RELAP5. The temperature difference was due primarily to different behavior in the steam generator inlet plenum.

Peak cladding temperatures were found to be higher in a RELAP5 calculation with fine steam generator nodalization than with coarse nodalization. These results are consistent with those previously reported by Argonne National Laboratory. In addition, significant previously unreported sensitivities of peak cladding temperature to initial steam generator secondary mass and separator modeling were discovered.

CONTENTS

FIGURES

TABLES

BREAK SPECTRUM ANALYSES FOR SMALL BREAK LOSS-OF-COOLANT ACCIDENTS IN A RESAR-3S PLANT

1. INTRODUCTION

In 1982, Test S-UT-8 was performed in the Semi-scale Mod-2A Experimental System at the Idaho National Engineering Laboratory (INEL). This test was designed to simulate a cold-leg, small-break, loss-of-coolant accident (LOCA) in a pressurized water reactor with U-tube type steam generators.

A significantly different hydraulic phenomenon was observed in this test as compared with previous small break LOCA tests in this and other experimental facilities. Specifically, in Test S-UT-8, the core level was observed to fall significantly below the elevation of the loop seals, for an extended period, before recovering at the time the loop seals were cleared of liquid. The loop seals are the low points in the cold legs between the steam generators and reactor coolant pumps. Previous experience indicated the core level would be depressed only to the elevation of the loop seals, and when this occurred, the loop seals were cleared and the core level was recovered. As a result of the lower-than-expected core level in Test S-UT-8, the core cladding temperatures increased significantly beyond those previously experienced in similar small break LOCA experiments.

The larger-than-expected core level depression was determined to be caused by a delayed draining of the upflow side of the steam generator U-tubes following the loss of loop natural circulation flow. Liquid inside the tubes was found to create a static pressure head that depressed the core level below what would exist with voided tubes. Important parameters affecting tube voiding characteristics were found to be: (1) wall condensation inside the U-tubes, (2) convection of liquid from the hot leg into the U-tubes via entrainment, (3) flooding phenomena inhibiting liquid backflow from the U-tubes (and steam generator inlet plenums) into the hot leg, and (4) the size of the reactor vessel internal bypass (from the downcomer inlet annulus to the upper head and plenum). A further discussion of the experimental findings is given in Reference 1.

Because of the safety implications of the heretofore unobserved core level depression below the loop seal elevation, much attention has been given consequently to simulating Test S-UT-8 using large thermal-hydraulic computer codes. The background of RELAP5/MOD2 and TRAC/PF1 computer simulations of Test S-UT-8 is discussed in Section 2.

The purpose of this report is to document an extension of the investigation into the excess core level depression to include a full scale pressurized water reactor (PWR); the RESAR-3S standardized-design plant. To this end, RELAP5/MOD2 and TRAC-PF1 models of the RESAR plant were used to simulate cold-leg, small-break LOCAs over a large spectrum of break sizes. The results of this study will be used by the U.S. Nuclear Regulatory Commission (NRC) to audit similar calculations performed by Westinghouse Electric Company using the NOTRUMP computer code. NRC comparisons of results using RELAP5 and TRAC with those using NOTRUMP will then be used as an aid in determining the suitability of the NOTRUMP code for licensing purposes.

RESAR-3S is a Westinghouse-design, four-loop plant. Two different steam generator configurations may be used in the plant; both are U-tube design. The Model D and F steam generators differ in feedwater injection location. In the Model D, feedwater is injected low in the downcomer, while in the Model F, the injection is high in the downcomer, near the steam separators. The analysis presented here considers both types of steam generators, because the differences between them were believed to possibly affect the U-tube condensation potential discussed above.

Previous analyses[2] at Argonne National Laboratory (ANL) indicated a potential exists for RELAP5 calculational results to be significantly affected by the extent of the steam generator modeling nodalization. The analysis presented here further investigates this sensitivity.

Section 3 describes the RELAP5/MOD2 and TRAC/PF1 models used. Section 4.1 presents the results of the RELAP5/MOD2 analyses including the effects of break size, steam generator configuration (Models D and F), steam generator nodalization, and code user experiences. Section 4.2 presents the results of the TRAC-PF1 analyses, including the effects of break size, and code user experiences. Section 4.3 presents a comparison of the RELAP5 and TRAC results for comparable calculations. Section 5 presents the conclusions of this study, and references appear in Section 6.

2. BACKGROUND

Semiscale-Mod-2A is a 1/1700 scale experimental facility representing a pressurized water reactor with U-tube steam generators. Test S-UT-8 simulated a 5% break in the cold leg of the reactor coolant system. Details of the experimental facility and a description of the test can be found in Reference 3.

Following the completion of Semiscale Test S-UT-8, much attention has been given to simulating this test using large thermal-hydraulic computer codes. The purpose of these simulations was to determine if holdup of liquid in the steam generator U-tubes and resultant depression of the core level below the lowest elevation of the loop seals, as occurred in the test, could be simulated using existing codes. Two such studies were performed at the Idaho National Engineering Laboratory (INEL)[4] and Los Alamos National Laboratory (LANL).[5]

The INEL study was performed with the RELAP5/MOD2 computer code and the LANL study was performed with the TRAC-PF1 computer code. These two codes were used at INEL to perform the RESAR plant calculations documented in this report. Results of comparisons between calculated and experimental data indicated both computer codes have the capability to simulate holdup of liquid in the steam generator tubes prior to the time of loop-seal clearing, and the resulting core level depression and core heatup. The comparisons also indicated a significant sensitivity of cladding temperature results to relatively minor changes in nodalization.

Thus, the comparisons of code calculations with experimental data for Test S-UT-8 give a qualitative indication that the TRAC-PF1 and RELAP5/MOD2 computer codes have the potential for calculating U-tube liquid holdup, and associated phenomena, in a full-size pressurized water reactor. The indication is only qualitative because the effects of break size, scaling, and nodalization on code capability to simulate key phenomena have not been established yet.

3. MODEL DESCRIPTIONS

The following sections describe the models used in this study. Section 3.1 describes the RELAP5 models of the RESAR-3S plant with Model D steam generators, and Section 3.2 describes the RELAP5 model of the plant with Model F steam generators. Section 3.3 describes the TRAC model. Section 3.4 provides documentation control information for input decks and computer codes used in this study. Section 3.5 discusses the common initial conditions and assumptions presented in this report. Section 3.6 discusses differences observed between the RELAP5 and TRAC models of the RESAR plant.

3.1 RELAP5 Models of RESAR Plant with Model D Steam Generators

The RELAP5 models used in this study were based on a model initially developed at INEL as part of another effort.[6] This initial model was subsequently transmitted to ANL for their use in other studies.[2] The original INEL model was modified by ANL to simulate a RESAR plant with finely-noded, Model D steam generators. Furthermore, ANL modified the boundary and initial conditions to agree with those to be used by Westinghouse Electric Company in analyses using the NOTRUMP code. ANL subsequently transmitted the modified model back to INEL, where it was used as the basis for the RELAP5 analyses presented in this report.

The base RELAP5 model used in the calculations presented in Section 4.1.3 consists of 188 volumes, 192 junctions, and 224 heat structures. Figure 1 shows a nodalization diagram of the model. Three of the four loops were lumped together as the intact loop. The length of corresponding components in each loop was the same, with the intact loop components having three times the volume and flow area of the broken loop components. The pressurizer surge line connects into the broken loop hot leg. Charging and safety injection pumps and accumulators were modeled only in the intact loop (see assumptions in Section 3.5). The charging flow was injected directly into the cold leg. The safety injection flow was injected into the accumulator line which was connected to the cold leg upstream of the charging line connection. The break causing the LOCA was located in the single loop at the location of the accumulator line connection with the intent of modeling a crack in the weld of the accumulator line-to-cold leg connection.

The steam generator primary and secondary sides were modeled including internal heat structures, main and auxiliary feedwater systems, steam line, relief valves, turbine stop valves, main steam isolation valves, and steam dump system.

The reactor coolant pumps were modeled using pump components. Homologous curves, two-phase difference curves, and two-phase multiplier tables for head and torque for Westinghouse PWR pumps were used for all input requirements except the two-phase difference curves for the energy dissipation region of the head and torque curves. Semi-scale two-phase difference data were the only information available for this input.

The pressurizer tank and surge line were modeled with pipe components. Eight nodes were used in the pressurizer tank so tank draining could be followed. The heaters and spray were not modeled since they were not needed to reach steady state and would not be used in the transients investigated here. The power-operated relief valve (PORV) was not modeled since it would not be challenged in this type of transient.

The reactor vessel model included a downcomer, lower plenum, core region, core bypass, upper plenum, and upper head with an "inverted top hat" configuration. The model included the upper head spray nozzle flow path. The core region had six volumes so the liquid level could be tracked, and the hydraulic conditions could be accurately calculated.

The connection between the reactor vessel upper plenum and hot legs is made from the lower cell adjacent to the hot leg centerline (Volume 120 in Figure 1). The significance of this nodalization choice is discussed in Section 4.1.5.

Heat structures were used to model the stored energy and heat transfer surfaces of the primary system loop piping; steam generator walls, internals, and tubes; and reactor vessel walls, internals, and fuel pins. One fuel pin was modeled as a hot pin, but no separate fluid volume was used for that pin. Heat losses to the ambient are negligible and

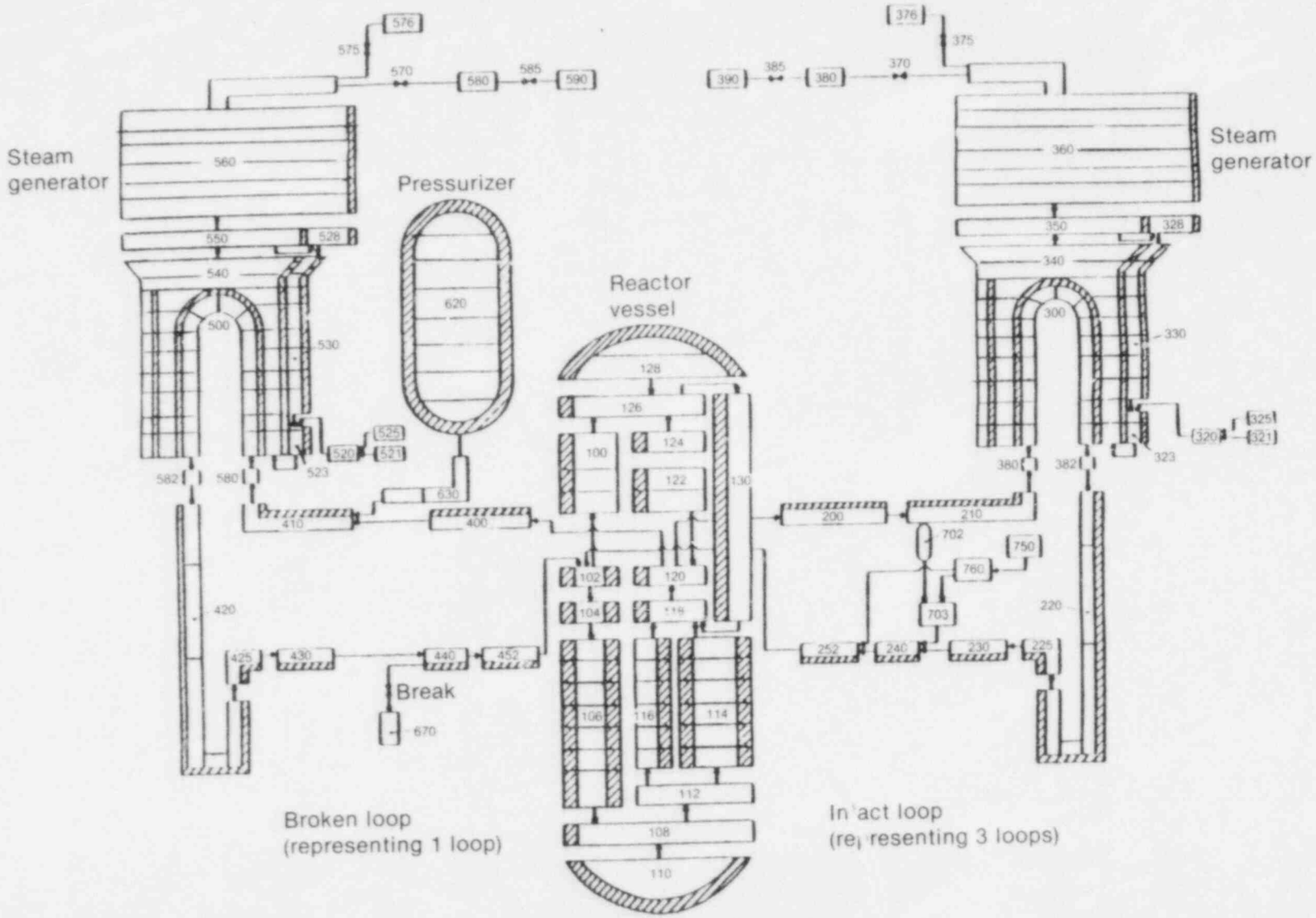

Figure 1. RELAP5 base nodalization for RESAR plant with finely-noded Model D steam generators.

were not modeled. Heat transfer coefficients were calculated within the code for all heat structures except the one in the vessel that was used to simulate gamma heating. This heat structure was modeled as a thin piece of steel with a large surface area and a high heat transfer coefficient so all energy generated within it would be immediately transferred to the fluid in the vessel.

Other user-selected code options include the following. Nitrogen was the noncondensible gas in the accumulator. Wall friction and unequal temperature options were implemented for all primary and secondary volumes except pumps and the steam line beyond the main steam isolation valves (MSIV). These options are not allowed for pumps. The main steamlines beyond the MSIV's were not regions critical to the calculation so the options were chosen to minimize problems in achieving steady state conditions. With a few exceptions to be discussed later, the following modeling criteria were applied at the junctions. As recommended by the RELAP5 development group, choking was allowed at all junctions except at the separators; the geometry determined whether a junction has a smooth or abrupt area change; and the full inertial treatment option was selected for all junctions. Liquid and vapor can have unequal velocities except at the separator inlets and the accumulator line-to-cold leg connections. These selections gave more realistic void distributions in the steam generators and prevented problems that could occur by injecting cold water into a two-phase system.

To perform the nodalization sensitivity study presented in Section 4.1.4, the base RELAP5 model was modified by combining adjacent cells in the steam generator tube, downcomer, boiler, and steam dome regions. The resulting nodalization is shown in Figure 2. The coarsely-noded model (Figure 2) represented the steam generators with about half the number of cells as in the base model (Figure 1) and contained 146 volumes, 150 junctions, and 174 heat structures.

3.2 RELAP5 Model of RESAR Plant with Model F Steam Generators

To simulate the RESAR plant with Model F steam generators, the base RELAP5 model described in Section 3.1 was modified by replacing the steam generators. The Model D steam generators were removed by breaking the nodalization pattern at the hot leg/inlet plenum, outlet plenum/cold leg, feedwater inlet, and steam dome/steam line junctions. Model F steam generators were then extracted from the original INEL RESAR plant Model[6] and inserted into the remaining part of the base model. The resulting nodalization for the RESAR plant with Model F steam generators is shown in Figure 3. By comparing Figures 1 and 3, the only significant difference in the nodalization patterns for the Models D and F steam generators is in the downcomer region. In the Model D steam generator, feedwater is injected low in the downcomer while in the Model F it is injected at the top of the downcomer. Both steam generators were investigated because the steam generator liquid holdup phenomenon would be affected possibly by the proximity of the auxiliary feedwater injection location to the steam generator U-tubes.

3.3 TRAC Model of RESAR Plant with Model F Steam Generators

The TRAC model of the RESAR plant with Model F steam generators is detailed in this section. The TRAC nodalization scheme is presented in Figure 4. The TRAC RESAR model consisted of a reactor vessel, intact (three lumped loops) and a broken loop. This model was based on a detailed deck supplied by LANL. The original detailed deck included 4 loops with a VESSEL component, consisting of 544 cells, employed to capture three dimensional flow phenomena.

The detailed LANL deck was simplified into a configuration similar to the RELAP5/MOD2 deck by combining three loops into a single lumped loop and reducing the detailed VESSEL component from three to two dimensions. The simplified loop nodalization for the RESAR plant was modeled with 42 one-dimensional components consisting of 191 computional cells. The coolant loops were proportionally sized with the intact loop having three times the broken loop volume. The degree of loop nodalization in the original LANL deck was maintained in the simplified deck. In the simplified vessel model, axial nodalization detail was maintained but radial nodalization was reduced to two regions, and azimuthal detail was removed completely. Thus, the simplified vessel model was reduced to approximately a one-dimensional configuration since, in most of the computational cells, flow was

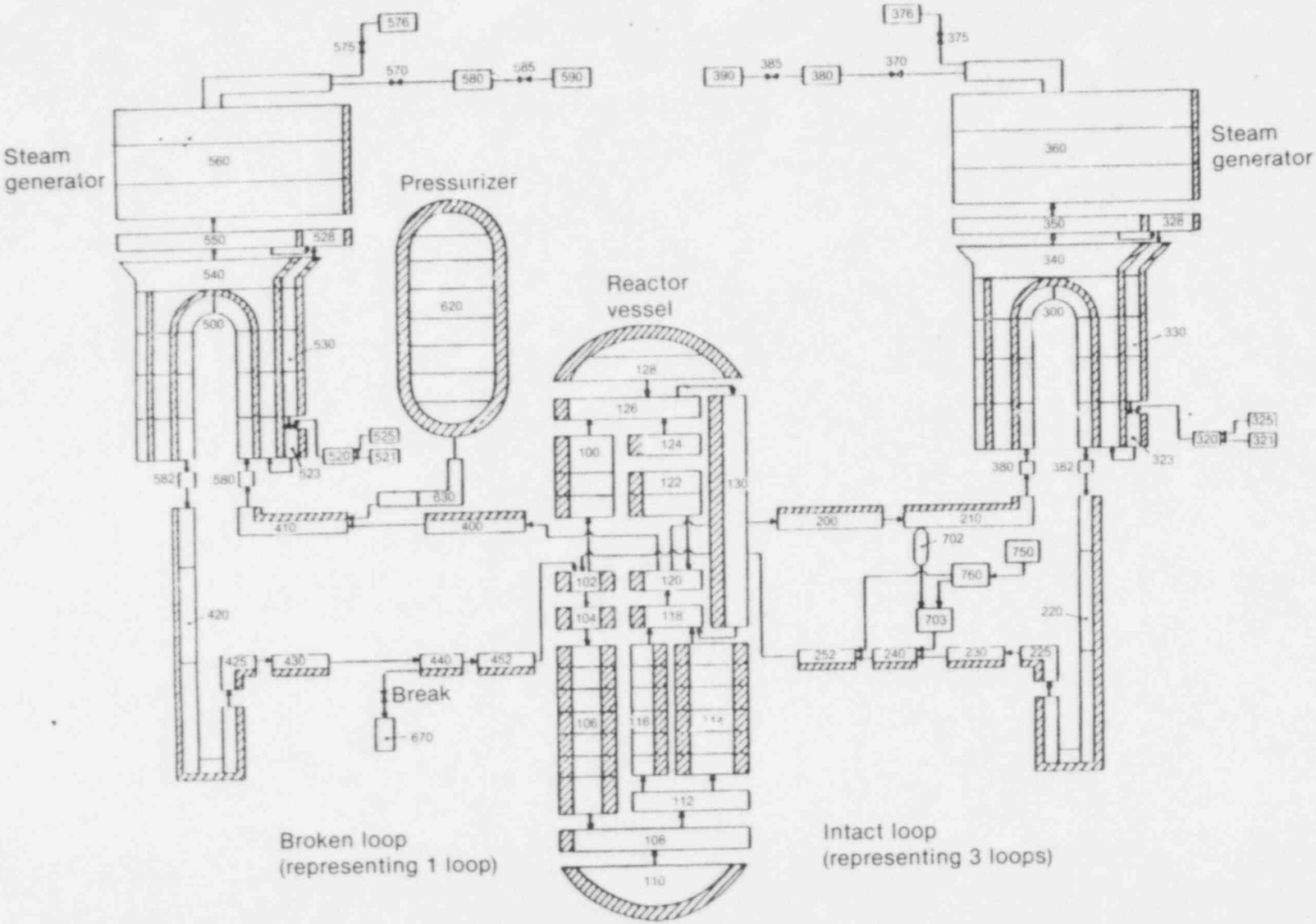

Figure 2. RELAP5 nodalization for RESAR plant with coarsely-noded Model D steam generators.

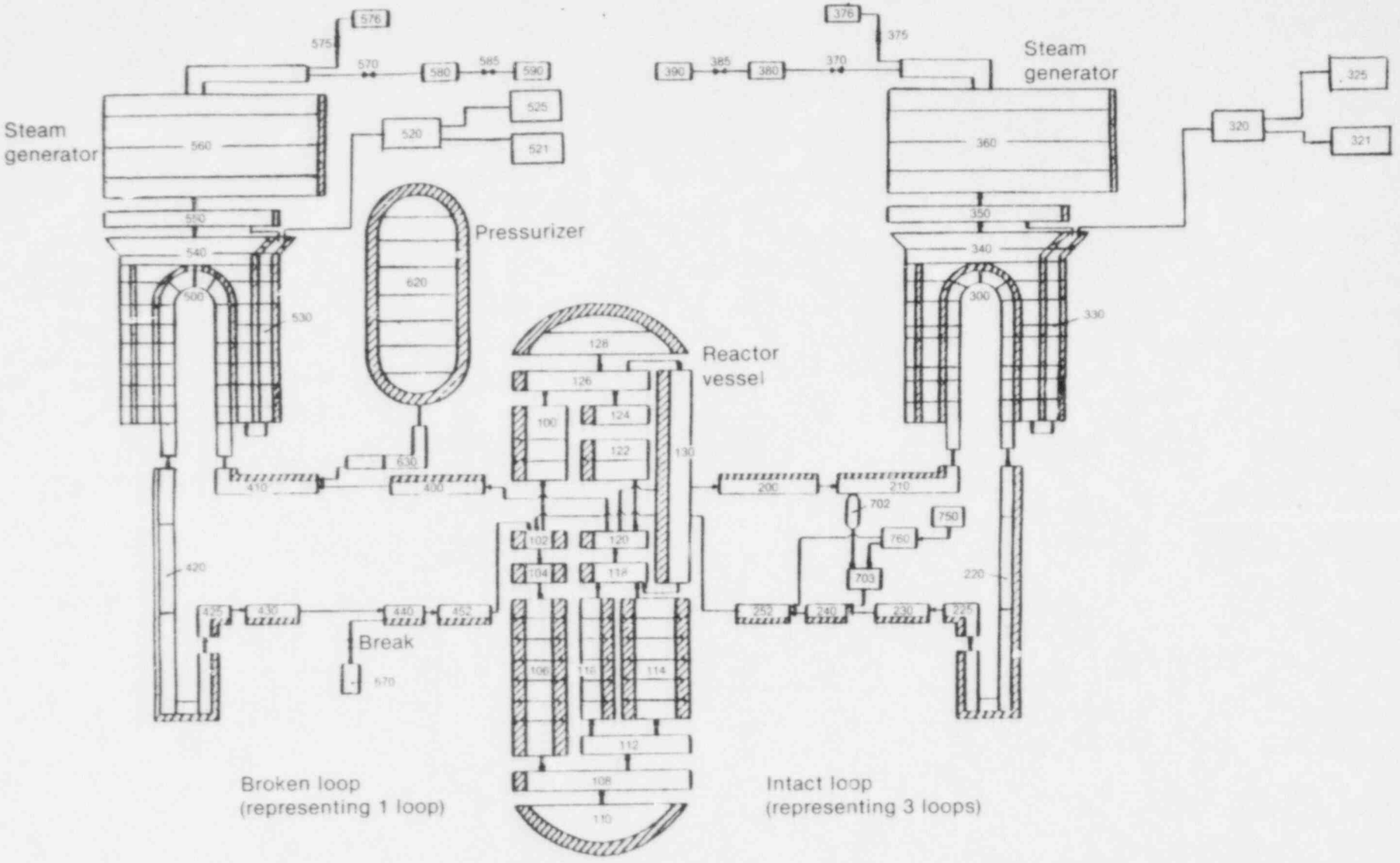

Figure 3. RELAP5 nodalization for RESAR plant with finely-noded Model F steam generators.

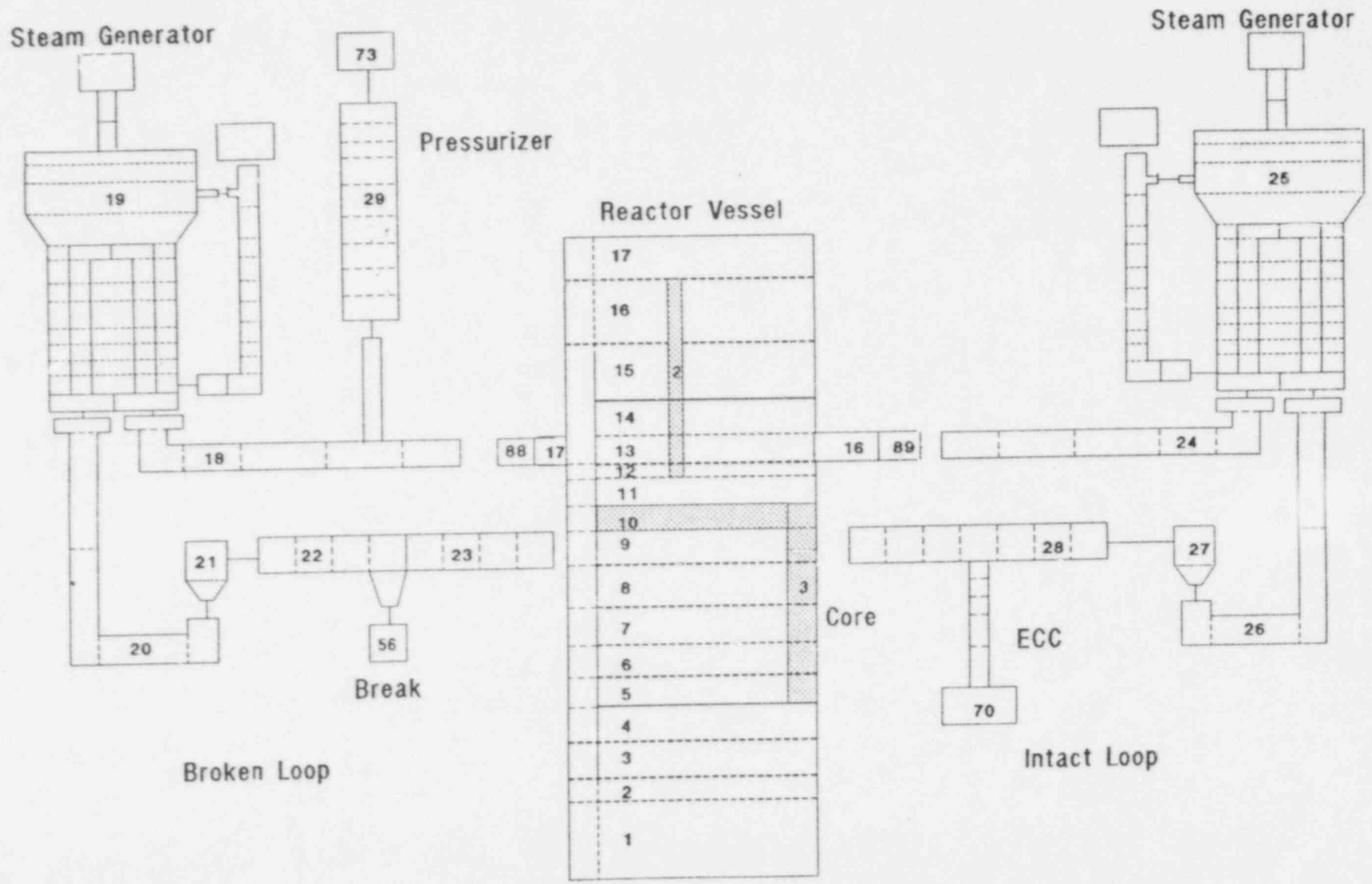

Figure 4. TRAC nodalization for RESAR plant with Model F steam generators.

limited to the axial direction only. In the process of collapsing the LANL input deck, flow areas, volumes, lengths, stored metal mass energy, and heat transfer surface areas were conserved.

Each steam generator was modeled with a STGEN component representing the tube bundles, boiler, downcomer, steam separator, and steam dome regions. The steam generator turbine stop valves and safety relief valves were modeled with TRAC VALVE components. Both the safety and stop valves were connected to common manifolds which were modeled with PLENUM components. The pressure boundaries at the valve outlets were modeled with FILL or BREAK components. FILL components provided the main and auxiliary feedwater into the steam generator downcomers. The FILLs were connected to common manifolds modeled as PLENUM components which were connected in turn to the steam generator downcomer inlets.

The primary coolant pumps were modeled with two-celled TRAC PUMP components. The ECCS boundary conditions were modeled to match the pressure flow curves from the RELAP5 input decks. ECCS was injected into the intact loop only. The ECCS modeling consisted of a PIPE/FILL combination to represent the combined flows from the charging, high pressure injection (HPI), and accumulator. The accumulator flow was based on the pressure and mass flow response calculated in the RELAP5 RESAR simulations. The break in the cold leg was modeled with a TEE/BREAK combination with the break-plane junction located at the TEE secondary/BREAK interface.

The reactor vessel nodalization scheme (Figure 4) used a 34-cell VESSEL component consisting of 17 axial levels, 2 radial regions, and no azimuthal regions. Two one-dimensional PIPE components were used to model the region between the core-baffle region and the lumped control-rod-guide assemblies. The lower plenum region was represented by levels 1 through 4 with the top of level 4 representing the interface of the lower support plate with the fuel region. Within the inner ring, the heated fuel length spans levels 5 through 9, and region 10 spans the upper core support plate regions. Running parallel with levels 5 through 9 is a PIPE component representing the core barrel/baffle annular flow region. Levels 11 through 14 and 15 through 17 represent the upper plenum and upper head regions, respectively. The downcomer spans levels 3 through 15 in the outer ring. The leakage path is located at level 15 between the downcomer and upper head interface. The control-rod-guide-tube assembly connects from the top of level 11 to the bottom of level 17. The leakage paths representing the hot leg nozzle/downcomer interface leakage gap was modeled with a VESSEL valve connection between the downcomer and upper plenum at level 14. Vessel-to-loop interfaces were modeled with PIPE/PLENUM combinations at the cold- and hot-leg connections. These interface volumes were modeled as part of the vessel, with the volume borrowed from the downcomer and upper plenum regions of the original LANL vessel. This modeling strategy approximated the vessel as a one-dimensional system since, in most cells, flow was constrained to the axial direction only. However, in the vessel, certain cells also had a radial flow component because cell-to-cell connections existed in the lower and upper plenums and upper head.

Heat transfer modeling in the reactor vessel and piping included both sensible heat from internal metal mass structures and heat generated by the nuclear fuel. The nuclear fuel simulation was based on Westinghouse standard 17 x 17 fuel assemblies. The fuel rod nodalization consisted of 6 axial and 8 radial temperature nodes. Both an average and a computational hot rod were used to simulate the core fuel response.

The principal options used in the TRAC model were the code transient option, the water packing option, the critical flow model at the break plane, and wall friction. The outer convergence criterion was set at 0.0001, and the maximum number of outer iterations was set at 10. Direct matrix inversion was used to calculate a numerical solution for the VESSEL component.

3.4 Code and Model Documentation Control

RELAP5 calculations presented in this report were performed using an updated version of RELAP5/MOD2, Cycle 21. The update was required to prevent code failure in the core gamma-heat structure (see description in 3.1) that occurred when portions of the core became completely dry.

TRAC calculations presented in this report were performed with an updated version of TRAC/

PF1/MOD1, Version 11.7. The update was required to correct errors in the PLENUM component.

Input decks and both codes that were used are stored at INEL on magnetic tape.

3.5 Assumptions and Boundary Conditions

As indicated in Section 3.1, the base RELAP5 model used in this study was obtained from ANL. This model was set up to calculate a small break LOCA sequence in the RESAR-3S plant. Furthermore, the boundary and initial conditions ANL specified in the model were selected to agree with those to be used by Westinghouse Electric Company in analyses using the NOTRUMP code. Boundary and initial conditions in the LANL-developed TRAC model were modified to agree with those of the base RELAP5 model. Thus, the RELAP5 and TRAC calculations presented here are comparable with each other, and with NOTRUMP calculations performed by Westinghouse. This section documents the significant common assumptions, and boundary and initial conditions used in these analyses.

Transient simulations were accomplished by first performing steady-state calculations to achieve plant operating conditions, then performing small break transient calculations, typically restarting them from the steady-state conditions. For the analysis presented here, the plant is assumed to be operating at 102% of full power. Initial steady-state conditions obtained are shown in Table 1. Comparisons show generally good agreement among all steady-state calculations. The TRAC and RELAP5 steady-state, steam generator secondary conditions differ moderately with the TRAC secondary system containing less liquid and operating at a higher pressure than that of RELAP5. These differences are not expected to be significant in comparison to the overall calculational results. However, a better comparison of initial secondary conditions could have been obtained if more time were available to perform the steady-state calculations.

Transient calculations were initiated by the break opening, and time zero corresponds to the break-opening time in all calculations presented in this report. Breaks were assumed to open instantaneously and were located at the cold leg centerline at the site of the accumulator line penetration. Standard best-estimate break flow models contained in the TRAC and RELAP5 codes were employed. The NOTRUMP calculations performed by Westinghouse will probably employ the Moody break flow model. Thus, results for a given break diameter will not be directly comparable. Because of the large number of break sizes investigated with TRAC and RELAP5, however, comparisons of TRAC and RELAP5 results with NOTRUMP results may be performed after appropriate adjustments for break flow modeling have been made.

Degraded performance of the emergency core cooling system (ECCS) was assumed. Only one high pressure injection (HPI) and one charging pump were assumed operable. Flow from these sources was injected only into the intact loop. The broken loop accumulator was assumed to be unavailable. Modeling of low pressure injection (LPI) was not required because calculations were terminated before initiation of LPI flow. Only one motor-driven auxiliary feedwater pump was assumed to be available. Characteristic curves for the ECC and decay heat removal systems are shown in Table 2.

Remaining assumptions concerning plant trips and control system functions are shown in Table 3.

To assure clearing of the liquid from the reactor coolant pump suction of the broken loop before that in the intact loop, the elevation of the loop seal to the intact loop was lowered by 2.0 ft. This modification was applied to all models used in this study. This modification assured the same loop seal was cleared first in all calculations, thus eliminating difficulties in comparing results of calculations where this is not the case.

Calculations were carried out to a point where indication of both short and long term core cooling was evident. For larger break sizes, this typically was when calculations were continued past initiation of accumulator flow and with an indication that clad temperatures had peaked. For some smaller break sizes, depressurization to the accumulator injection pressure was not encountered, but core cooling was assured by a covered core, stable pressure, and safety injection flow exceeding break flow.

Table 1. Initial steady state operating conditions

Parameter	RELAP5 Model D SG	Coarse Node RELAP5 Model D SG	RELAP5 Model F SG	TRAC Model F SG
Reactor Power, MW(t)	3479.0	3479.0	3479.0	3479.0
Hot Leg Temperature, °F	623.3	623.4	622.9	624.2
Cold Leg Temperature, °F	562.8	562.9	561.8	562.8
Pressurizer Pressure, psia	2269.5	2273.5	2273.5	2244.0
Loop Flow (Total 4-Loop), lbm/s	38789.0	38755.0	38495.0	38229.0
Feed/Steam Flow, lbm/s/SG	1063.5	1066.2	1064.7	1058.2
Feed Temperature, °F	437.2	437.2	437.2	436.5
Secondary Pressure, psia	987.8	961.3	996.4	1030.2
Secondary Mass, lbm/SG	113806.0	105760.0	111026.0	87[illegible]
Steam Generator Level, ft	43.8	41.8	44.8	39.05

3.6 Differences Between TRAC and RELAP5 Models

Comparison of TRAC and RELAP5 calculations for identical sequences is an important part of this report. Therefore, differences between the TRAC and RELAP5 modeling of the RESAR plant must be documented. This section discusses differences between the models presented in Section 3.2 (RELAP5) and 3.3 (TRAC).

Both models portray a RESAR-3S plant with Model F steam generators. As discussed in Section 3.5, good agreement between models was obtained for the initial steady-state operating conditions. Furthermore, assumptions and boundary conditions for the TRAC model were adjusted to agree with those of the RELAP5 model. Thus, the initial and driving conditions for the two models are in good agreement.

Both models have similar nodalization schemes. Comparing Figures 3 and 4, only minor differences in the nodalization are observed. In the reactor vessel, the core region consists of 6 cells in the RELAP5 model and 5 in the TRAC model. In the reactor coolant loops, the TRAC model generally has finer nodalization in the hot legs and pumps. Steam generator nodalization of the two models is virtually identical.

Geometrical data of the two models were compared prior to performing the calculations. Some significant differences were noted, and these are discussed below. Most of these differences are traced directly to the RELAP5 and TRAC models developed at INEL and LANL, respectively. Since the basis for the LANL TRAC model is unknown, neither the RELAP5 nor the TRAC model geometries can be judged to better simulate the plant.

In the reactor vessel, the core bypass (lower plenum to upper plenum) was handled differently between the two models. The RELAP5 steady-state bypass flow was approximately 10 times that of TRAC. Bypass flow volumes compared well. The different bypass flow rates appear to be caused by different interpretations of the leakage flows within the barrel-baffle region. These differences are not expected to significantly affect the calculated results.

Table 2. ECCS and decay heat removal characteristic curves

High Pressure Injection Characteristics (90°F Liquid)		Charging Injection Characteristics (90°F Liquid)	
Pressure (psia)	Flow Rate (lbm/s)	Pressure (psia)	Flow Rate (lbm/s)
≤ 14.7	63.84	≤ 14.7	47.76
114.7	61.56	114.7	45.91
214.7	59.17	314.7	42.11
314.7	56.59	514.7	38.15
414.7	53.92	714.7	33.99
514.7	51.15	914.7	29.64
614.7	48.27	1114.7	25.09
714.7	45.27	1314.7	20.34
814.7	42.10	1514.7	15.31
914.7	38.72	1714.7	9.73
1014.7	35.02	1914.7	4.91
1114.7	30.85	≥ 2114.7	0.0
1214.7	25.83		
1314.7	18.90		
1414.7	5.12		
≥ 1514.7	0.0		

Accumulator

Total Volume	4050 ft^3
Liquid Volume	3150 ft^3
Initial Temperature	90°F
Initial Pressure	600 psia

Motor-Driven Auxiliary Feedwater

Flow Rate	20.7 lbm/s (per steam generator)
Liquid Temperature	90°F

Two bypass leakage paths exist in the upper region of the reactor vessel. One path connects the upper region of the downcomer with the upper head (DC-UH path). The other path represents leakage between the downcomer and upper plenum regions (DC-UP path) around the circumference of the hot leg nozzle penetrations. The models simulate these leakage paths differently. In the TRAC model, both paths are present, but the elevation of the DC-UP path is above its true elevation at the hot-leg centerline. In the RELAP5 model, only the DC-UH path is present. The DC-UP path appears to have been deleted by ANL; it was included in the original RELAP5 RESAR model[6] but not in the model received from ANL. The TRAC DC-UH path is smaller than that of RELAP5 model, however, such that the total, steady-state, upper reactor vessel bypass flow (DC-UH plus DC-UP) is about

Table 3. Plant trip and control system assumptions

Event	Assumptions
Reactor Trip	Scram when pressurizer pressure is less than 1860 psia. 1979 American Nuclear Society (ANS) + 20% power decay.
Reactor Coolant Pump Trip	1 s after scram.
Safety Injection	25 s after pressurizer pressure falls below 1760 psia.
Turbine Trip	At time of scram.
Auxiliary Feedwater Injection	Initiate 61 s after scram, control to maintain 41.833 ft of steam generator (SG) downcomer collapsed level.

7% larger with TRAC than with RELAP5. Although results of a small-break LOCA calculation may be expected to be sensitive to differences in total upper reactor vessel bypass, the difference noted above is not considered significant. This judgment is based on the findings of bypass-sensitivity studies presented in Reference 1.

As indicated in Section 3.5, the initial steady-state, steam-generator secondary mass and level were lower and secondary pressure was higher with TRAC than with RELAP5. Geometrical differences were also noted between the steam-generator secondary regions of the two models. In general, the TRAC steam generator was found to be larger than that of RELAP5. As examples, TRAC steam generator tube volume was 18% larger than RELAP5, tube length was 6% longer, and boiler volume was 35% larger. Possible effects of these and other geometrical differences will be discussed in Section 4.3.

4. RESULTS

Results of the analyses are presented in this section. Section 4.1 presents results from the RELAP5 analysis, Section 4.2 presents results from the TRAC analysis, and Section 4.3 presents a comparison of the RELAP5 and TRAC results. Peak cladding temperature results for all calculations are summarized in Section 5.

4.1 RELAP5 Results

Results of the RELAP5 analysis are presented in this section. Section 4.1.1 presents a detailed discussion of the results for a representative calculation. Section 4.1.2 discusses the effects of break size, Section 4.1.3 discusses the effects of steam generator configuration, and Section 4.1.4 discusses the effects of steam generator model nodalization. Section 4.1.5 presents user experiences gained from employing the RELAP5 code in this application.

4.1.1 Representative Results. RELAP5 calculations were performed for 1.5-, 2- 3-, 4-, 5-, 6-, and 7-in.-diameter cold leg breaks in a RESAR plant with Model F steam generators and for 2-, 3-, 4-, 5-, 6-, and 7-in.-diameter cold leg breaks in a RESAR plant with Model D steam generators. These calculations were performed with the finely-noded steam generator models described in Sections 3.1 and 3.2. An additional RELAP5 calculation was performed to investigate the effects of variation in steam generator nodalization for a 2-in.-diameter, cold-leg break in a RESAR plant with Model D steam generators.

The trends of plant response for all the RELAP5 calculations were similar in most respects. To simplify discussion of results, a detailed discussion of results for one calculation (3-in.-diameter break, Model F steam generators) is presented here. A sequence of events for this calculation is shown in Table 4. Then the following subsections discuss the effects of varying the break size, steam generator model type, and degree of steam-generator model nodalization.

The transient begins with the opening of a 3.0-in.-diameter break in the cold leg at zero time. As shown in Figure 5, the primary system pressure fell rapidly as a result of the break. At 35 s, the pressurizer pressure reached 1860 psia, causing a reactor trip. This resulted in a turbine trip, causing isolation of main feedwater and steam flows, and tripped the reactor coolant pumps.

The high pressure injection and makeup flows to the intact loop were initiated at 65 s. This time corresponds to 25 s after the time the pressurizer pressure reached 1760 psia. Auxiliary feedwater was initiated at 96 s, corresponding to 61 s after the reactor trip.

The decline in primary system pressure was terminated as the pressure approached that of the secondary system. This indicates the energy removal rate at the break was not sufficient to remove decay heat. Thus, the secondary system was required to remove part of the decay heat, and as a result, the primary system pressure remained above that of the secondary system.

As a result of the reactor coolant pump trip, the loop flow rates declined rapidly as shown in Figure 6. Following coastdown of the pumps, loop flow entered a period of natural circulation. As shown in Figures 7 and 8, the injection flow from HPI and makeup was exceeded by the break flow. As a result, the primary system began to void as indicated by the hot-leg void fractions shown in Figure 9.

As the loop void fractions increased, an asymmetry in the steam generator upside and downside tube levels developed. The terms upside and downside level refer to the collapsed levels in the portions of the U-tubes that experience vertically upward and downward flow, respectively, during normal plant operation. Figure 10 shows the tube level responses within the intact loop steam generator; responses in the broken loop were virtually identical to those in the intact loop. In Figure 10, the zero level corresponds to the bottom end of the tube (bottom surface of the tubesheet). The asymmetry between the upside and downside levels is caused by the opposite effect the force of gravity has on these two fluid flow paths. In the upside, gravity opposes positive flow, i.e., normal direction, while in the downside it supports positive flow. As the loop flow rate slows, this difference causes the downside to drain more rapidly than the upside. Thus, resulting two-phase flow patterns are concurrent downward in the downside of the tube and countercurrent (vapor upward, liquid downward) in the upside of the tube.

Table 4. RELAP5 calculated sequence of events for 3-in. break, Model F steam generators

Events	Time (s)
Break opens in cold leg	0
Reactor trip, reactor coolant pump trip,turbine trip, main feedwater isolated, turbine stop valves closed	35
HPI and makeup flow initiated	65
Auxiliary feedwater initiated	96
Core heatup begins	814
Broken loop seal clears, core temperatures decrease	873
Auxiliary feedwater throttled when level setpoint attained	1230
Accumulator injection begins	2104
End of calculation	2928

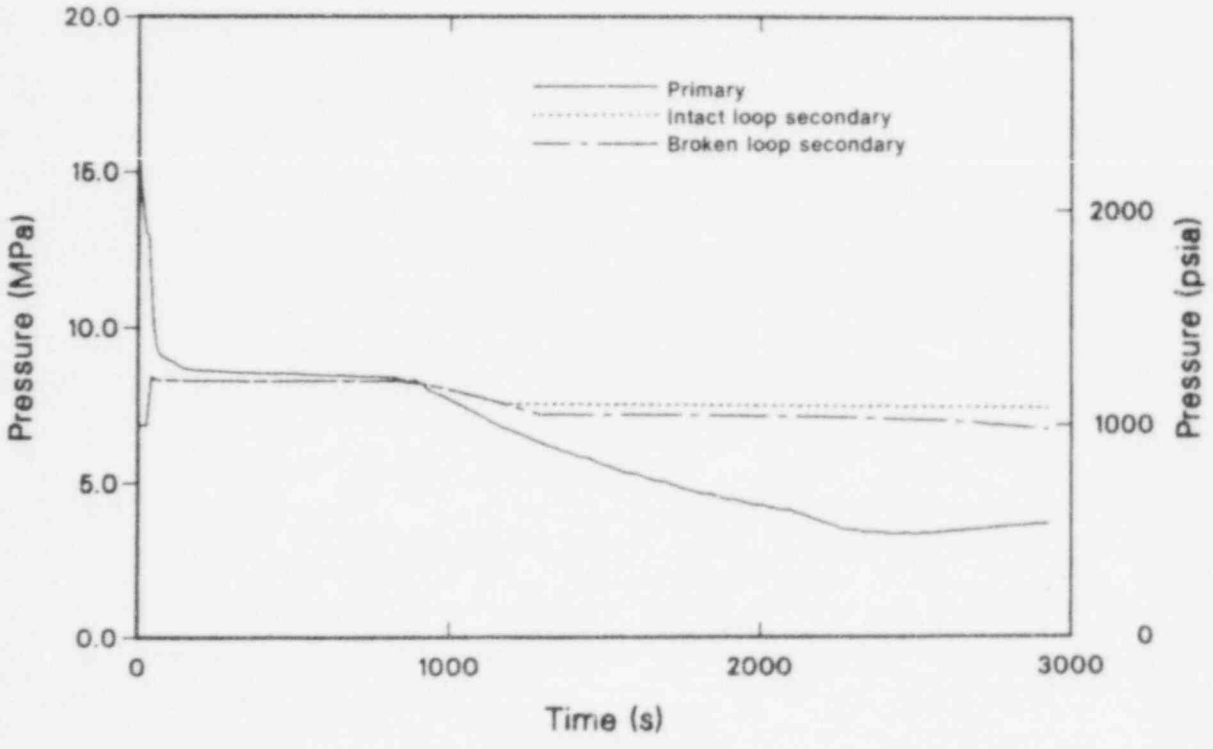

Figure 5. RELAP5 primary and secondary system pressures for 3-in. break, Model F SG.

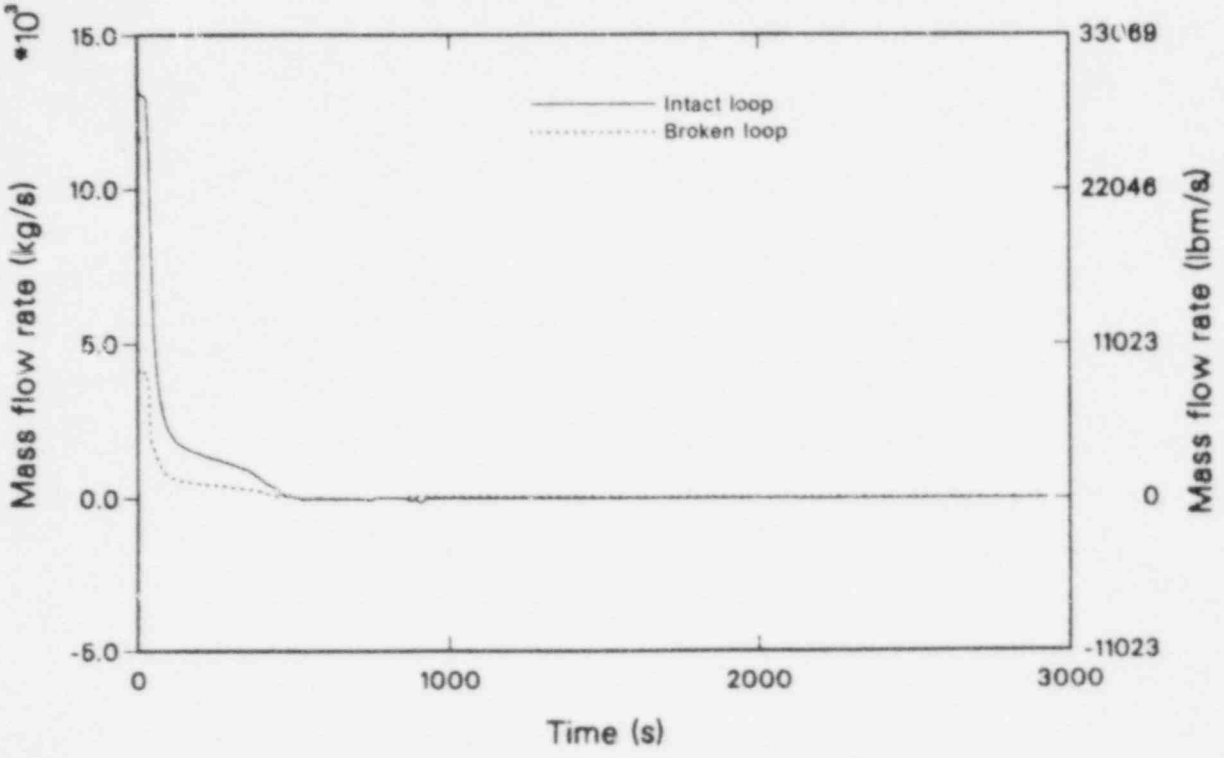

Figure 6. RELAP5 hot leg mass flow rates for 3-in. break, Model F SG.

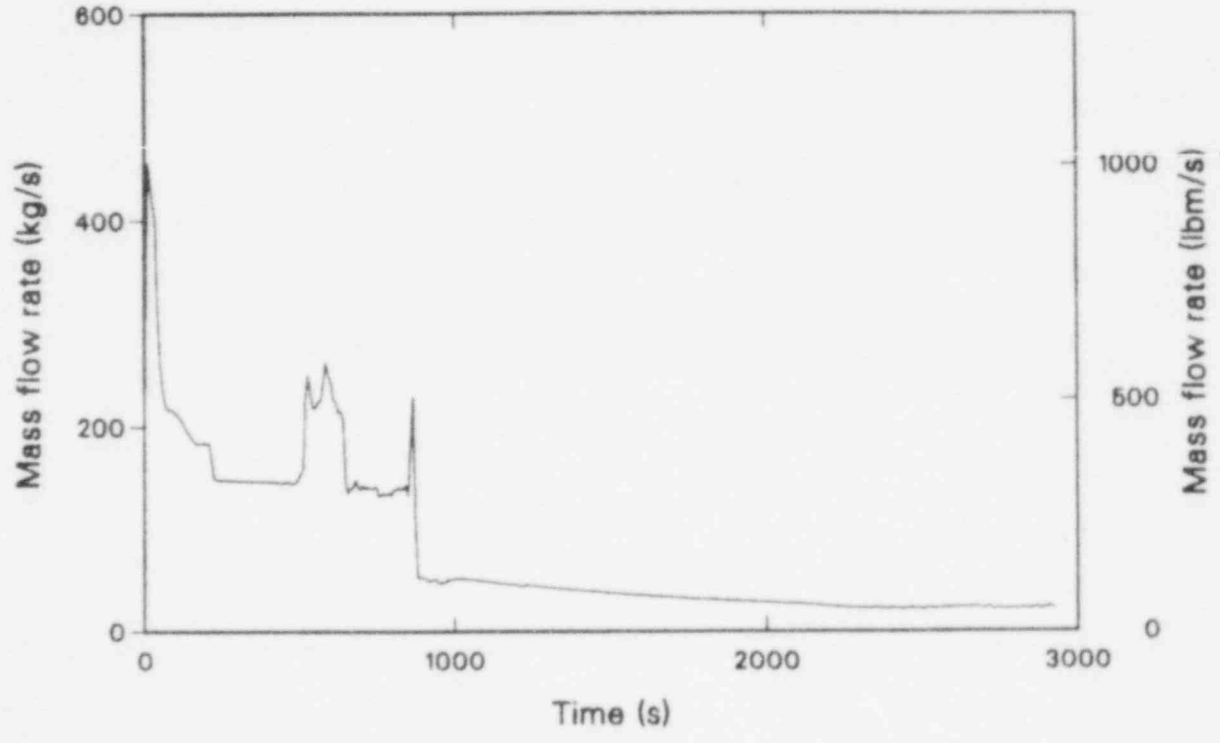

Figure 7. RELAP5 break mass flow rate for 3-in. break, Model F SG.

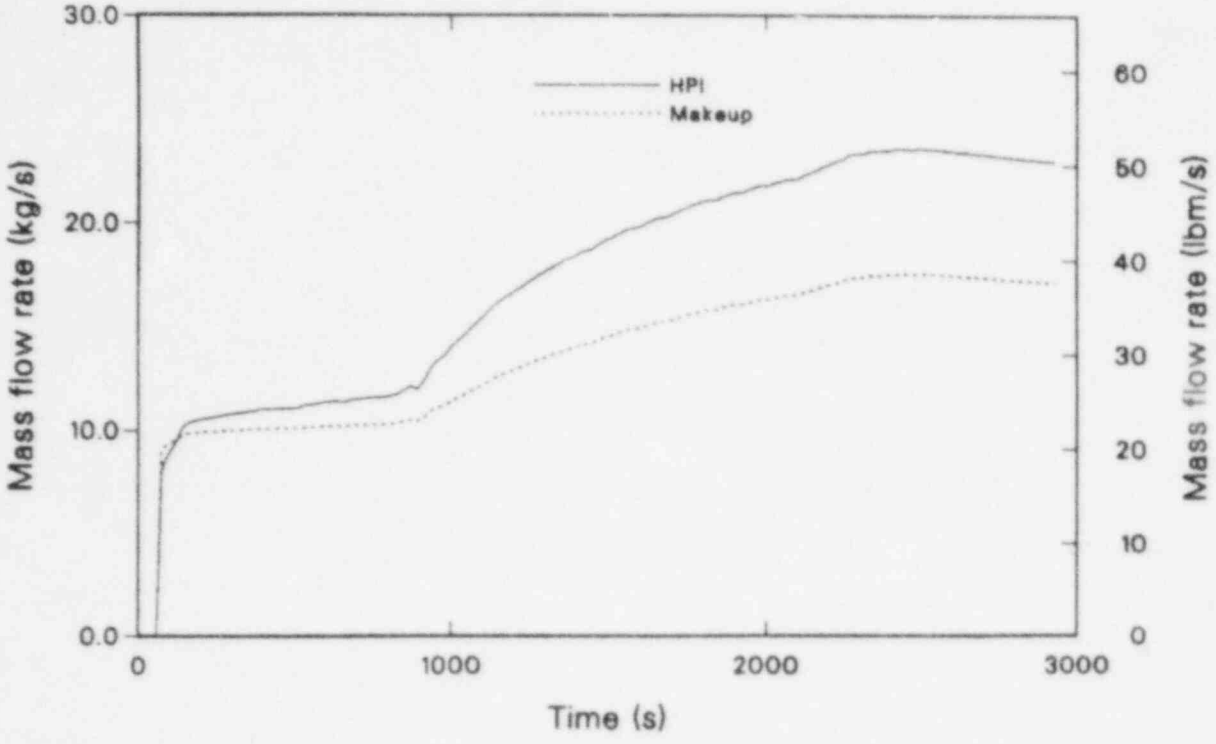

Figure 8. RELAP5 HPI and makeup flow rates for 3-in. break, Model F SG.

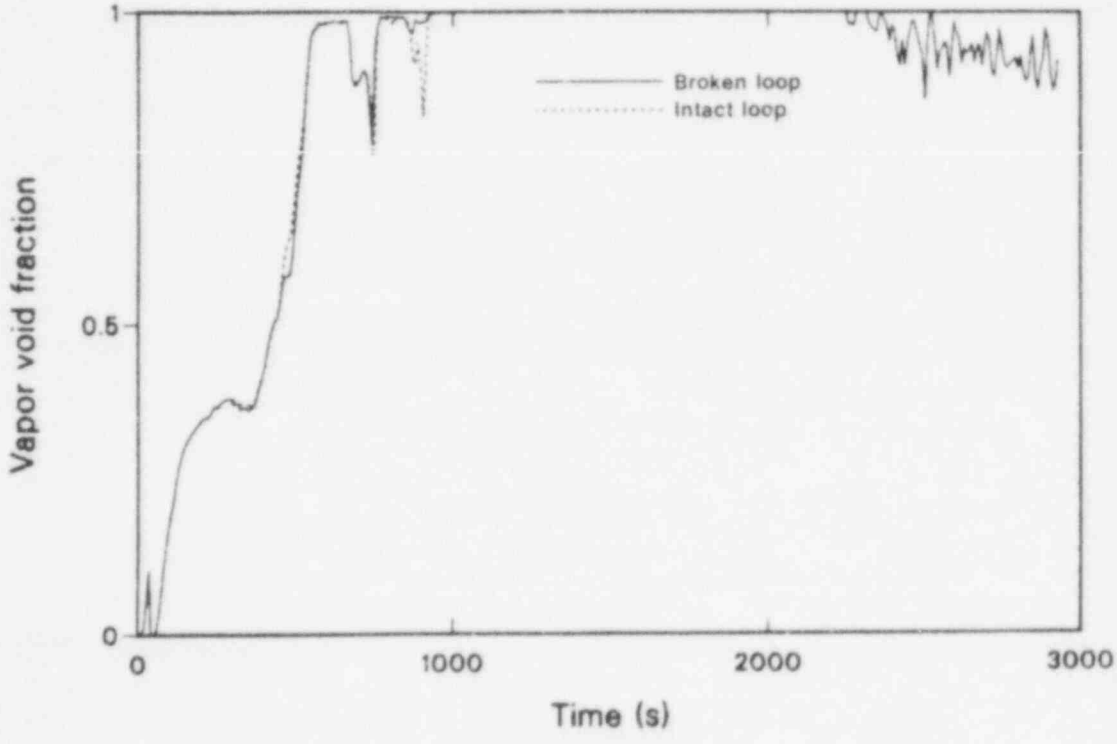

Figure 9. RELAP5 hot leg void fractions for 3-in. break, Model F SG.

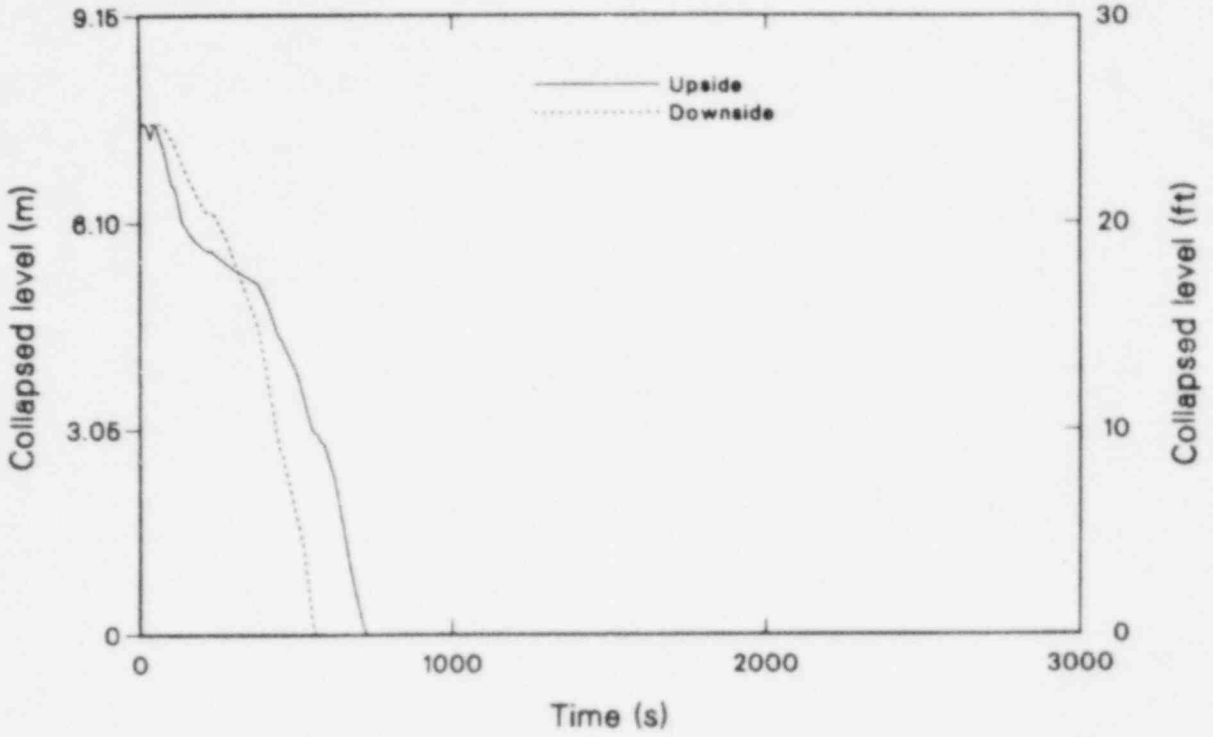

Figure 10. RELAP5 intact loop SG tube levels for 3-in. break, Model F SG.

Figure 11 shows the liquid fractions in the intact loop steam generator plenums and the sloped section of the intact loop hot leg. The asymmetry of liquid distribution between the inlet and outlet plenums is similar to that discussed for the steam generator upside and downside tube levels.

The asymmetries discussed above are significant because they directly affect the core level during periods of stagnant loop flow. Specifically, the difference between the total upside collapsed level (sloped hot leg, plus inlet plenum, plus tube upside) and total downside collapsed level (outlet plenum plus tube downside) creates a static head imbalance. Due to manometric considerations, the imbalance results in a core level depression below, and downcomer level elevation above, the level expected without the imbalance. Without the asymmetry, the collapsed core level needs to be depressed only to the elevation of the loop seals to allow clearing of the seals. With the asymmetry, however, the core level must be depressed below the loop-seal elevation to compensate for the static-head imbalance. As shown in Figure 12, the core level was depressed to 3.58 ft above the bottom of the core before the loop seal cleared. This was 3.36 ft below the loop seal elevation.

As a result of the additional depression of the core level, a heatup of the fuel rod cladding occurred in the top three core sections as shown in Figure 13. Comparing Figures 12 and 13, the initial core heatup began when the collapsed core level fell to 6.01 ft above the bottom of the core.

Continued voiding of the broken loop caused the downside of the broken loop pump suction to begin draining after the tube downside and outlet plenum had drained. As shown in Figure 14, the pump suction drained steadily until the loop seal elevation was reached at about 873 s. At that time, the loop seal was cleared, causing liquid in the broken loop pump suction upside to be swept toward the reactor vessel. As steam reached the break, the break mass flow rate dropped significantly (Figure 7), and the increasing break volumetric flow caused the primary system pressure to begin decreasing again (Figure 5). The decreasing pressure caused an increase in HPI and makeup flow rates (Figure 8) and this, along with the liquid entering the reactor vessel from the broken cold leg, caused the collapsed core level to rapidly increase as shown in Figure 12.

With the increasing core level, the heatup in the upper portion of the core was reversed, and the

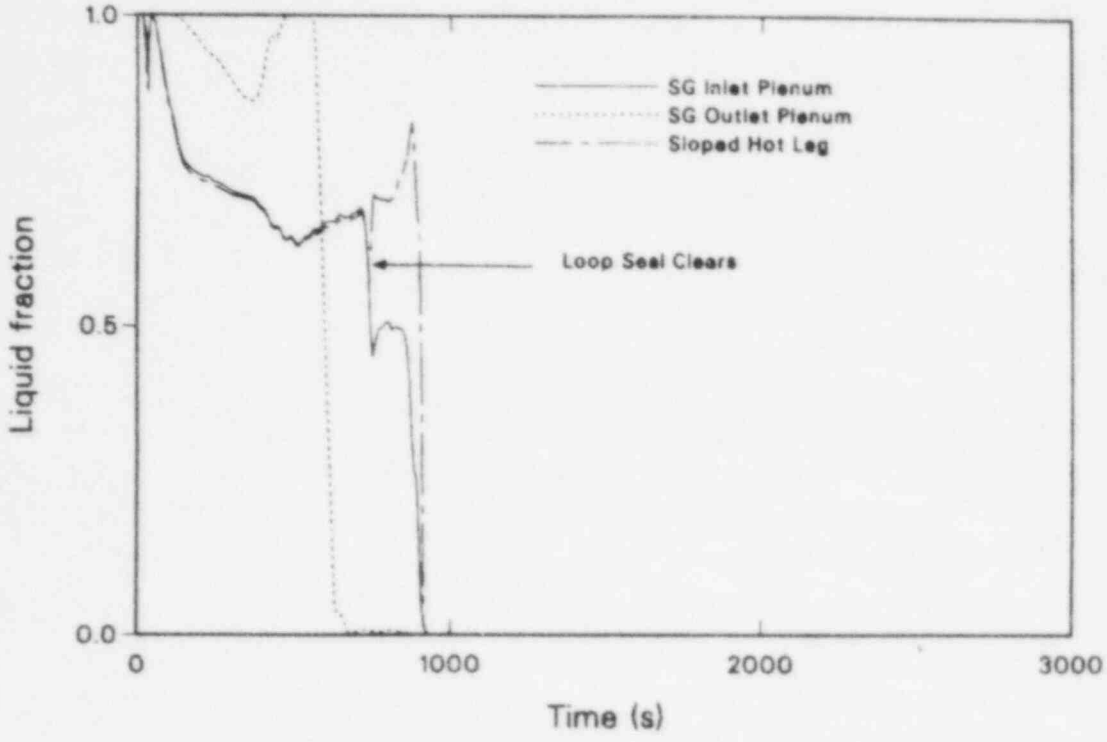

Figure 11. RELAP5 intact loop SG plenums and sloped hot leg liquid fractions for 3-in. break, Model F SG.

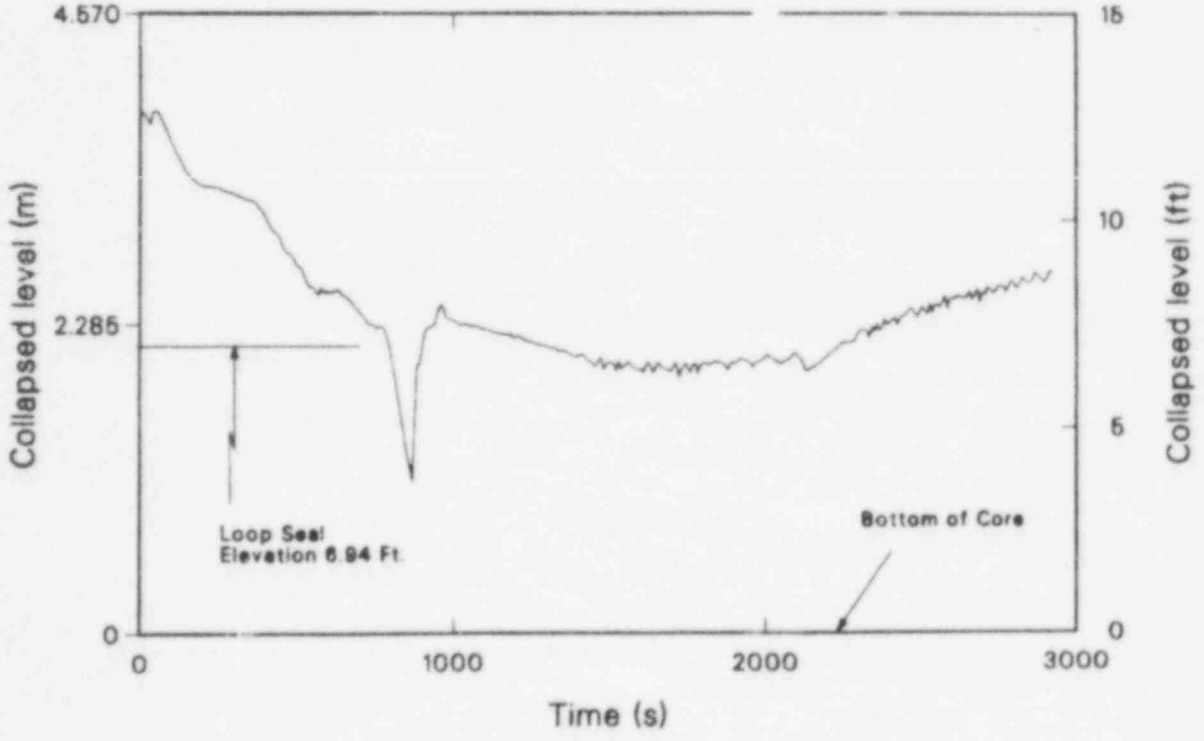

Figure 12. RELAP5 collapsed core level for 3-in. break, Model F SG.

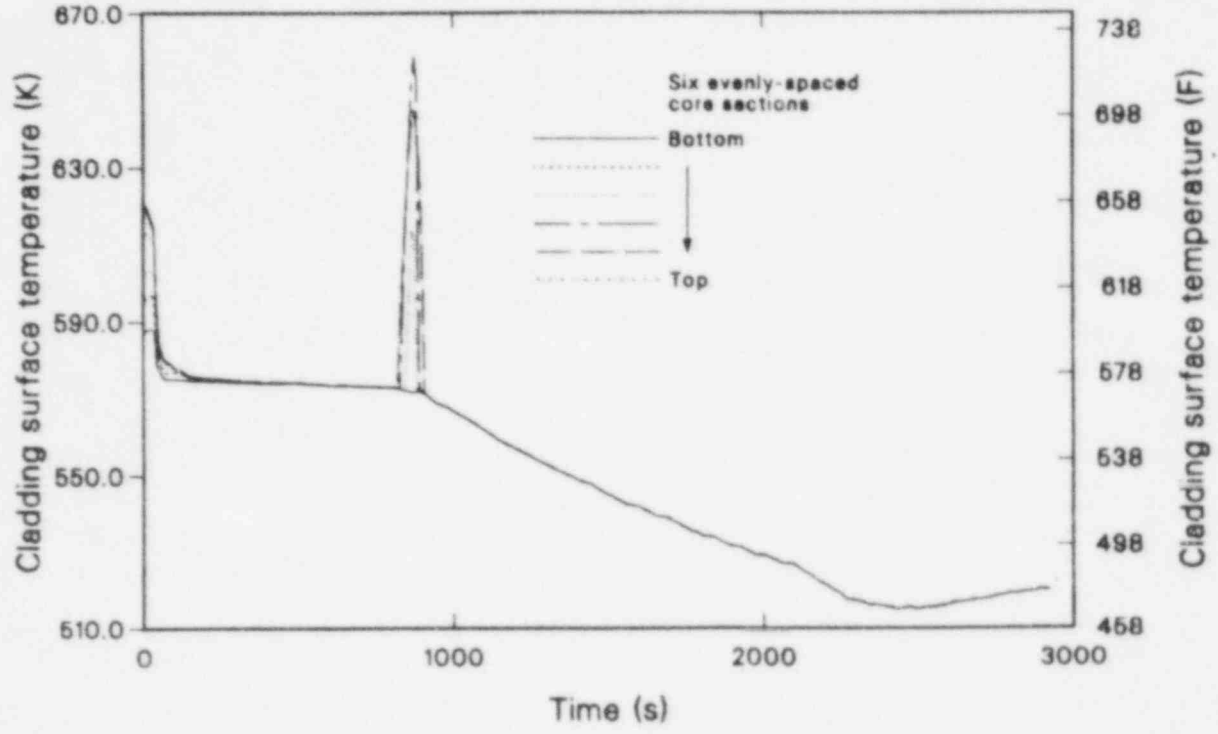

Figure 13. RELAP5 average core cladding temperatures for 3-in. break, Model F SG.

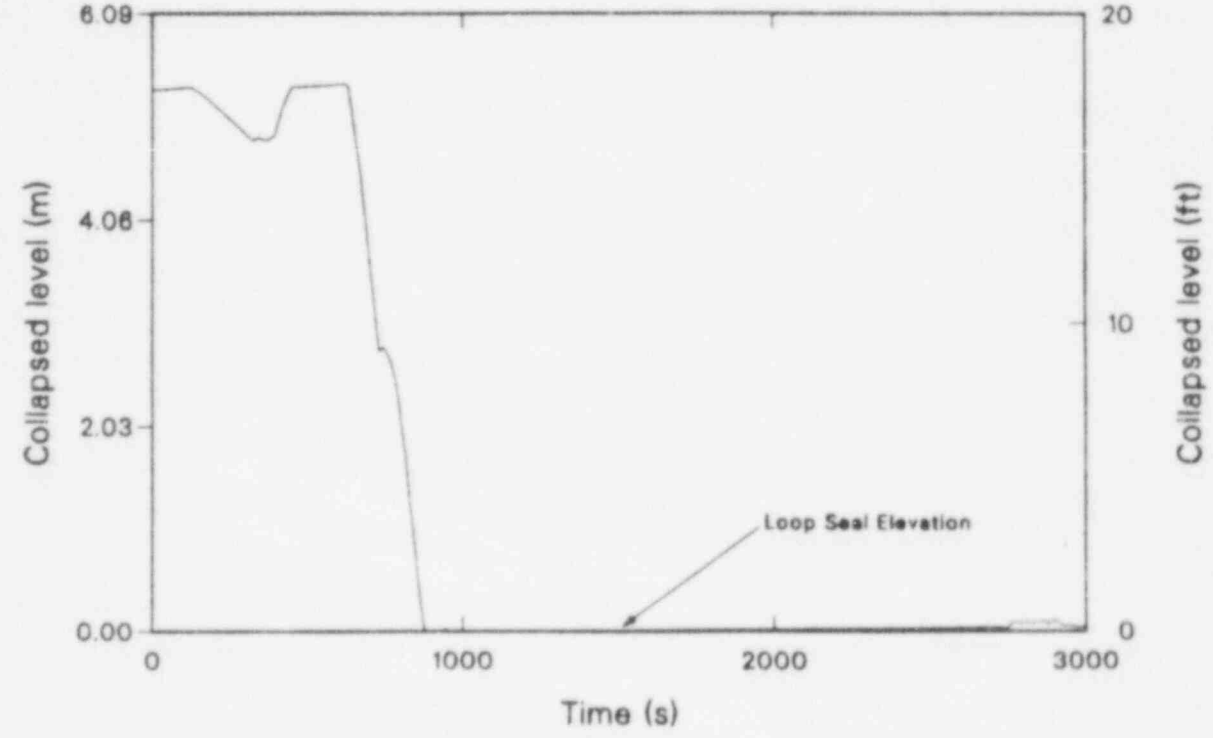

Figure 14. Broken loop pump suction downside level for 3-in. break, Model F SG.

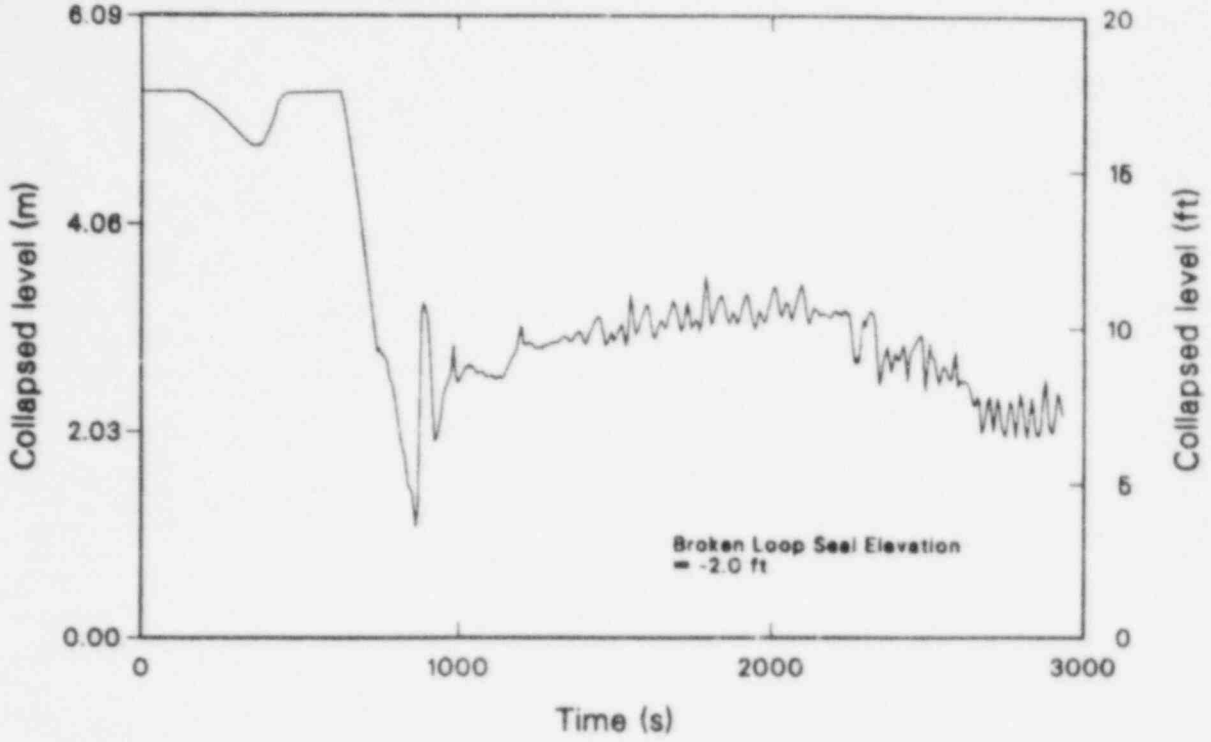

Figure 15. Intact loop pump suction downside level for 3-in. break, Model F SG.

cladding temperatures returned to saturation as shown in Figure 13. Maximum cladding temperatures attained were 730°F in the average core and 790°F in the hot pin.

Clearing the loop seal in the broken loop allowed significant steam flow to reach the break. As a result, clearing of the intact-loop seal did not occur. As shown in Figure 15, the intact loop pump suction downside level increased when the broken loop seal cleared.

Continued primary system depressurization initiated accumulator flow at 2104 s when the pressure reached 600 psia. As will be discussed in the following sections, a second core heatup was observed during this depressurization phase for larger break sizes. With a 3-in. break size, however, the depressurization was gradual, and flashing within the core was not sufficient to cause a second heatup.

The calculation was terminated at 2928 s with the reactor pressure and temperature increasing slowly and the core level increasing. Injection flow from the HPI and makeup systems exceeded the break flow as shown by comparing Figures 7 and 8.

For assurance that RELAP5-calculated results for the prototype RESAR pressurized water reactor (PWR) are reasonable, comparisons of the countercurrent flow behavior in the steam generator inlet regions were performed. Representative comparisons are shown here for the 3-in.-diameter break RELAP5 calculation with Model F steam generators. First, the comparisons assume the RELAP5-calculated vapor upflow velocity is correct. Next, a liquid downflow velocity is calculated according to a countercurrent flow limiting (CCFL) correlation. Finally, a comparison between the correlated and RELAP5-calculated liquid velocities is made. Thus, the comparisons are an indication of the reasonableness of the RELAP5 flooding behavior.

At the connection between the steam generator inlet plenum and tubes (inlet of the tubesheet), the Wallis CCFL correlation[7] is applicable because of the small hydraulic diameter of the U-tubes. The Wallis correlation relates the dimensionless vapor and liquid volumetric fluxes as follows.

$$j_g^{*\frac{1}{2}} + j_f^{*\frac{1}{2}} = 0.775 \qquad (1)$$

where

$$j_g^* = V_g \alpha \rho_g^{\frac{1}{2}} x$$

$$j_f^* = V_f (1 - \alpha) \rho_f^{\frac{1}{2}} x$$

V_g = vapor velocity (upward)

V_f = liquid velocity (downward)

α = void fraction

ρ_g = vapor density

ρ_f = liquid density

$$x = \left[gD(\rho_f - \rho_g) \right]^{-\frac{1}{2}}$$

D = hydraulic diameter

g = acceleration due to gravity.

Given V_g, α, ρ_g, and ρ_f from the RELAP5 calculation, and D from the plant geometry, equation (1) was solved for V_f (Wallis). Figure 16 compares the RELAP5 and Wallis liquid velocities at the intact loop steam generator inlet plenum-to-tube connection. The period of interest is from 500 to 750 s when the loop flow has stopped and the tube upside levels are decreasing as shown in Figure 10. The comparison shows the RELAP5-calculated U-tube upside level draining process occurred slightly slower than predicted by the Wallis correlation. Thus, the RELAP5 calculation is conservative, compared to Wallis, because a higher tube level creates the potential for greater core level depression and peak clad temperatures.

As discussed earlier, core heatup began after the U-tubes had completely drained and was caused by the static head of liquid remaining in the steam generator inlet plenum and vertical sections of the hot legs. Thus, while the tube liquid level did not directly cause the core heatup, the delayed draining of the U-tubes caused delayed draining of the steam-generator inlet plenum and vertical hot leg sections, which allowed the core to heat up. The overall draining process may be thought of as a cascade, with the tubes draining to the plenum and the plenum draining to the hot legs.

The geometry of the hot leg/inlet plenum connection is quite different from that at the plenum/tube connection. Specifically, at the former, the hydraulic diameter is much larger; equaling the hot leg diameter. The Wallis correlation has not been shown to be applicable for such large diameters. Instead, the Kutateladze correlation is generally applied in larger diameter situations. The Kutateladze correlation is not explicitly dependent on diameter; however, the Kutateladze constant is often varied to obtain good agreement with available experimental data. No data are available for the hot leg/inlet plenum geometry of the RESAR plant. For this analysis, a Kutateladze constant of K = 3.2 was assumed based on the reference countercurrent-flow-limiting model of the TRAC-BD1 computer code.[8] The Kutateladze correlation relates the dimensionless vapor and liquid velocities as follows:

$$K_g^{\frac{1}{2}} + K_f^{\frac{1}{2}} = K^{\frac{1}{2}} = 3.2^{\frac{1}{2}} \qquad (2)$$

where

$$K_g = \alpha V_g \left[\frac{(\rho_f - \rho_g)\sigma g}{\rho_g^2} \right]^{-\frac{1}{4}}$$

$$K_f = (1 - \alpha) V_f \left[\frac{(\rho_f - \rho_g)\sigma g}{\rho_f^2} \right]^{-\frac{1}{4}}$$

σ = surface tension.

Given V_g, ρ_f, ρ_g, and α from the RELAP5 calculation, and the physical property σ, Equation (2) was solved for V_f (Kutateladze). Figure 17 compares the RELAP5 and Kutateladze liquid velocities at the intact loop hot leg-to-inlet plenum connection. Two periods of interest are noted: first, while the tubes are draining from 500 to 750 s, and second, after the tubes have drained and before clearing of the broken loop seal from 750 to 873 s. During the first period, the RELAP5 calculation showed significant liquid drainback while the Kutateladze correlation predicted no liquid drainback. During the second period, RELAP5 and Kutateladze liquid velocities were in excellent agreement.

Thus, the RELAP5 liquid velocity at the hot leg-to-inlet plenum connection was nonconservative from 500 to 750 s by about 0.3 ft/s. This correlates to about 4.7 ft^3/s of excessive liquid flow from the intact loop inlet plenum to the hot leg. As shown in Figure 16, however, RELAP5 was conservative at

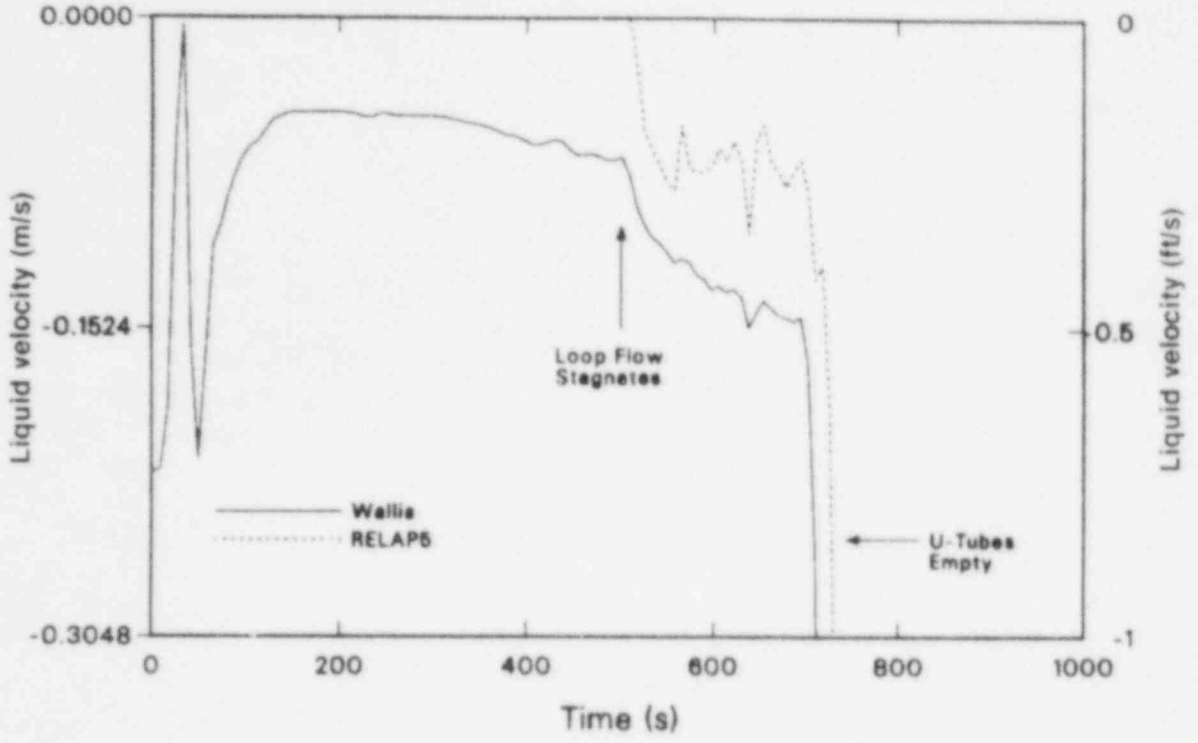

Figure 16. Comparison of RELAP5 and Wallis liquid velocities at intact steam generator tube entrance.

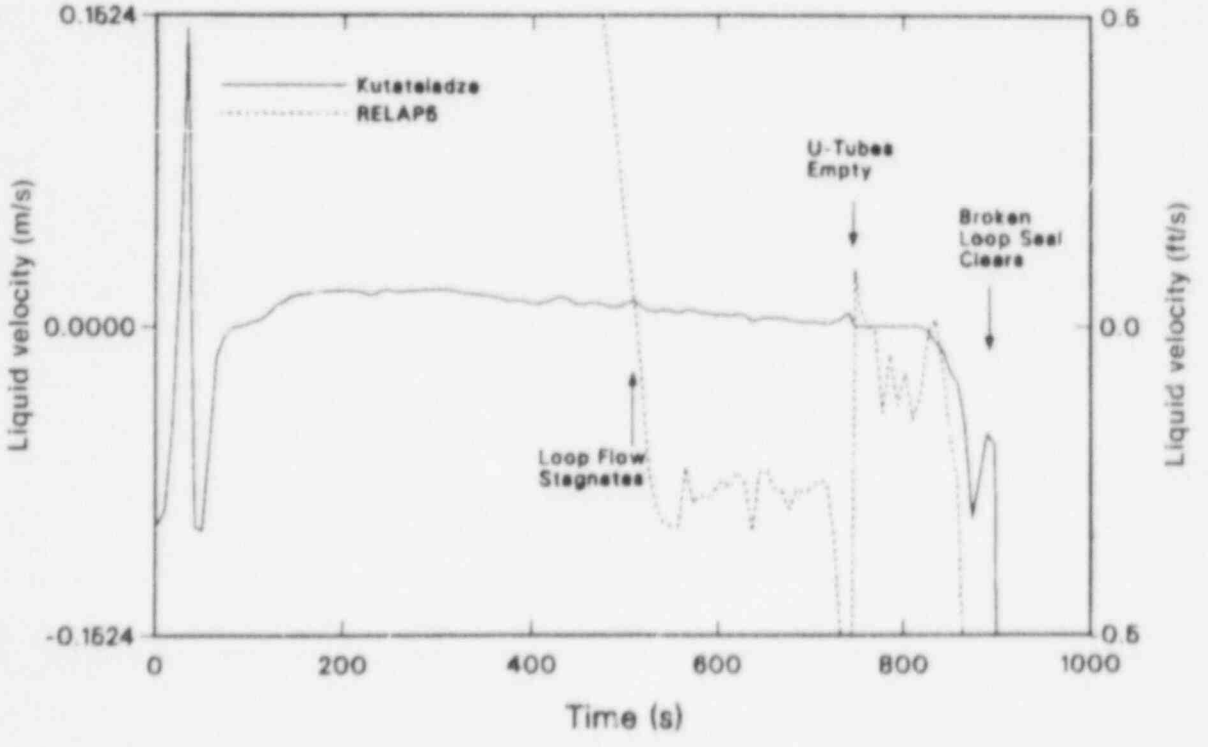

Figure 17. Comparison of RELAP5 and Kutateladze liquid velocities at intact hot leg/steam generator plenum connection.

the plenum-to-tube connection by about 0.2 ft/s (or 6.6 ft^3/s) during the same period.

In summary, the countercurrent flow behavior of RELAP5 in the hot leg/inlet plenum/tube region is in general agreement with that predicted by the Wallis and Kutateladze correlations. From 500 to 750 s, RELAP5 was found to drain the inlet plenum too quickly and to drain the tubes too slowly by approximately the same differences in liquid volume. Thus, the net rate of static head loss with RELAP5 is in excellent agreement with that predicted by the flooding correlations from 500 to 750 s. From 750 s to the time of loop-seal clearing at 873 s, draining of the inlet plenum is in excellent agreement with that predicted by the Kutateladze correlation. The above discussions are presented only to assure the reader that the countercurrent flow behavior calculated by RELAP5 is reasonable. Quantification of the reasonableness is difficult, however, due to uncertainties involved in determining the flooding correlations and associated constants applicable to the specific RESAR plant geometry and flow conditions.

4.1.2 Break Size Effect. This section discusses the parametric break size effects observed in the RELAP5 small-break LOCA calculations for the RESAR plant with Model F steam generators. Break diameters of 1.5, 2, 3, 4, 5, 6, and 7 in. were investigated. The parametric effects observed in calculations for the RESAR plant with Model D steam generators were similar to those discussed here.

Obviously, sequence event timing is accelerated as the break size is enlarged. Table 5 displays this acceleration for two key events: reactor trip and initial loop-seal clearing time.

Primary system pressure responses for the seven break sizes are compared in Figure 18. For the 1.5- and 2-in.-diameter breaks, depressurization to the accumulator injection pressure did not occur. For these breaks, a steady condition was attained with HPI and makeup injection flow exceeding break flow, and the primary system pressure exceeding the accumulator pressure. For the 3-in. break and larger, depressurization to the accumulator injection pressure was encountered.

Differences in loop seal clearing behavior were observed as a function of break size. As discussed in Section 3.5, the intact-loop seal was arbitrarily lowered by 2.0 ft to assure clearing of the broken loop seal first. For the 1.5- through 4-in.-diameter breaks, only the broken-loop seal cleared. For the 5- through 7-in.-diameter breaks, both loop seals cleared. The faster depressurization rates associated with the larger breaks (shown in Figure 18) caused a higher overall vapor production rate (due to flashing) than for smaller breaks. For these larger breaks, clearing a path around the broken loop to the break was insufficient to remove all the vapor generated, so the intact-loop seal was cleared as well.

Core-collapsed level and peak-cladding-temperature responses for the seven break sizes are shown in Figures 19 and 20, respectively. The peak cladding temperature shown in each case is the highest temperature reached in each of the calculations. In all cases, this temperature occurred in the hot pin. In most cases, this temperature occurred in the sixth (top) core section (see Figure 3); however, for the 2-in.-diameter break it occurred in the fifth core section, and for the 5-in.-diameter break, in the third core section. The peak cladding temperatures are summarized in Table 6 as a function of break size. Two distinct peaks are observed: first at 2 in., and second at 6 in. For the 2-in. break, only a pre-loop-seal-clearing heatup was observed. For the 6-in. break, clearing of the broken-loop seal did not cause a rewet of the hot pin; rewetting was delayed until initiation of accumulator injection.

Core heatup was observed prior to loop-seal clearing for all break sizes. Subsequent to loop seal clearing, a second heatup was not observed for the 1.5-, 2-, 3-, and 5-in.-diameter breaks but was observed for the 4-, 6-, and 7-in. breaks. The previously discussed clearing of both loop seals for the 5-in. break allowed rapid primary system depressurization to the accumulator-injection setpoint pressure, thus preventing a second heatup with this break size.

Table 7 presents the effect of break size on the core level at which heatup of the core rods begins. A dramatic sensitivity of this parameter to break size is observed. For the smallest break (1.5 in.), core heatup begins when the collapsed core level is about 60% of the core height. As the break size increases, the core level at which heatup begins decreases uniformly. For the largest break (7 in.), heatup does not begin until the collapsed level decreases to 7% of core height. This variation is caused by the additional flashing and level swell associated with the larger breaks. Core heat

Table 5. Effect of break size on sequence event timing

Break Diameter (in.)	Time of Reactor Trip (s)	Time of Loop Seal Clearing (s)
1.5	129	4844
2	72	1934
3	35	873
4	22	529
5	16	347
6	12	290
7	11	191

is removed by the additional flashing, and the vapor generated by the flashing causes the core to be wetted with a frothy mixture. For the smaller breaks, the core voids are not as large, and a quiescent boiloff is experienced. The data shown in Table 7 are inconsistent with the experimental results of the Semiscale S-UT test series.[9] Both Test S-UT-6 (5% break, 6.7 in. equivalent) and Test S-UT-1 (10% break, 9.5 in. equivalent) showed a heatup beginning at about 53% collapsed core level. Thus, these results differ with

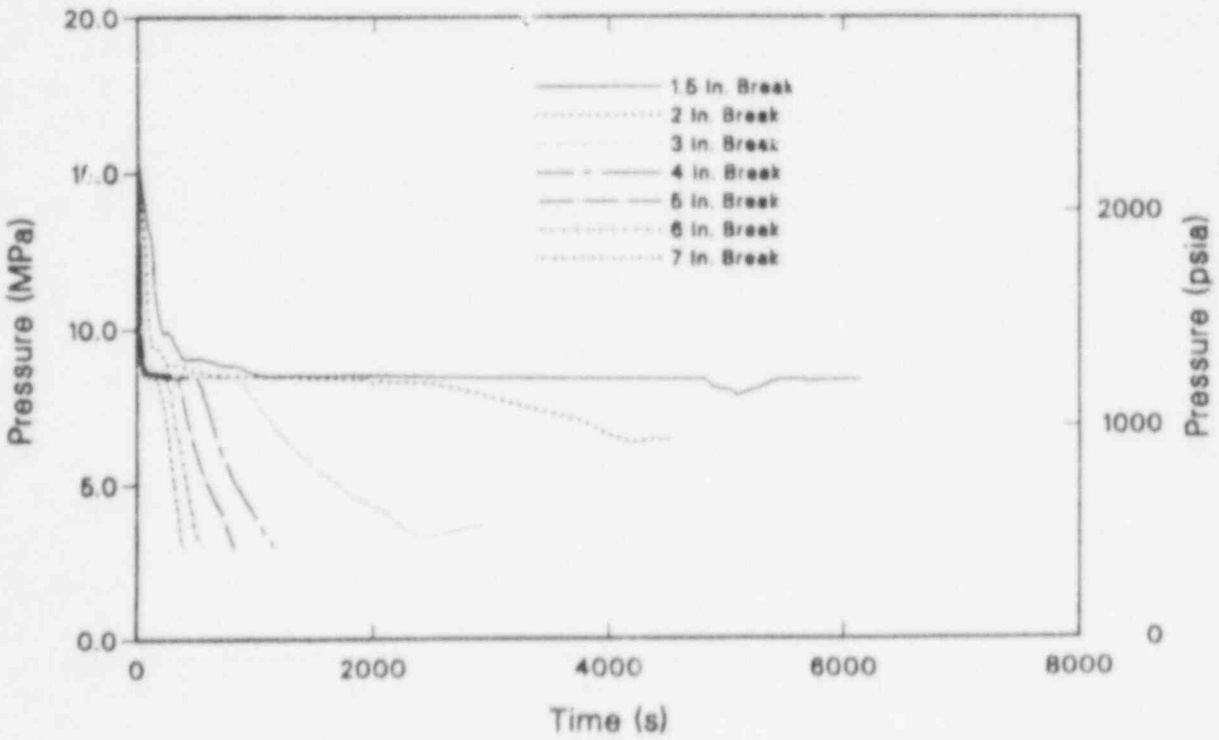

Figure 18. Effect of break size on primary system pressure.

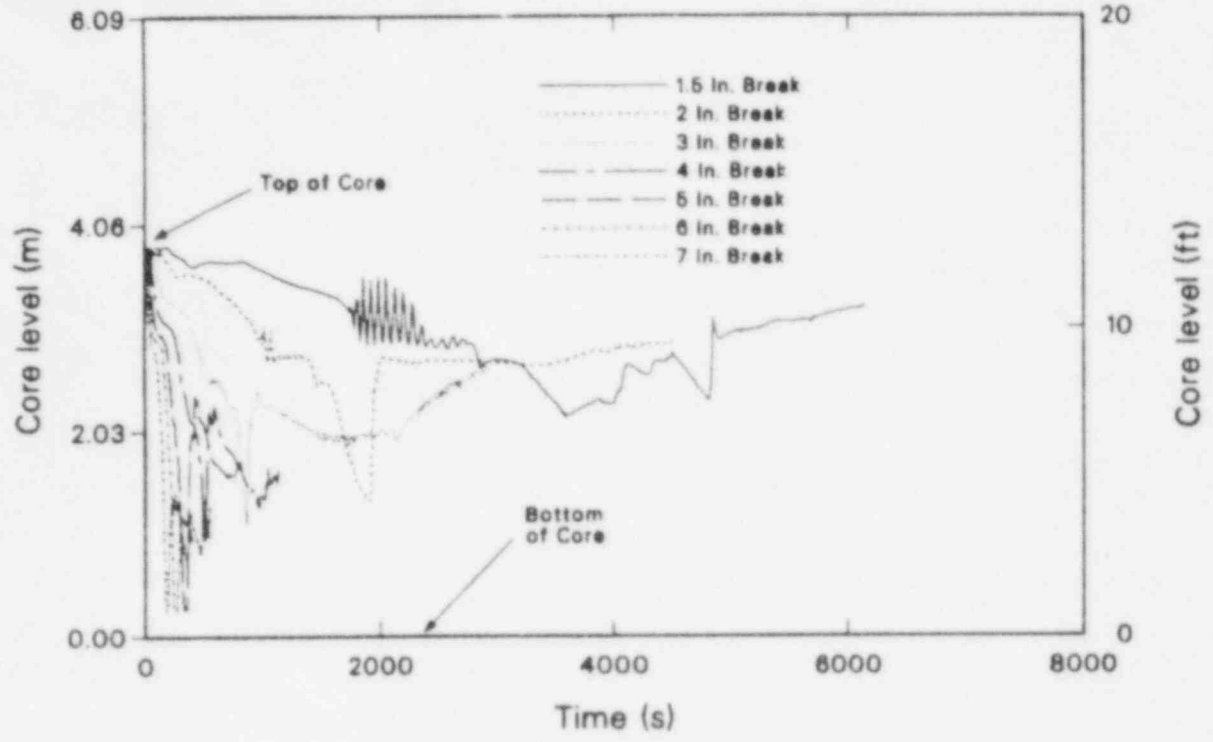

Figure 19. Effect of break size on core level.

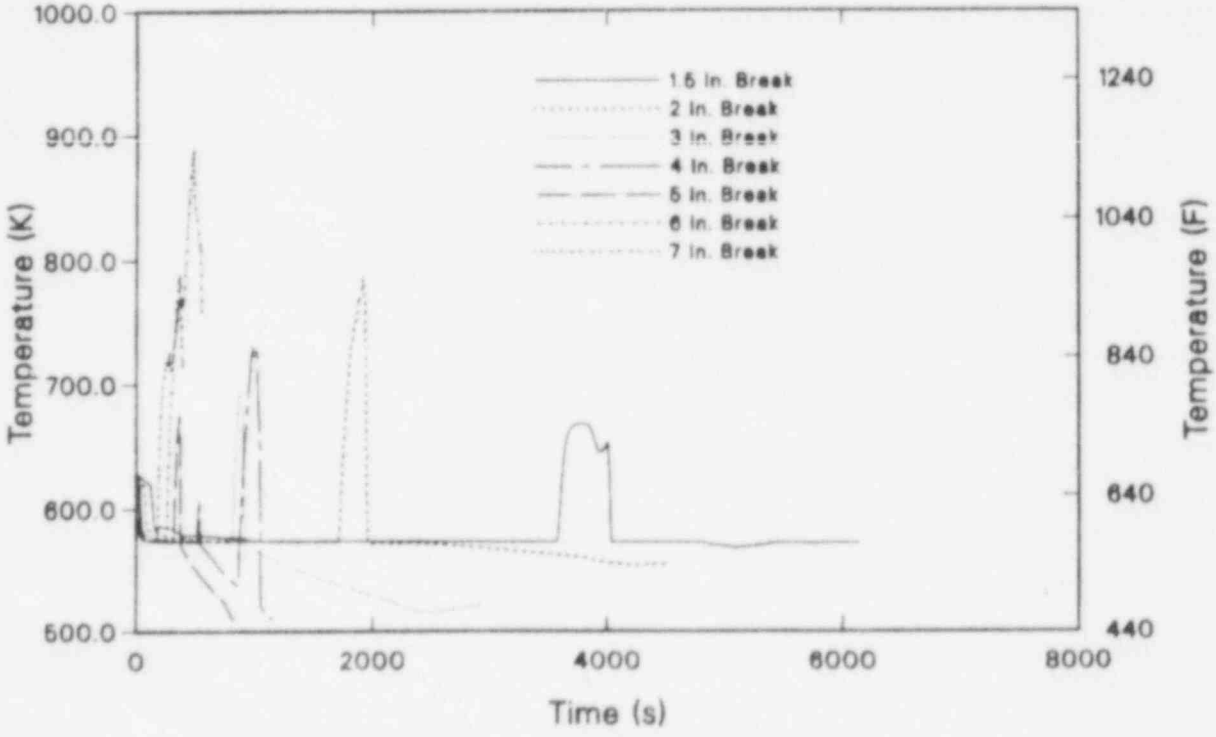

Figure 20. Effect of break size on peak cladding temperature.

Table 6. Effect of break size on peak cladding temperature

Break Diameter (in.) Model F SG	Peak Cladding Temperature (°F)
1.5	744
2	959
3	790
4	360
5	760
6	1148
7	962

those of the RESAR calculations, both in the magnitude of core level at which heatup begins and in the sensitivity of that level to break size. Further investigation of this discrepancy appears warranted.

Table 7. Effect of break size on core level at which heatup begins

Break Diameter (in.) Model F SG	Collapsed Core Level When Heatup Begins (ft)
1.5	7.28
2	6.15
3	6.01
4	4.23
5	2.08
6	0.947
7	0.894

4.1.3 Steam Generator Configuration Effect. This section discusses the sensitivity of the RELAP5 calculational results to steam generator configuration. The Models D and F steam generators differ primarily in the injection location for main feedwater and auxiliary feedwater and in the configuration of the downcomer region.

As indicated in Figures 1 and 3, main feedwater and auxiliary feedwater injection in the Model D steam generator is near the bottom of the downcomer and is at the top in the Model F. The impetus for analyzing the same break sizes with both steam generators was to examine the sensitivity of liquid holdup within the steam generator U-tubes to auxiliary feedwater injection location. Intuitively, the lower downcomer injection location of the Model D steam generator was expected to cause a colder fluid to wet the outside tube walls than for the Model F steam generator. This colder fluid was expected to provide extra condensation potential for the fluid within the tubes, thus increasing the liquid level there.

Another difference between the two steam generator configurations concerns the downcomer volume distribution. The Model D steam generator upper downcomer cross sectional flow area is roughly twice that of the Model F. Since throttling of auxiliary feedwater (AFW) occurs when a setpoint downcomer level is reached, and since the setpoint level is within this region of different areas, throttling for the two different steam generator configurations occurred at significantly different times. This effect is only applicable to the calculations of the smaller break sizes because the longer sequence timing for these calculations spanned one or both of the auxiliary feedwater throttling times. As an example, for the 2-in. break, auxiliary feedwater was throttled at 2825 s with the Model D steam generator, and at 1100 s with the Model F steam generator. For the 4-in. break and larger, the calculations were completed before the time of auxiliary feedwater throttling to either steam generator. Thus, for the larger breaks, this difference is inconsequential.

Results of the 4-in.-diameter break calculations with Models D and F steam generators were compared. This comparison investigates the effects of steam generator configuration independent of the auxiliary feedwater throttling difference just discussed. Figure 21 compares the liquid temperatures in the lower sections of the broken loop steam

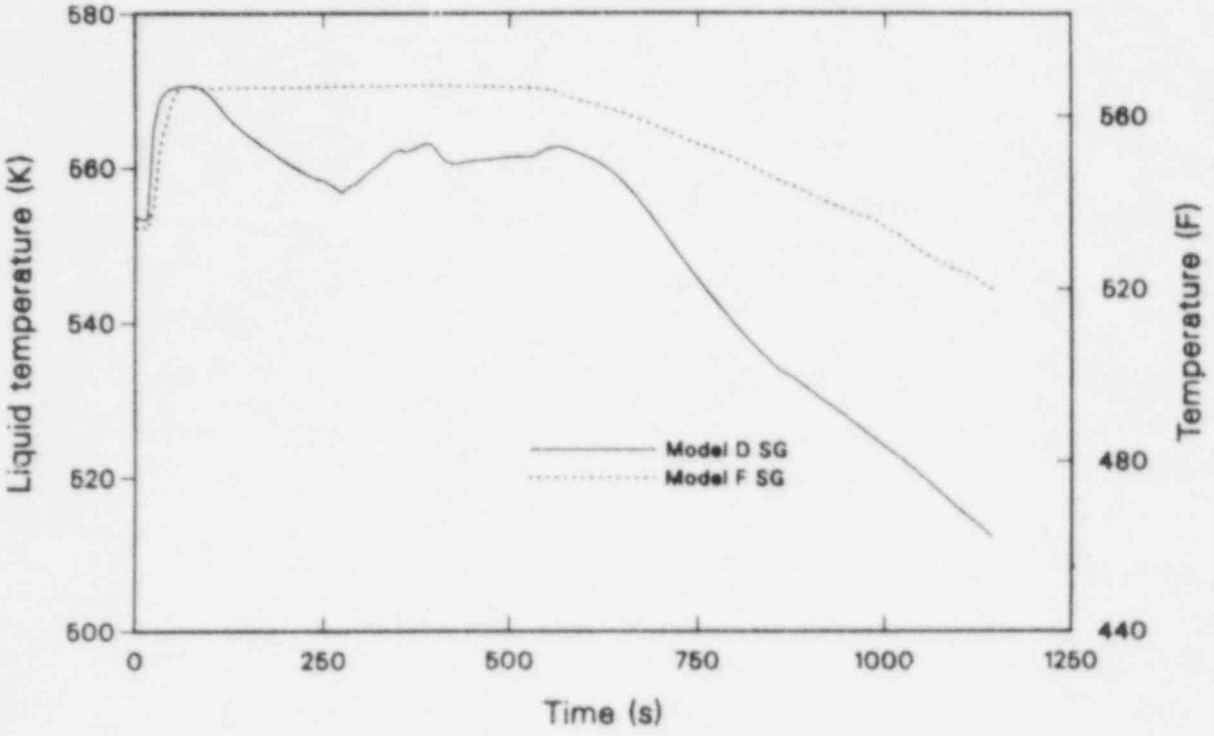

Figure 21. Effect of steam generator configuration on boiler temperature.

generator boilers. As was intuitively expected, this temperature is lower by about 18°F, for the Model D steam generator during the pre-loop-seal-clearing period.

The temperature difference shown in Figure 21 was caused by the effect the feedwater injection location has on the steam generator recirculation ratio (the ratio of the liquid mass flow rate entering the boiler section to the feedwater injection rate). A higher ratio indicates more recirculation flow occurred between the steam generator boiler and downcomer. Thus, a low recirculation ratio produces colder boiler entrance temperatures than a high ratio. Because the cold auxiliary feedwater is mixed with a warm downcomer flow before entering the boiler, the elevation difference between the Models D and F steam generator auxiliary feedwater injection locations creates less recirculation driving head for Model D than for Model F. The driving head is higher with the Model F steam generator because the elevation difference is filled with cooler water than with Model D. For full-power, steady-state operation, the Models D and F recirculation ratios compare favorably (3.53 for Model D and 3.60 for Model F) due to the high recirculating flow rates and the relatively warm main feedwater. Following turbine and main feedwater trips, however, and with cold auxiliary feedwater injection, the above effects cause the Model F recirculation ratio to be about twice that for Model D.

The lower boiler temperature difference between the Models D and F steam generators did not, however, have a significant effect on U-tube collapsed levels. As shown in Figure 22, the broken-loop, U-tube upside collapsed, steam-generator levels with the Model D and F steam generators are in good agreement. The agreement for the U-tube downside levels was even better.

The core levels, shown in Figure 23, differ moderately, with the minimum core level for the Model D steam generator calculation depressed slightly below that of the Model F. Also, core level depression proceeded with the Model D steam generator for a longer period of time. Since the cladding temperature is sensitive to the extent and duration of core level depression, the peak temperature for the Model D calculation was above the Model F calculation (860°F versus 657°F) during the pre-loop-seal-clearing time period.

The different core level depression behavior in the Models D and F calculations was traced to minor differences in the manner in which the pump

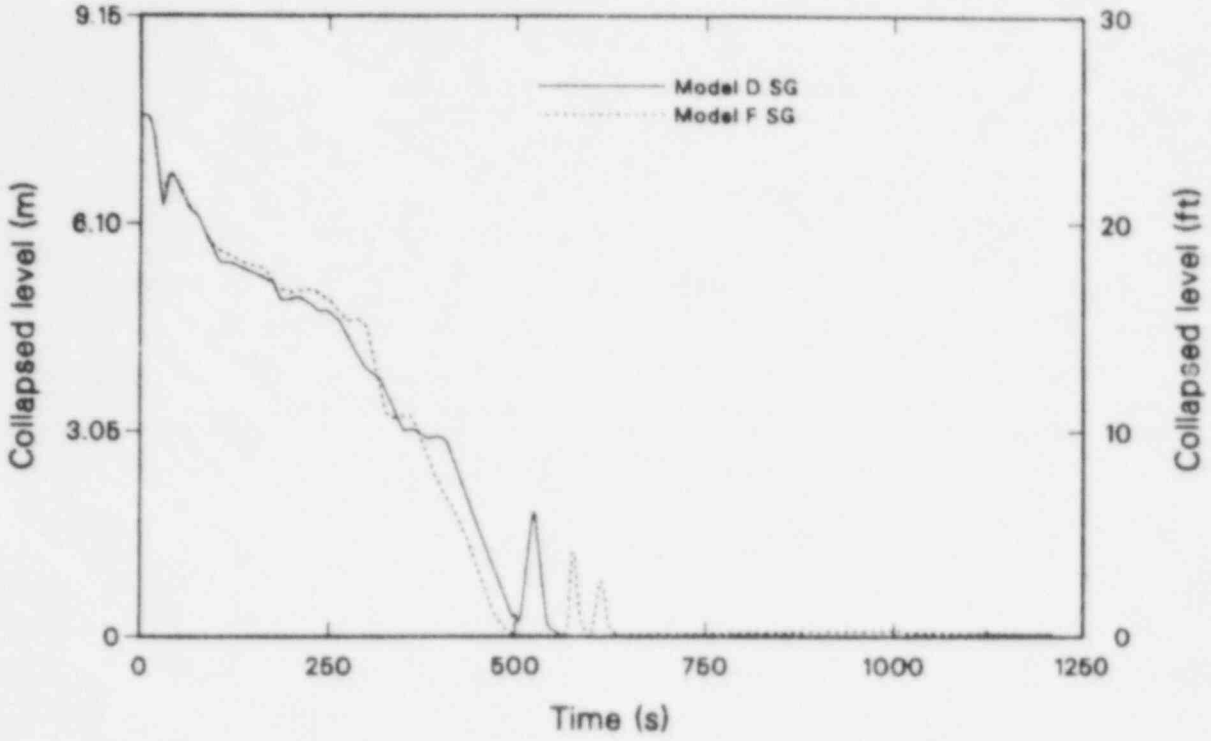

Figure 22. Effect of steam generator configuration on U-tube upside level.

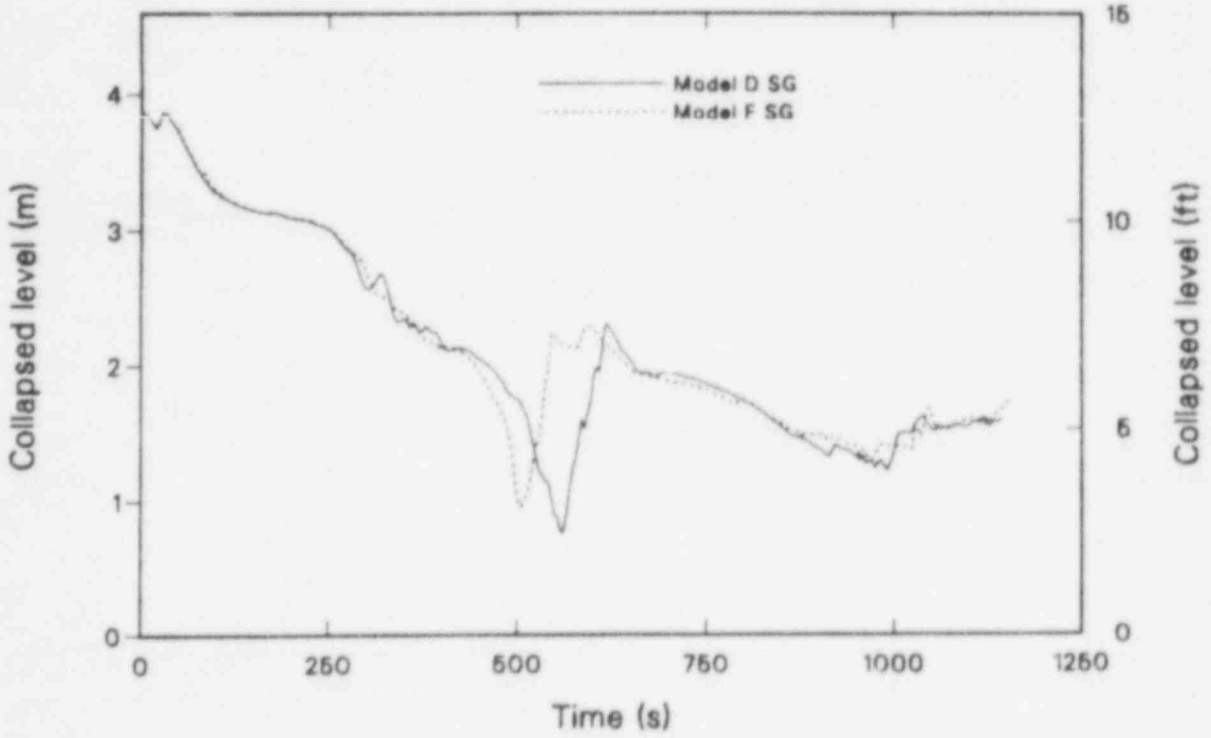

Figure 23. Effect of steam generator configuration on core level.

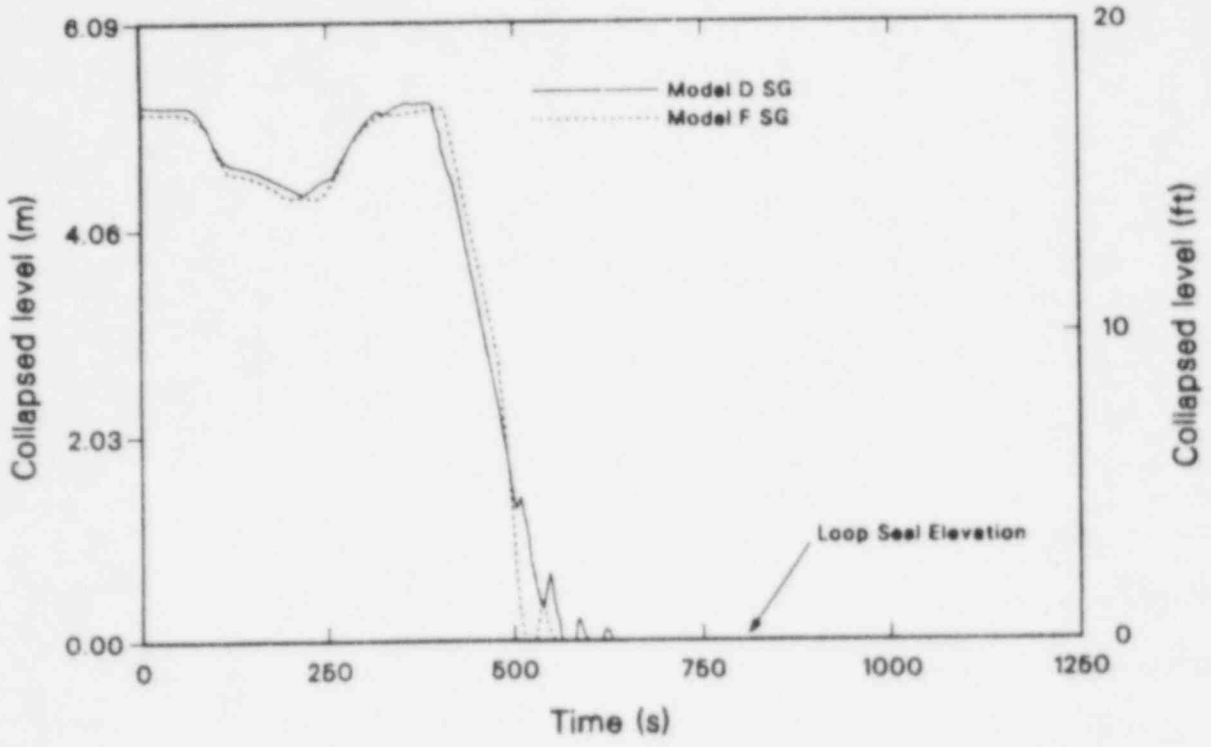

Figure 24. Effect of steam generator configuration on pump suction downside level.

suction downside, and inlet plenum/hot leg vertical section levels completed their draining processes. This is illustrated in Figure 24 for the broken loop, pump suction downside level. Responses of this level for the Models D and F calculations are virtually identical until the levels reach about 5 ft. After that, the Model D level decreased more slowly than the Model F level. A similar, and slightly larger, difference existed in the steam generator and vertical hot leg sections. The result is a delay in the calculated Model D loop-seal clearing time (561 s) compared to that of Model F (529 s). Thus, the core heatup with the Model D steam generator lasted 32 s longer than with Model F.

These differences in the draining processes appear to be caused by the temperature difference displayed in Figure 21. However, while this was shown not to significantly affect the tube levels, it did provide in the Model D calculation for additional condensation of the steam passing through the voided tubes, after they have drained. This additional condensation with the Model D steam generators did two things: (a) produced the additional condensate apparent in Figure 24 and (b) removed some of the vapor in the process. As a result, the calculation with Model D steam generators resulted in a slightly more depressed core level and a delayed loop-seal clearing, compared with the Model F calculation.

In summary, only minor differences in behavior were observed between 4-in.-diameter break calculations with Models D and F steam generators. The behavior differences were found to be caused by the different auxiliary feedwater injection locations of the two configurations. Peak cladding temperatures, prior to loop-seal clearing, were found to be slightly higher for the Model D steam generator than for the Model F. In general, the results discussed here were also observed for the other break sizes as well. For break diameters smaller than 4-in., however, differences in auxiliary feedwater throttling behavior between the two steam generator configurations affected the results. For break sizes larger than 4-in. the effects discussed above were less significant because of the accelerated sequence timing.

4.1.4 Steam Generator Nodalization Effect. Argonne National Laboratory's analyses[2] indicated a potential exists for RELAP5 small break LOCA calculational results to be significantly affected by the extent of the steam generator nodalization. To investigate this possibility,

Table 8. Calculated sequence event timing fc fine and coarse nodalization steam generators

Event	Time of Events (s)	
	Coarse Nodalization	Fine Nodalization
Break opens in cold leg	0	0
Reactor trip	66	72
HPI and makeup initiated	97	103
Auxiliary feedwater initiated	127	130
Core heatup begins	2003	1629
Broken loop seal clears	2110	1979
Auxiliary feedwater throttled	—	2825
Intact loop seal clears	—	3542
Calculation ended	3254	4515

RELAP5 calculations of 2-in.-diameter breaks were performed using the basic (fine) and coarse Model D steam generator nodalization schemes presented in Section 3.1. The basic steam generator nodalization contained about twice the number of calculational cells as the coarse nodalization. For example, the U-tube primaries were simulated with 16 cells in the fine nodalization and 8 cells in the coarse nodalization. Results of the Model D steam generator 2-in.-diameter break calculations with fine and coarse nodalization are discussed in this section.

Table 8 compares the sequence event timing for the coarse and fine nodalization calculations. The sequence timing for the two calculations compare well for early events. However, for later events (such as clearing of the broken loop seal), the sequence of events was slower with the coarse nodalization than for the fine nodalization.

The effect of steam generator nodalization on primary system pressure is shown in Figure 25. No major differences are observed for this parameter.

The nodalization effect on core level is shown in Figure 26, and significant differences are noted. With the fine nodalization, the core level decreases relatively steadily while, with the coarse nodalization, major perturbations are observed from about 800 to 2000 s. Also, the minimum core level was about 2 ft lower with the fine nodalization.

Comparing Figures 27 and 28, the different core level behavior is shown to cause a more significant heatup with fine nodalization than with coarse. With fine nodalization, the core level decreased sufficiently to cause a heatup in the top four core sections while with coarse nodalization only the top two core sections experienced a heatup. Also, the duration of the heatup was longer with fine nodalization (107 s). The resulting fine nodalization peak cladding temperature (1199°F) was higher than that for coarse nodalization (840°F).

The different core level response was caused by significantly different hydraulic behavior in the steam generator secondaries. An indication of this difference is shown by the intact loop steam generator recirculation ratio in Figure 29. As shown, with the fine

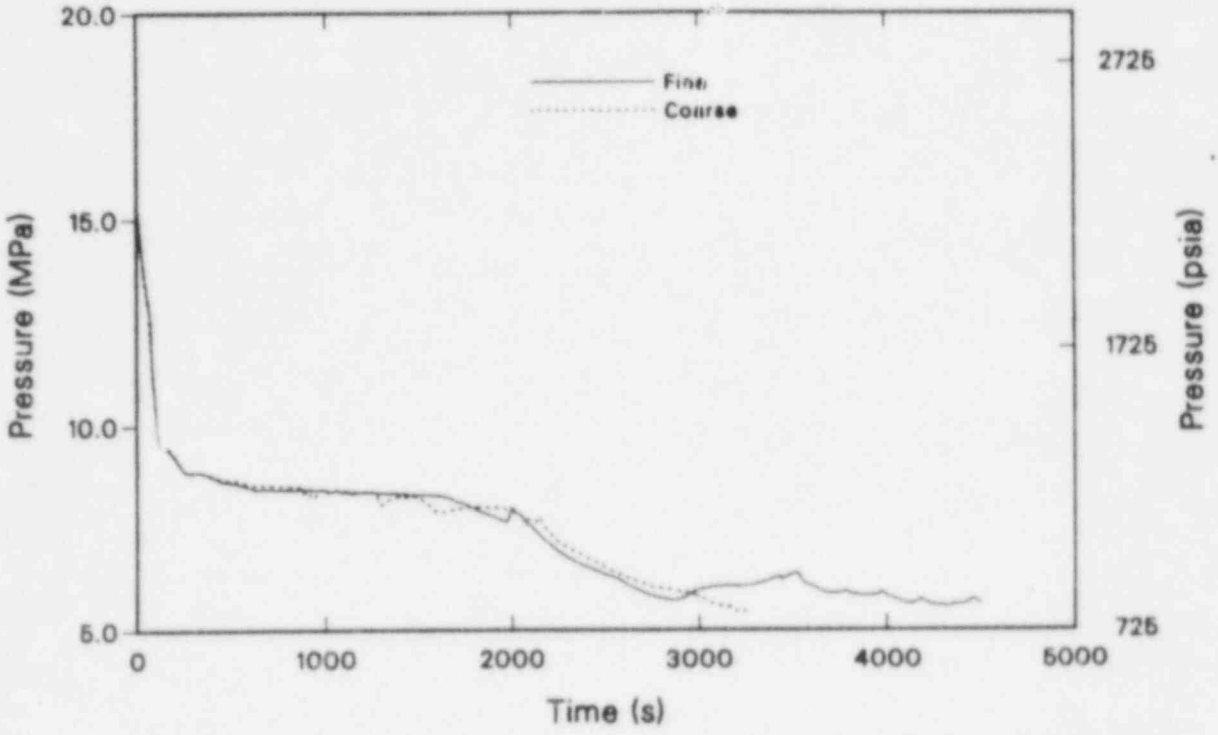

Figure 25. Effect of steam generator nodalization on primary system pressure.

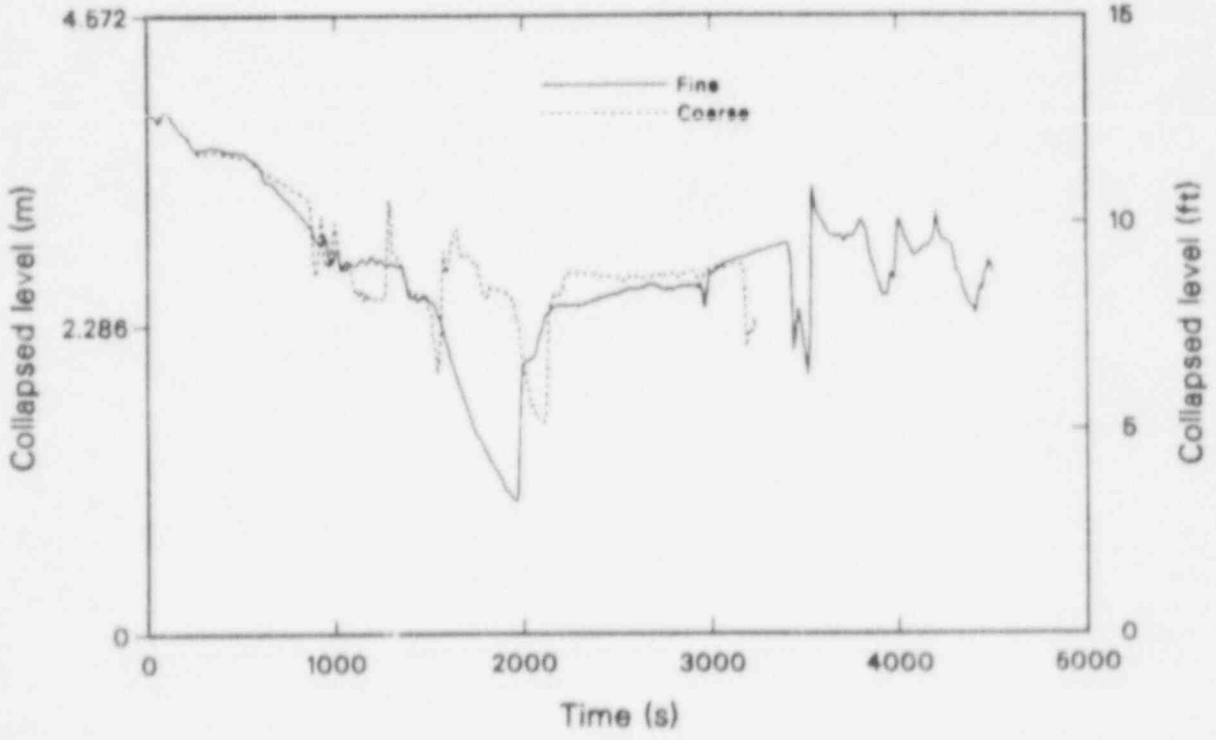

Figure 26. Effect of steam generator nodalization on core level.

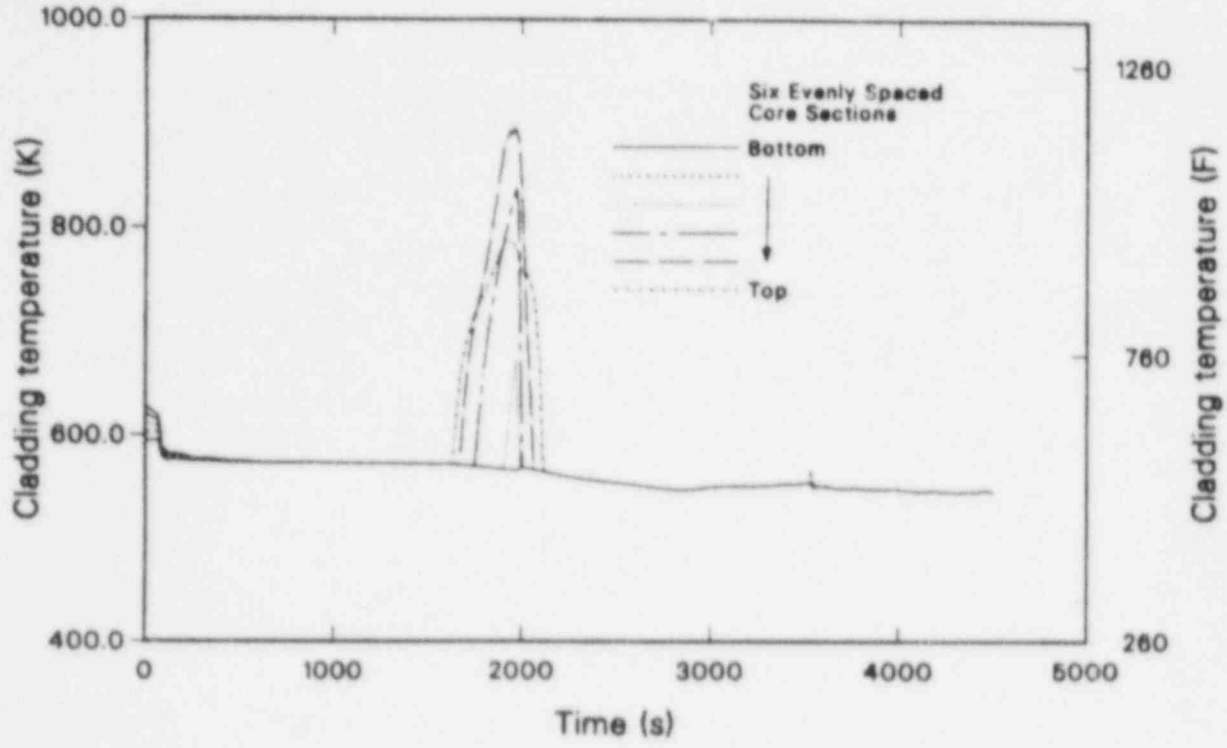

Figure 27. Hot pin cladding temperatures with fine nodalization.

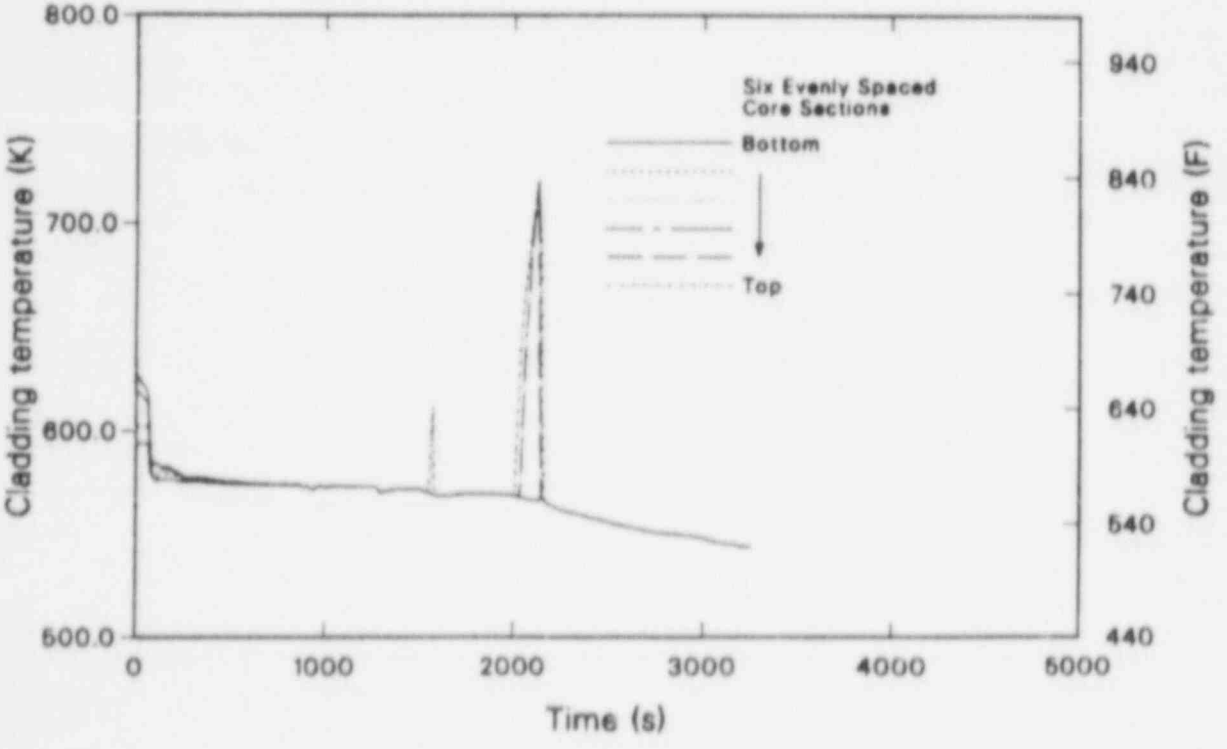

Figure 28. Hot pin cladding temperatures with coarse nodalization.

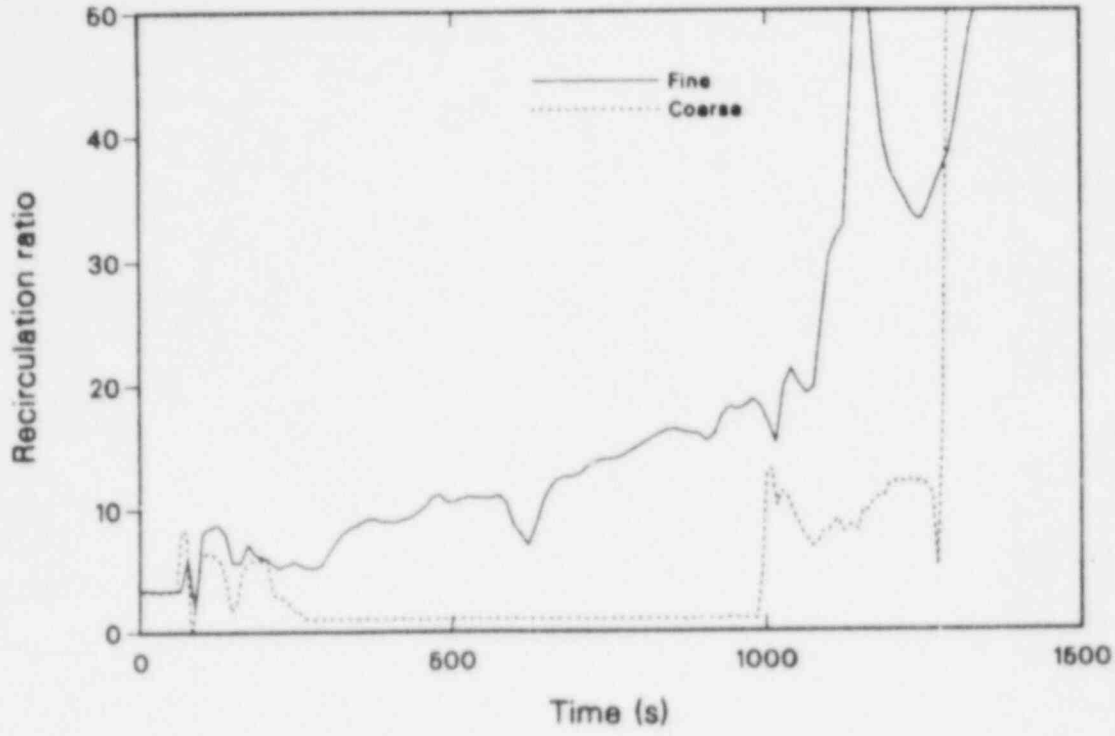

Figure 29. Effect of steam generator nodalization on recirculation ratio.

nodalization, the steam generators tended to recirculate continuously and in a somewhat regularly increasing manner. With coarse nodalization, however, no recirculation occurred from about 250 to 1000 s. Then, moderate recirculation is observed from about 1000 s until a step jump in recirculation occurs at about 1250 s. This irregular behavior with coarse nodalization resulted in small steam generator heat removal rates during periods of no recirculation and large removal rates during periods of high recirculation. This effect is shown in Figure 30 for the intact loop steam generator.

The sudden dramatic increases in steam generator heat removal rate with the coarse nodalization caused significant condensation to occur, and as a result, U-tube collapsed levels (upside and downside) increased suddenly. As shown in Figures 31 and 32, these effects caused significantly different U-tube collapsed level behavior with coarse and fine steam generator nodalization. The divergence in the U-tube level behaviors shown in Figures 31 and 32 corresponds to the core level divergences shown in Figure 26 from about 800 to 1500 s.

The perturbations in primary system liquid distribution in the coarse nodalization calculation affected the break mass flow rates as indicated by comparing Figures 33 and 34. With fine nodalization, break mass flow decreased uniformly from 1000 to 1979 s when the broken-loop seal cleared. With coarse nodalization, the break flow was affected significantly as the primary liquid shifted with changing steam generator behavior. The associated differences in break energy removal rate caused a shift in the timing of the remaining sequence events. As a result, the broken-loop seal was cleared 131 s later in the coarse nodalization calculation than in the fine.

To determine the cause of the different steam generator secondary hydraulic behavior in the coarse and fine nodalization models, the major edits at 500 s were examined. This is in the time period when the coarse nodalization steam generator was not recirculating but the fine nodalization steam generator was (see Figure 29). The edits exhibit similar steam generator void distributions in the two calculations. However, about 8000 lbm more liquid and about 3 ft higher steam generator downcomer level were present within the fine nodalization steam generator than within the coarse. As shown in Table 1, 8000 lbm is the approximate difference between the initial coarse and fine nodalization steam generator masses. Thus, the different behavior observed between the coarse and fine nodalization calculations is primarily due, not to a sensitivity of nodalization, but rather, to a

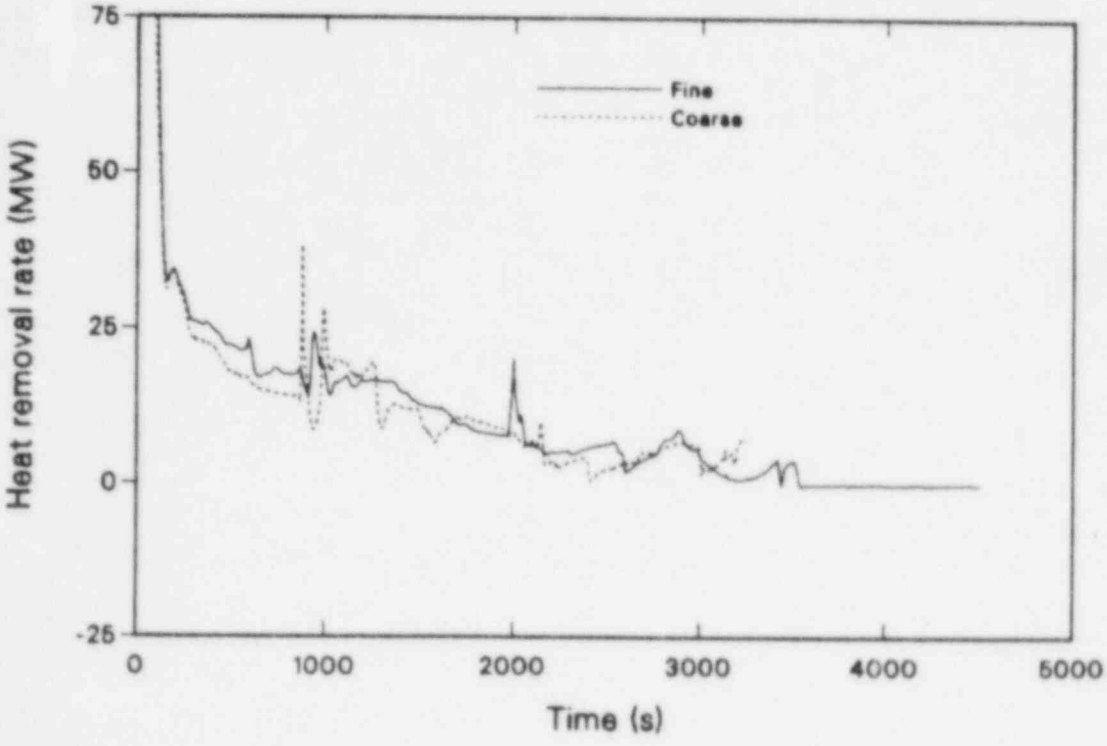

Figure 30. Effect of steam generator nodalization on steam generator heat removal rate.

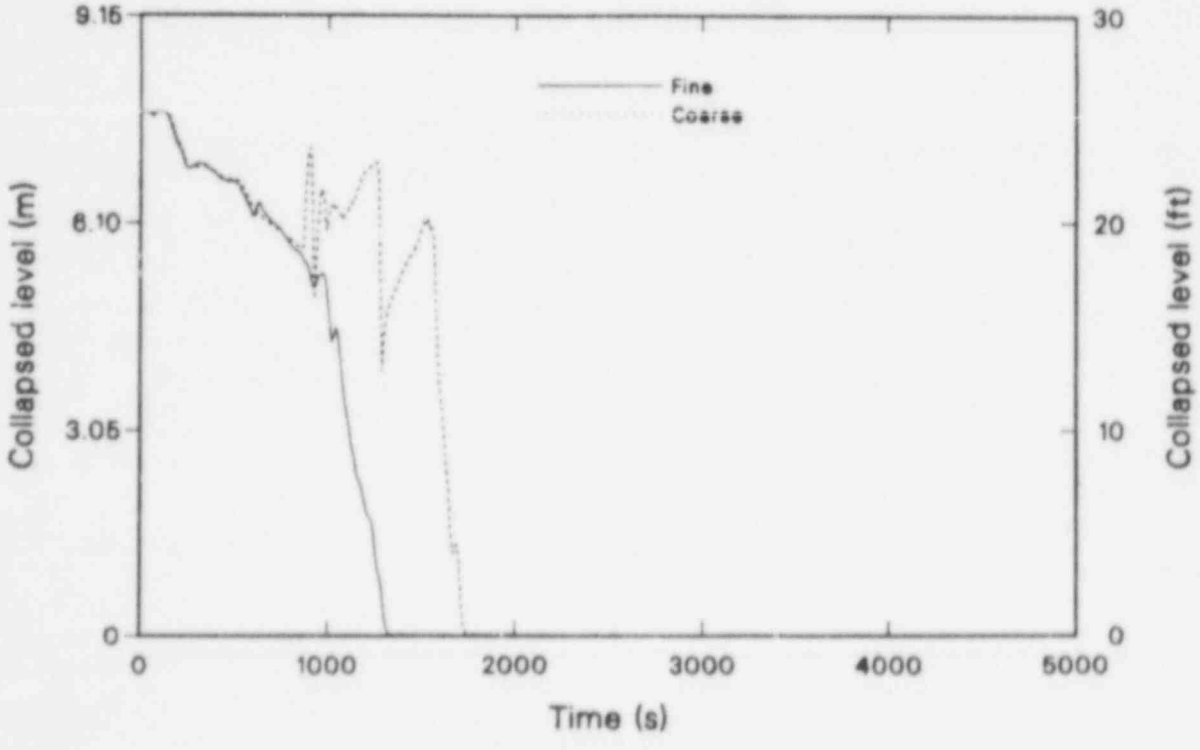

Figure 31. Effect of steam generator nodalization on U-tube upside level.

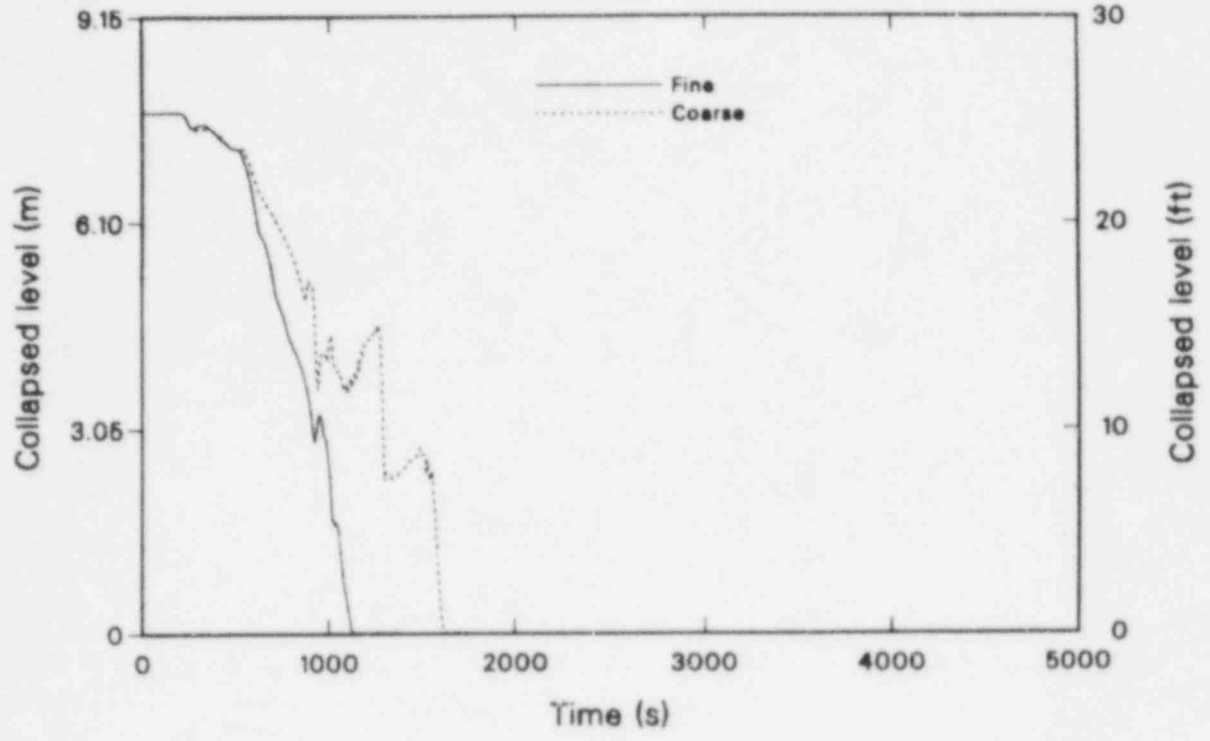

Figure 32. Effect of steam generator nodalization on U-tube downside level.

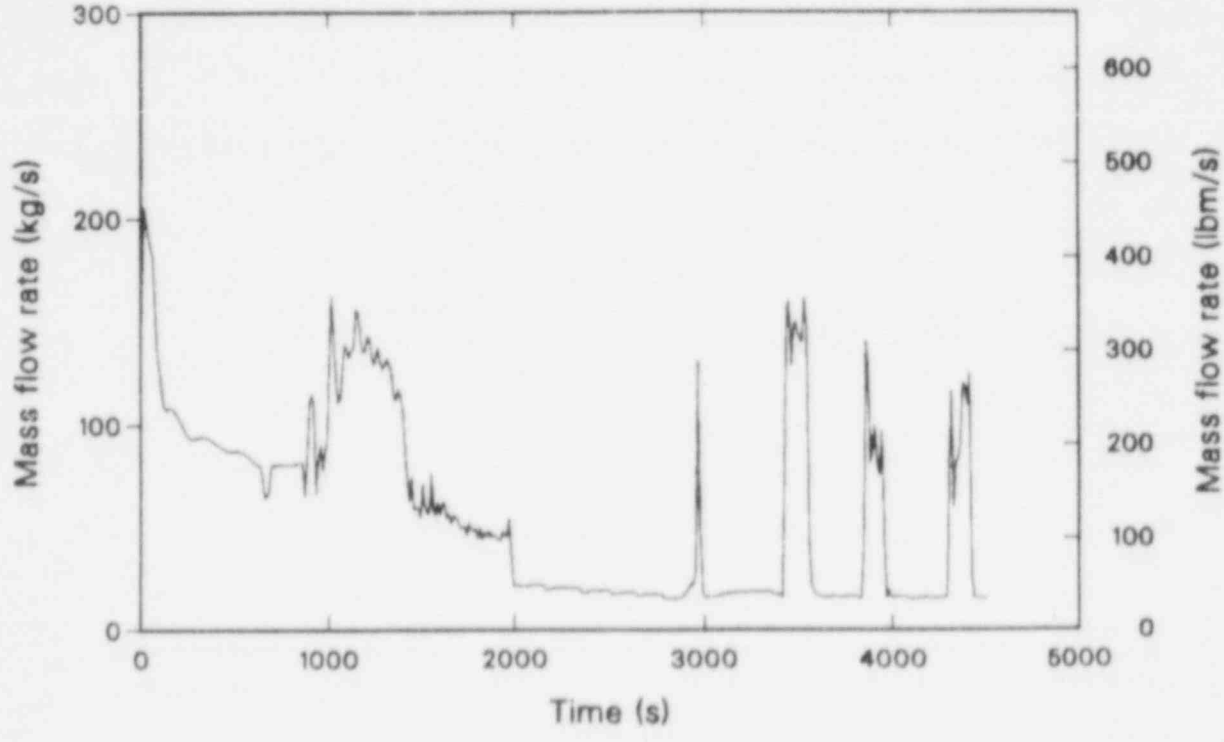

Figure 33. Break mass flow rate with fine nodalization.

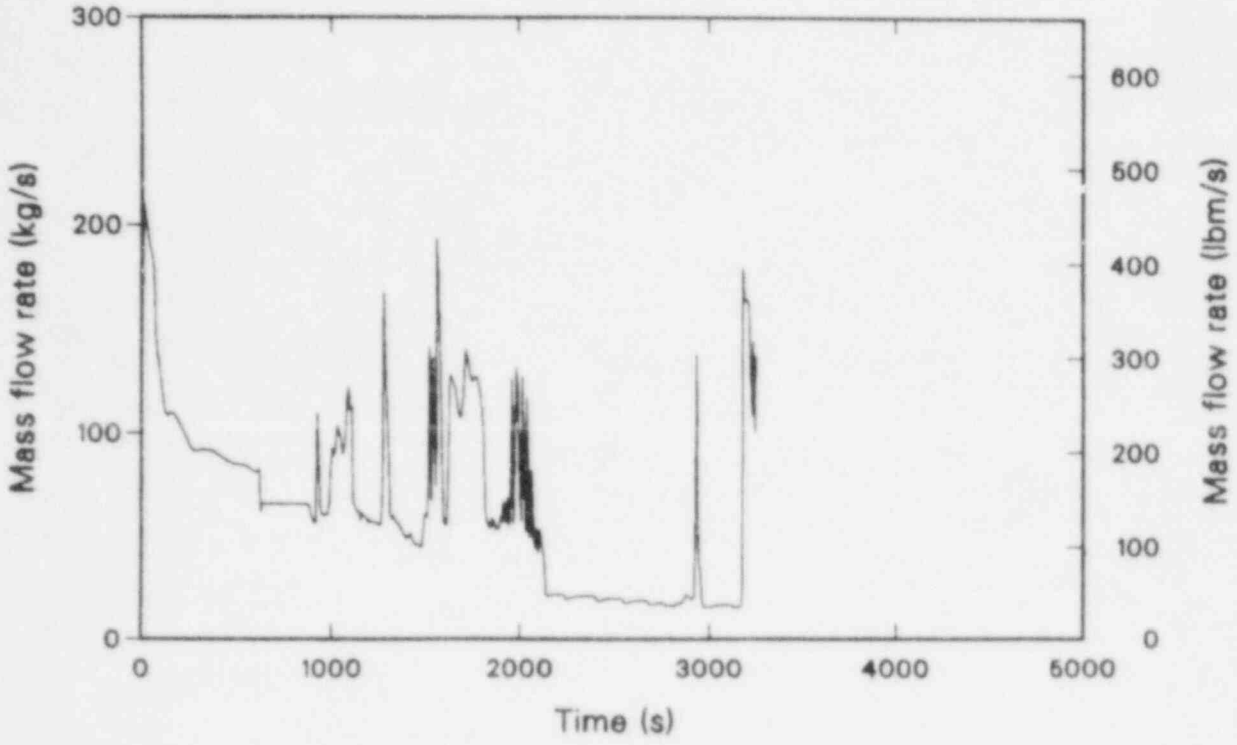

Figure 34. Break mass flow rate with course nodalization.

sensitivity of initial secondary inventory. The fine nodalization steam generator secondary contained sufficient initial inventory to permit continuous recirculation. The coarse nodalization model, however, did not have sufficient inventory until about 1000 s when auxiliary feedwater addition had allowed liquid to enter the separator, restarting recirculation.

Results of the calculations shown here indicate lower peak cladding temperatures are associated more with the coarse steam generator nodalization than with the fine nodalization. These findings are consistent with those of Argonne.[2] These calculations also indicate a potentially significant, and previously unobserved, sensitivity of core level and peak cladding temperature results to initial steam generator secondary mass.

With a low initial mass, a period with no recirculation existed followed by a recurrence of recirculation after sufficient secondary mass addition. With a higher initial mass, recirculation was not lost. The difference in recirculation response caused a corresponding difference in U-tube and core-collapsed-level responses. The behavior observed with the higher initial secondary mass is typical of that observed in previous calculations of this type. This does not mean, however, that the behavior observed with the lower initial secondary mass is not reasonable as well. The 8000 lbm difference in initial secondary mass is well within the uncertainty in that plant parameter. A threshold secondary mass could reasonably exist below which recirculation is lost. With no recirculation, the steam generator downcomer fluid temperatures can be expected to plunge which, upon restart of recirculation, will cause the outside of the tubes to be swept with cold water. The resulting increased condensation rate inside the U-tubes has the potential to delay or reverse the decline in tube levels as observed in Figures 31 and 32. Some Semiscale experimental data[10] indicate a condensation-induced level increase of this type. Further investigation of the sensitivity to initial steam generator inventory appears warranted.

The observed sensitivity to initial steam generator secondary inventory implies a sensitivity likely also exists to steam generator separator modeling. In RELAP5 model development, the separator region is constructed typically to span the elevations of the separators and steam dryers. The intent of this modeling criteria is to place the center of the modeled separator cell near the center of the combined regions where separation actually occurs. This results in a RELAP5 separator model that resides higher than the separators and lower than the dryers in the prototype steam generator. For example, in the RESAR Model D

Table 9. RELAP5 run time statistics

Break Diameter (in.)	SG Model	Transient Time (s)	CPU Time Required (s)	CPU Time/ Transient Time
1.5	F	6157	18902	3.67
2	D(Fine)	4512	13855	3.07
2	D(Coarse)	3254	7658	2.35
2	F	4518	14951	3.31
3	D	2529	7942	3.14
3	F	2928	9951	3.40
4	D	1144	3740	3.27
4	F	1152	3695	3.21
5	D	789	5011	6.35
5	F	824	5192	6.30
6	D	548	3481	6.35
6	F	554	3474	6.27
7	D	398	2533	6.36
7	F	396	2512	6.34

steam generator RELAP5 model, the separator extends from 38.4 to 45.1 ft above the top of the tubesheet. In the prototype, the separator inlet is at 35.8 ft and the swirl vane centerline is at 43.2 ft. In the RELAP5 model, separation, and therefore recirculation, recurs when significant liquid fractions appear at the 38.4 ft elevation. The corresponding elevation for beginning of separation in the prototype is not known; however, it may be as high as 43.2 ft. Further investigation into determining the elevation required for separation in the prototype appears warranted. Once determined, this information could then be used to revise the RELAP5 separator modeling philosophy.

4.1.5 RELAP5 User Experiences. This section describes the user experiences from performing the RELAP5 calculations presented in this report.

4.1.5.1 Rate of Computer Time Usage. In general, the RELAP5/MOD2 computer code performed conveniently and economically. Computer run time statistics for the 14 calculations are shown in Table 9. The models with fine steam generator nodalization contained 188 volumes, 192 junctions, and 225 heat structures. The model with coarse steam generator nodalization contained 146 volumes, 150 junctions, and 175 heat structures. As shown, the ratio of central processing unit (CPU) to transient time ranged from 3.07 to 6.36 with the fine nodalization model. Calculations for break diameters smaller than 5 in. were performed specifying a 0.1 s maximum time step size, while for the calculations with larger break diameters 0.05 s maximums were specified. This was done as an expediency to avoid possible code running problems when using a larger time step for transients with accelerated sequence timing. Had budget, rather than schedule considerations been paramount, all RELAP5 calculations could have been performed at CPU-to-real time ratios from 2 to 3.

4.1.5.2 Code Failures Due to Moderator Heating Modeling. The RELAP5 RESAR model simulated the direct moderator heating of fluid within the core through auxiliary heat structures (other than those representing the core rods) connected to the core hydraulic cells. These heat structures simulated moderator heating by delivering the appropriate power fraction to the liquid phase within each core cell. Because some small break calculations performed involved total dryout (void fraction = 1.0) of regions of the core, this scheme for moderator heating resulted in a code failure when all liquid in any core cell vanished. This failure was encountered in only two calculations. When this failure occurred, it was circumvented by removing the moderator heat source momentarily, then restoring it, after a liquid inventory had returned in all core cells. While this was a practical solution for the calculations performed here, it was inconvenient. Moderator heating simulation is recommended, using the option for it on the source data cards for the core rod heat structures rather than

through separate heat structures as was done here. Using this option, moderator heating is properly simulated, and the inconvenience of circumventing code failures is eliminated.

4.1.5.3 Separator Modeling Philosophy. As discussed in Section 4.1.4, a new sensitivity to initial steam generator secondary mass and philosophy of steam separator modeling has been identified. Steam separators have been modeled with a single cell simulating both the separators and dryers. This cell typically has been centered at the midpoint of the separators and dryers. The effects discussed in Section 4.1.4 suggest, however, separators may be modeled more appropriately with the bottom of the cell at an elevation coinciding with the prototype minimum steam generator boiler level required for recirculation. While this minimum required level is not known with certainty, it is likely near the swirl-vane elevation. Using current practice, the bottom of the separator cell is typically modeled below the swirl-vane elevation. More investigation of this modeling effect appears to be warranted.

4.1.5.4 Upper Plenum to Hot Leg Connection. A RELAP5 code user decision is required for modeling the connections between the reactor vessel upper plenum and the hot legs. Two options are available for these junctions in RELAP5/MOD2, Cycle 21, the code used in these analyses. The junctions may be connected either from the upper or lower reactor vessel cells adjacent to the hot leg centerline. Referring to Figure 1, the hot legs may be attached either to the bottom of cell 122, or the top of cell 120. Preliminary calculations were performed using each option. Nonphysical draining behavior of the RESAR hot legs was observed using the connection to the upper cell. Specifically, using this option, no liquid drainback from the hot legs to the reactor vessel was observed following termination of loop natural circulation flow; the hot legs remained liquid filled. Using connections to the lower cell, however, resulted in reasonable countercurrent flow behavior in the horizontal sections of the hot legs, with increasing void fractions typified in Figure 9. As a result of these findings, all calculations presented in this report were performed using connections from the lower reactor vessel cell to the hot legs.

4.2 TRAC Results

Results of the TRAC analysis are presented in this section. Section 4.2.1 presents a discussion of the results of a representative calculation. Section 4.2.2 discusses the effects of break size, and Section 4.2.3 presents user experiences using the TRAC code for this application.

4.2.1 Representative Results. TRAC calculations were performed for 2-, 3-, and 4-in.-diameter cold leg breaks in a RESAR plant with Model F steam generator. This section describes the simulation of the 3-in.-diameter cold-leg break beginning from full power conditions. Although event times differ, the 2- and 4-in. breaks produce similar phenomena.

The calculated sequence of events for this scenario is presented in Table 10. The transient was initiated at zero seconds (0.0 s) by opening a 3-in.-diameter break in the cold leg. Initially the primary system pressure fell rapidly as shown in Figure 35. Within 16 s, the reactor tripped on a low pressurizer pressure signal at 1860 psia. This resulted in turbine and reactor coolant pump trips. A safety injection signal was generated at 27.5 s on a low pressurizer pressure signal at 1760 psia, and HPI was initiated at 52.5 s. At 77 s, the auxiliary feedwater system was activated. This time corresponded to 61 s after the reactor trip.

During the initial 200 s of the transient, the primary system pressure was characterized by a continuous decrease due to decreasing core decay heat and shrinkage of the primary coolant mass. The shrinkage was caused by mass removal from the break and primary-to-secondary heat transfer. After approximately 200 s, the primary system pressure response leveled at approximately 1189 psia, slightly above the secondary system pressure. The lower secondary system pressure enabled the secondary side to function as a heat sink, permitting natural circulation to continue after reactor coolant pump coastdown. Figure 36 presents the total (4-loop) cold-leg and hot-leg mass flow rates.

The steam generator secondary pressures initially increased (Figure 35) as a consequence of feedwater and steam stop valve closure. Pressure relief in the secondary system was maintained by the steam generator safety relief valves. The safety relief valves maintained the secondary system pressures below the primary system pressure. The lower secondary system pressures maintained the steam generators as heat sinks until 900 s when the loop seals cleared.

After 200 s, upper head flashing slowed the decrease in the primary system pressure. The steam

Table 10. TRAC calculated sequence of events for 3-in. break, Model F steam generators

Event	Time (s)
Break initiated	0
Reactor trip, turbine trip, trip reactor coolant pumps	16
Initiate high pressure injection (HPI) and makeup flow to intact loop only	52
Initiate auxiliary feedwater (AFW)	77
Broken loop seal clears	900
Intact loop seal clears	950
Accumulator injection begins	2200
End of calculation	2457

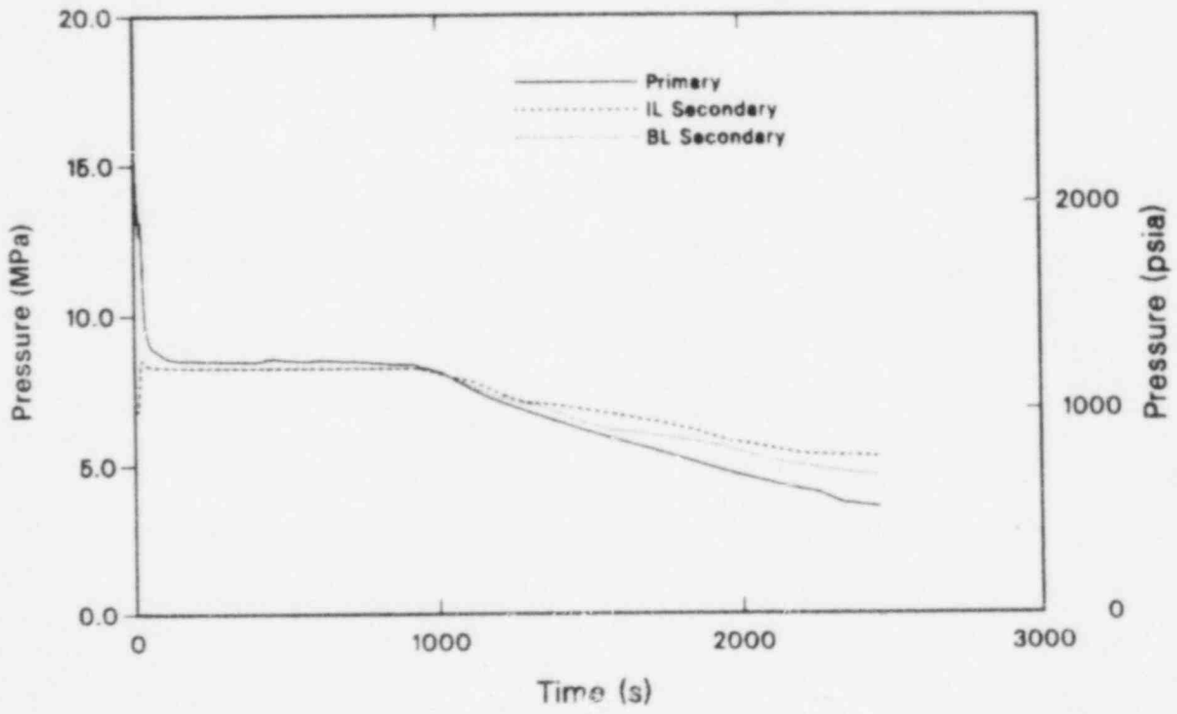

Figure 35. TRAC primary and secondary pressures, 3-in. break, Model F SG.

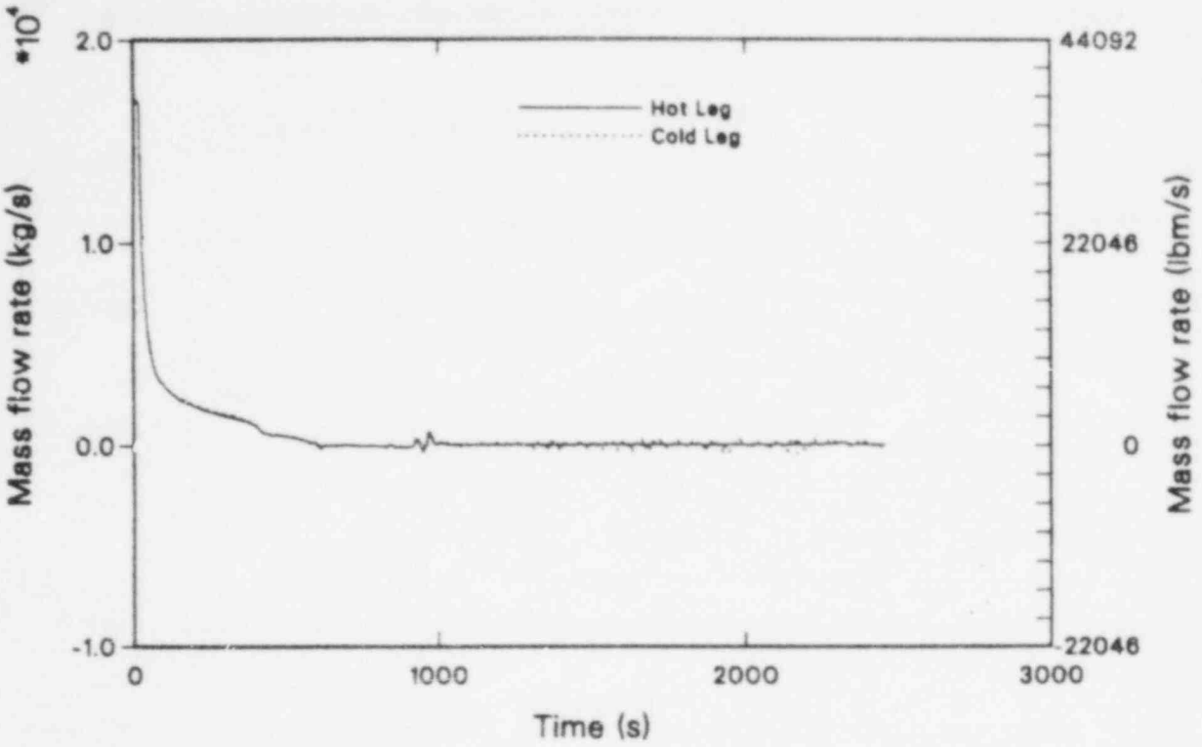

Figure 36. TRAC hot and cold leg mass flow rates, 3-in. break, Model F SG.

bubble formed in the upper region of the reactor vessel contained sufficient expansion energy to stabilize the primary system pressure. The transition from forced circulation to natural circulation loop flow significantly reduced primary-to-secondary heat transfer so the primary system cooldown was retarded also.

During the period of loop natural circulation flow, the primary system mass inventory was progressively reduced since the break flow exceeded the total ECCS injection flow (Figure 37). Loop stagnation occurred at approximately 900 s when voiding at the top of the steam generator U-tubes prevented liquid from flowing through the U-tubes in both the intact-loop and broken-loop steam generators.

Figures 38 and 39 present the collapsed liquid levels in the upside and downside of the U-tubes of the intact-loop and broken-loop steam generators. The upside and downside levels span the lengths from the tops of the SG U-tubes to the inlet and outlets of the U-tubes, respectively. The tube level responses in the intact loops and broken loops were virtually identical.

The asymmetric behavior between the U-tube upside and downside levels is the consequence of asymmetries in the flow regimes at the steam generator tube inlets and outlets. At the steam generator inlets, upward flow induces a countercurrent flow regime at the tube entrances which retards liquid drainage into the hot legs and inlet plenum due to steam originating in the core. At the tube outlets, the column of liquid is not supported by the upward thrust of steam exiting the core. As a consequence, the drainage rate in the steam generator downside regions exceeds the drainage rate in the upside tube regions.

Unlike the RELAP5 simulation presented in Section 4.1.1, the steam generator level asymmetries in the TRAC calculation did not induce a significant core level depression after the loss of natural circulation. A detailed explanation for this difference is discussed in Section 4.2.2. Figure 40 presents the collapsed liquid levels spanning the top of the reactor vessel upper plenum to the bottom of the lower plenum for the core and downcomer regions. After the loss of natural circulation, liquid remaining in the hot legs drained back into the top of the core, replacing the core inventory. As a consequence, sufficient core cooling occurred to prevent any rod temperature excursion. Figure 41 presents response of the cladding surface temperature at each

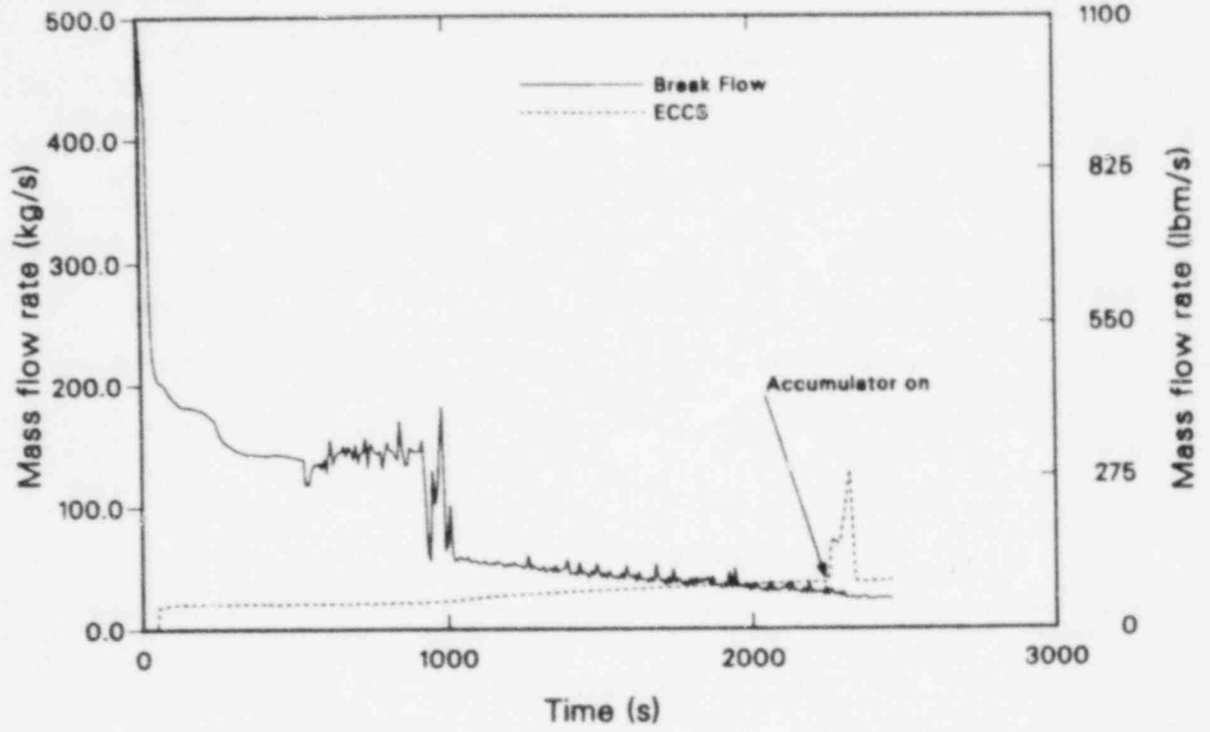

Figure 37. TRAC break mass flow rate and ECCS mass flow rate, 3-in. break, Model F SG.

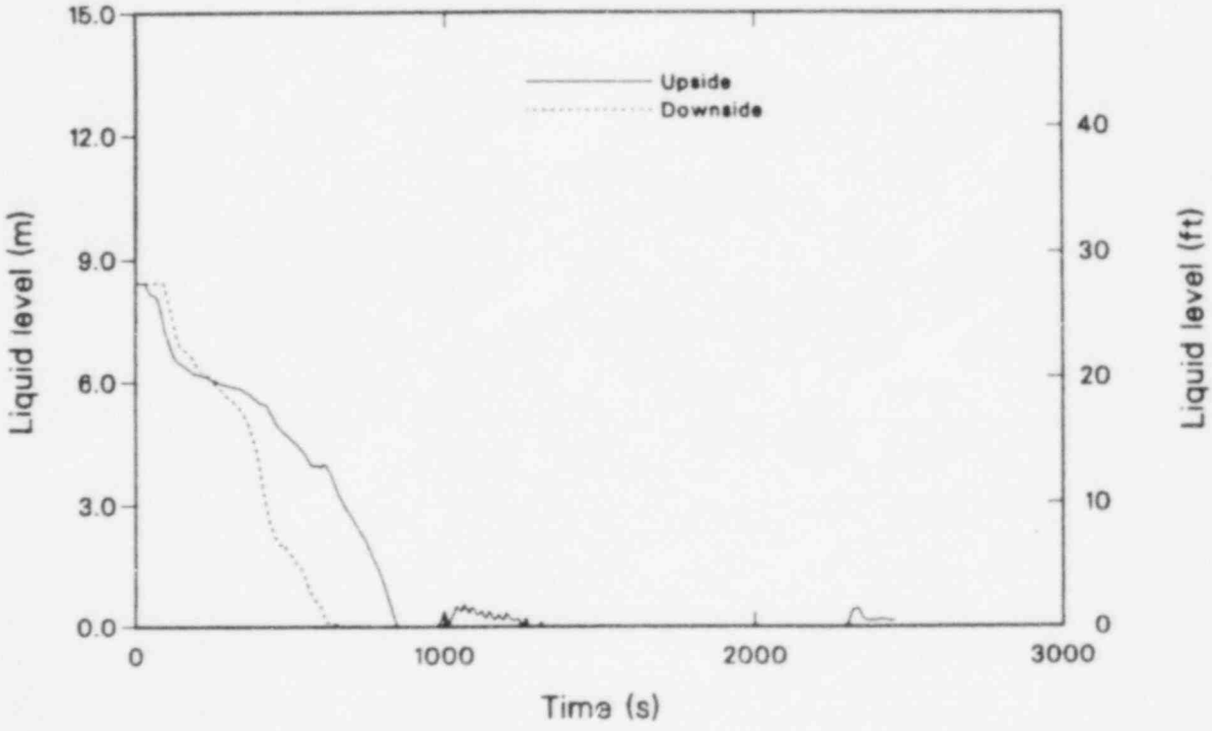

Figure 38. TRAC collapsed U-tube levels for intact loop steam generator, 3-in. break, Model F SG.

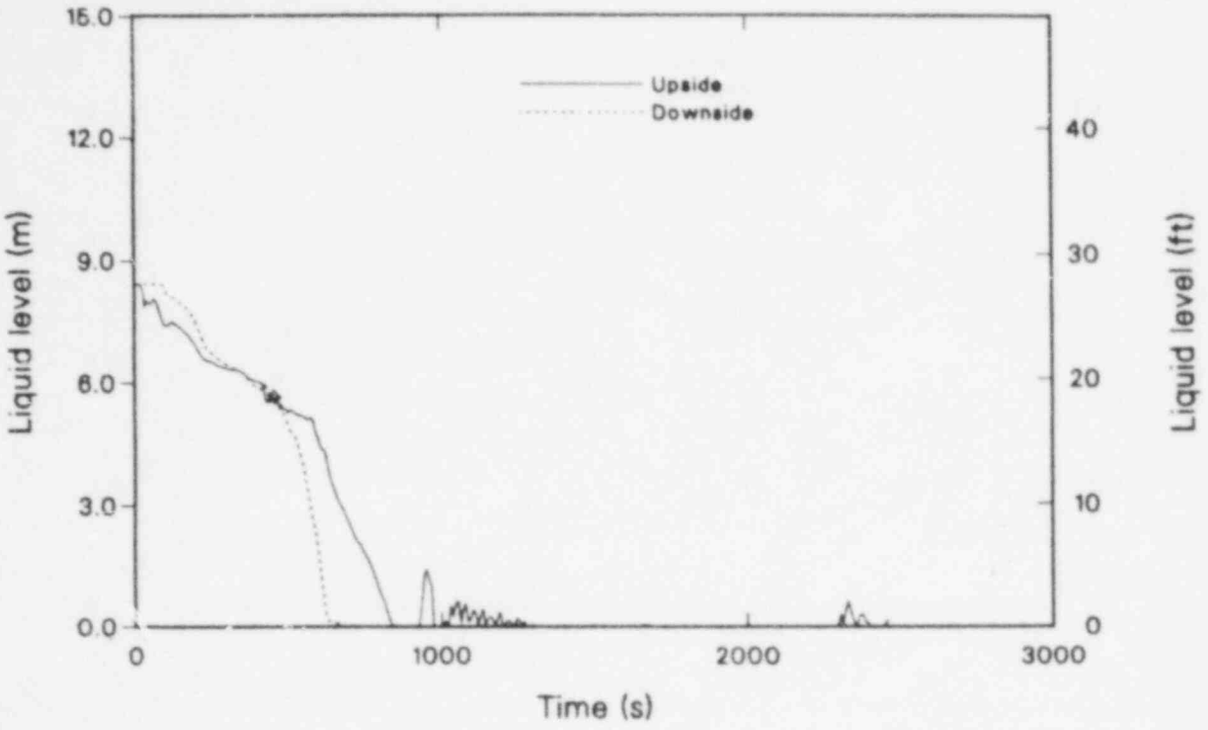

Figure 39. TRAC collapsed U-tube levels for broken loop steam generator, 3-in. break, Model F SG.

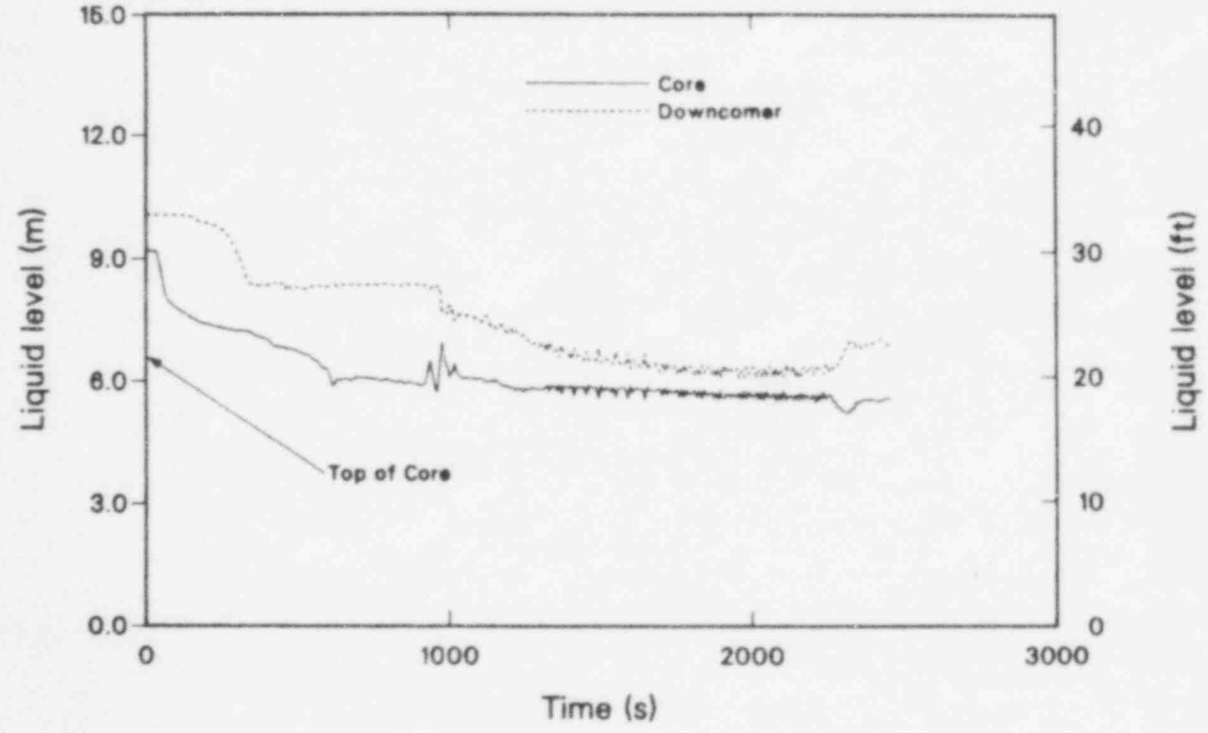

Figure 40. TRAC collapsed core and reactor vessel downcomer levels, 3-in. break, Model F SG.

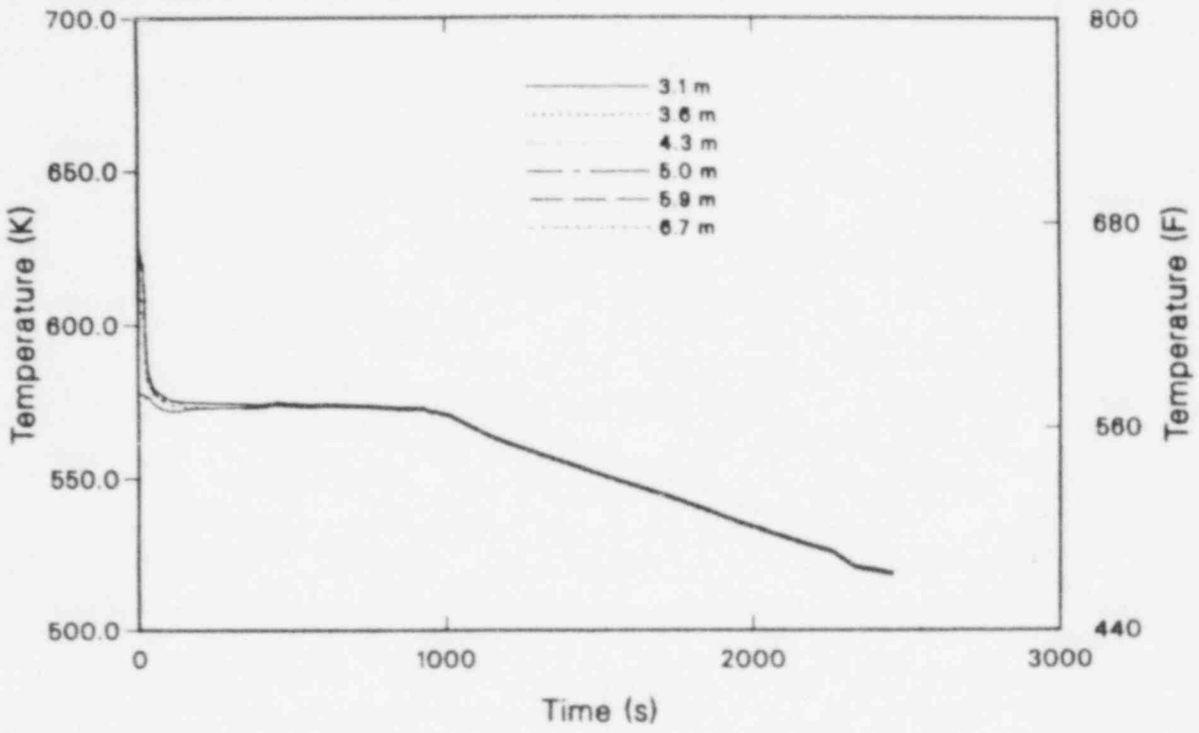

Figure 41. TRAC cladding temperatures, 3 in. break, Model F SG.

elevation. The core temperatures approximately follow the surrounding fluid saturation temperature.

At 970 and 1000 s, respectively, the broken-loop and intact-loop pump seals cleared. As a consequence, a direct steam path from the reactor vessel outlet to the break was established. As steam reached the break, the break flow transitioned to single-phase steam, producing a decrease in the mass flow rate and an increase in the volumetric flow rate. The increased break volumetric flow caused the primary system pressure to decrease (Figure 35).

As the pump loop seals were cleared, liquid from both the intact loop and broken loop was swept into the reactor vessel downcomer. The corresponding level increase can be seen in Figure 40. However, after 930 s, the liquid forced into the vessel was convected out of the vessel back into the hot legs. Most of this liquid was convected into the inlet plenums of the steam generators. During the loop seal clearing process, the interfacial drag in the reactor vessel region was probably overcalculated by TRAC. The continued suspension of liquid in the steam generator inlet plenum is the principal cause of the downcomer level exceeding the core level. A further discussion of this problem will be presented in Section 4.2.3.

Continued primary system depressurization caused initiation of the accumulator flow at 2300 s when the pressure reached 600 psia. The initial accumulator injection caused cold leg steam condensation. This condensation induced a temporary manometer oscillation between the core and downcomer regions, followed by increased levels in both regions (Figure 40). Prior to accumulator injection, the ECC flow had begun to exceed the break flow. The calculation was terminated at 2400 s with the primary system pressure decreasing and with the net reactor vessel liquid inventory increasing.

As was done in Section 4.1.1, a comparison of the TRAC results with empirical countercurrent flow limiting (CCFL) correlations was made. At the junction between the steam generator tube sheets and inlet plenums, the Wallis correlation was employed. Figure 42 shows a comparison of the TRAC-calculated liquid velocities and the Wallis-correlation liquid velocities at this junction. The period of interest is from 600 to 900 s when the loop flows stagnated, causing the flows in the steam generator inlet plenum to transition to CCFL conditions. The comparison indicates the upside

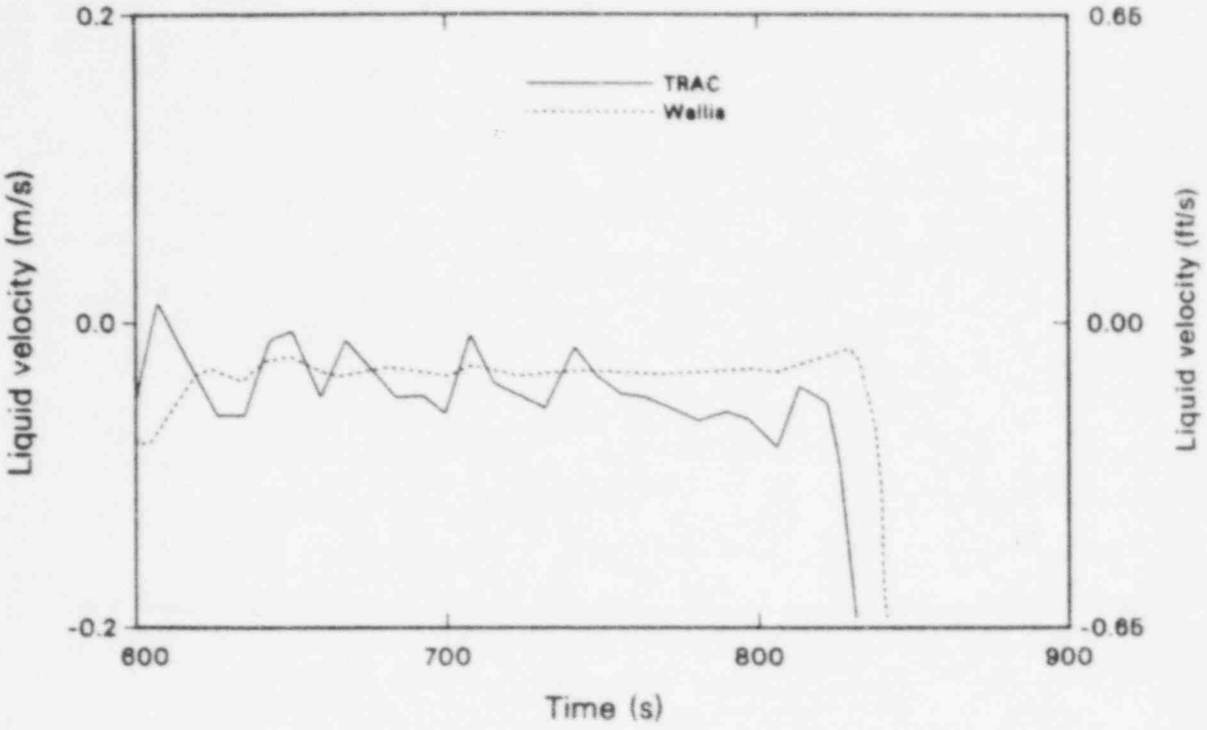

Figure 42. Comparison between TRAC simulated and Wallis correlated liquid velocities.

level draining process occurred, on the average, slightly faster than predicted by the Wallis correlation in the time interval from 600 to 850 s. By 850 s, the tubes had emptied. Thus, the TRAC calculation is slightly nonconservative because the U-tube upsides drain faster than expected using the Wallis correlation. This, in turn, produces a lower gravity head relative to core-level-depression dynamics, which lessens the chance of a core rod heatup developing.

Liquid cascaded from the steam generator tubes into the steam generator inlet plenum which, in turn, cascaded into the hot legs. An investigation of the drainage dynamics at the steam generator inlet plenum/hot leg interface was made using the Kutateladze correlation previously employed in Section 4.1.1. Figure 43 presents the calculated and empirical liquid velocities at this interface. Initial agreement was obtained between the calculated and empirical liquid junction velocities. The overall results between 600 and 1000 s show significantly more liquid drained back in the calculation compared to the correlated rate. As stated in Section 4.1.1, a significant number of uncertainties exist relative to using experimental correlations at junctions with complex geometries. The concern is regarding the correlation constants to be employed. Thus, the results shown in Figure 43 should be considered only as a possible indication that the TRAC results may be overcalculating the drainage rate out of the steam generator plenum prior to loop-seal clearing.

After loop seal clearing, the flow regime at the steam generator plenum/hot leg interfaces oscillated between concurrent upflow and countercurrent flow conditions (Figure 44). This oscillatory behavior tended to maintain significant amounts of liquid in the steam generator plenums after loop-seal clearing. The periodic flow regime transitioning prevented a continuous draining of the steam generator plenums. Some of this oscillatory behavior may be model-dependent and not physical. An additional discussion of the TRAC calculated behavior is covered in Section 4.2.3. Continued suspension of liquid in the steam generator inlet plenums was concluded to have made the TRAC simulation more conservative due to manometric considerations.

The principal conclusion drawn from analysis of the 3-in.-diameter-break TRAC simulation was that adequate core cooling was maintained during both the pre- and post-loop-seal-clearing phases of the transient. The principal concern was the

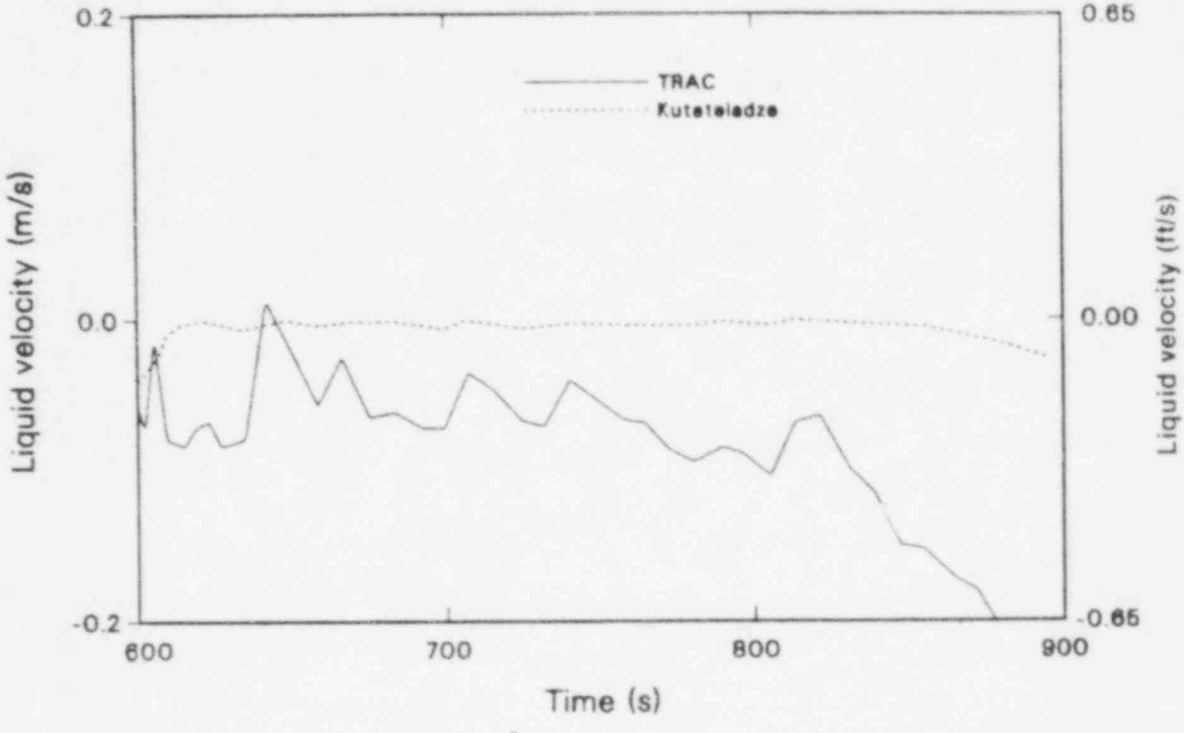

Figure 43. Comparison between TRAC simulated and Kutateladze liquid velocities.

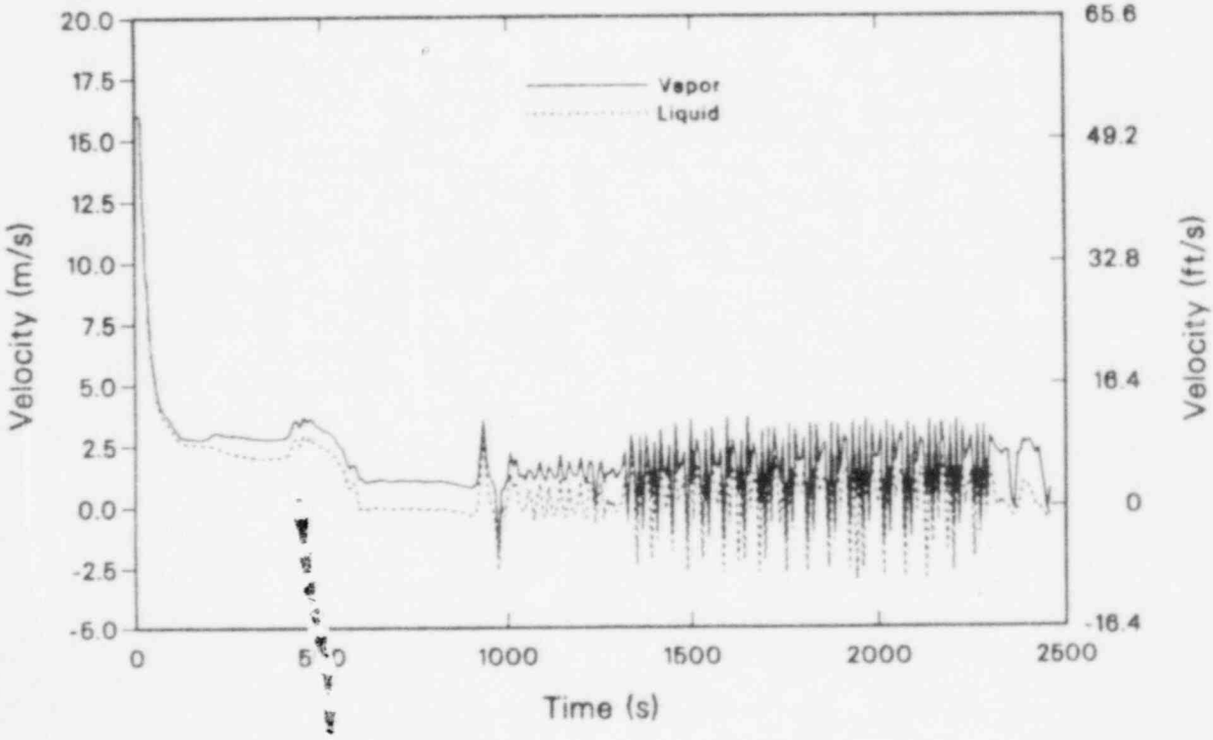

Figure 44. TRAC liquid and vapor velocities at broken loop hot leg/SG inlet plenum interface, 3-in. break, Model F SG.

Table 11. Event times for 2-, 3-, and 4-In.-diameter break TRAC calculations

Event	Time (s) 2-Inch	3-Inch	4-Inch
Break initiated	0.0	0.0	0.0
Reactor trip, reactor coolant pump (RCP) trips, shut turbine stops, main feedwater (MFW) stops	36	16	8
Initiate high pressure injection (HPI) and makeup flow	68	52	41
Initiate auxiliary feedwater (AFW)	97	77	69
Broken loop seal clears	2500	900	480
Intact loop seal clears	—	950	520
Accumulator injection begins	—	2200	1200
End of calculation	2826	2457	1300

anomalous convection of liquid from the core region to the steam generator inlet plenums after loop-seal clearing. This behavior tended to make the simulation conservative based on core-level-depression response. But, this overcalculated convection behavior should be resolved to ensure that future TRAC simulations represent best estimate plant behavior. Rod heatup was not encountered in this calculation because the drain rate from the U-tubes and steam generator inlet plenum was larger than predicted by flooding correlations.

4.2.2 Break Size Effect. This section deals with the parametric differences observed between the 2-, 3-, and 4-in.-break simulations. The trends for all three transients were very similar. Table 11 presents a summary of key events for each transient. The principal effect of varying break size in the TRAC simulations was to affect timing changes in key events. Break size reduction delayed such key events as time to loop stagnation, and loop seal clearing. Each simulation exhibited the same qualitative trends relative to system depressurization, break flow response, and level trends in key regions such as the reactor vessel, steam generators, and pump suctions. None of the three TRAC simulations exhibited core level depression sufficient to induce cladding temperature excursions. Specific reasons why the TRAC simulations did not produce temperature excursions, and the RELAP5 calculations did, are detailed in Section 4.3.2.

Figure 45 presents comparisons of the primary system pressure responses for the three break sizes. Each calculation had a period of rapid depressurization followed by a relatively long period of stable pressure response. As break conditions transitioned from single-phase liquid to predominately single-phase vapor conditions, the calculated depressurization rates increased. The final increase in the calculated depressurization rates were coincident with loop seal clearing. The mechanisms applicable during the period of primary system pressure stabilization were discussed in Section 4.2.1.

Figure 46 presents a comparison of the vessel collapsed liquid levels spanning the top of the reactor vessel upper plenum to the bottom of the lower plenum. Each calculation was characterized by an initial drop in level during the periods of pump coastdown, and natural circulation loop flow conditions were reached when the collapsed levels stabilized. The stabilization was the consequence of sufficient liquid drainback from the hot legs to maintain the levels. In each simulation, liquid drainage from the hot legs was sufficient to replace liquid which was flowing out the reactor vessel downcomer.

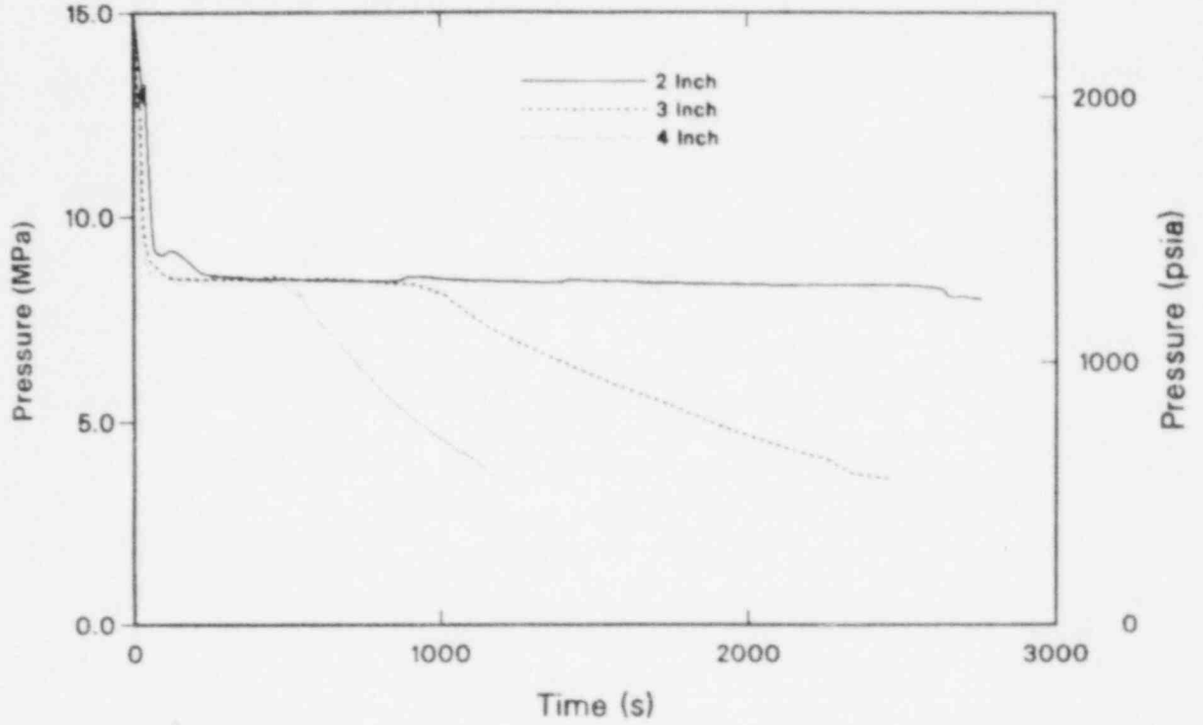

Figure 45. TRAC primary system pressure responses for 2-, 3-, and 4-in.-diameter breaks.

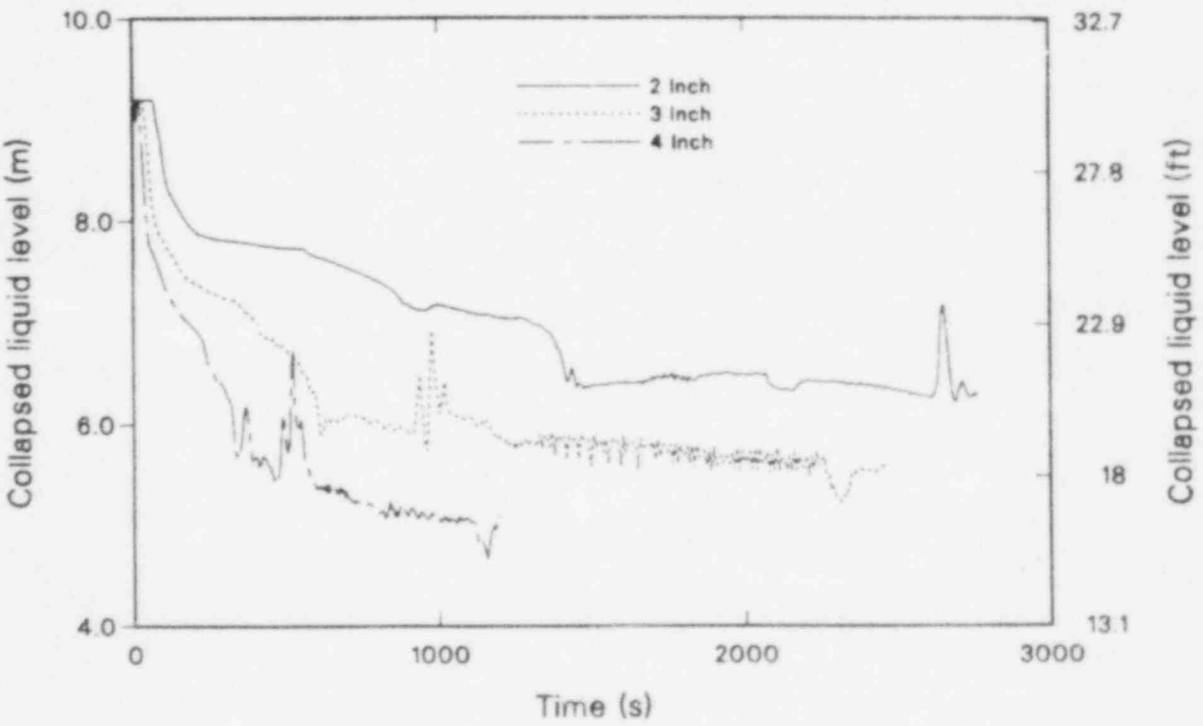

Figure 46. TRAC reactor vessel level responses for 2-, 3-, and 4 in.-diameter breaks.

Table 12. TRAC run time statistics

Break Diameter (in.)	SG Model	Transient Time (s)	CPU Time Required (s)	CPU Time/ Transient Time
2	F	2727	58394	21.4
3	F	2457	26994	10.98
4	F	1200	13764	11.47

After the upflow sides of the loop seals cleared (2-in. break simulation was stopped after intact-loop-seal clearing), each calculated collapsed vessel level was characterized by a temporary level increase followed by a decrease back to approximately the level present before loop-seal clearing. The return to pre-loop seal conditions was caused by liquid convected out of the reactor vessel back into the steam generator inlet plenums and hot legs. This convective phenomenon may not be physical since the rate of convection greatly exceeds any core decay heat boiloff rates. This convection is suspected to be related to the manner in which the TRAC code calculates interfacial friction.

The 3- and 4-in.-diameter break simulations indicated that after loop-seal clearing sufficient ECC liquid replacement would be available to maintain core cooling. The 2-in.-diameter break simulation was not continued to the time where the calculated ECC mass flow rate exceeded the break mass flow rate. However, by extrapolating the results from the 3- and 4-in.-break scenarios, the rate of core boiloff was concluded to be insufficient to significantly deplete the core liquid inventory by the time ECC would exceed the break flow rate. Therefore, post-loop-seal-clearing core temperature excursions would not occur.

4.2.3 TRAC User Experiences. This section details user experience relative to using the TRAC-PF1 (Version 12) code in performing the 2-, 3-, and 4-in.-diameter break calculations. Recommendations will be made for improving code run times, improving code accuracy, and enhancing user modeling capabilities.

Table 12 summarizes the run time statistics for the 2-, 3-, and 4-in.-diameter LOCA calculations. One conclusion was that code run time statistics could be improved by addressing the following questions:

1. What methods can be employed to simplify the model to reduce computer run times without significantly reducing code accuracy?

2. What additional coding modifications can be made to further improve code run times?

One recommendation is that further work be done to determine what is the minimum noding requirements for accurately simulating small-break transients. Clearly, this investigation requires additional code benchmarking with experimental data. Also, preliminary indications from the TRAC RESAR simulations show detailed simulation of three dimensional reactor vessel flow dynamics are not necessarily applicable to the question of how the core liquid level is depressed during a small-break loss-of-coolant accident (SBLOCA). Again, additional experimental and theoretical work should be done to investigate when reactor vessel multi-dimensional flow dynamics are important. Using simplified reactor vessel models will significantly reduce computational run-time requirements because of significant reductions in storage requirements.

Run-time efficiency was also limited by calculated thermal-hydraulic conditions. In particular, the average size of the computational time step was limited by nonequilibrium thermal-hydraulic conditions in the intact-loop cold-leg region, where subcooled ECCS was injected, and the tops of the steam generator downcomers where subcooled auxiliary feedwater was injected. Typically, computational time-step problems would result in a code abort rather than any obvious computational distortions. After a code abort, the simulation can be restarted by reducing the size of the maximum time step. However, the attendant cost of reducing the

time step below a threshold of 0.001 s tended to make the simulation extremely expensive.

Due to the intrinsic structure of the TRAC code, some reduction in computational time-step size as well as additional computational iterations will occur in order to simulate nonequilibrium conditions. However one conclusion was that a further investigation must be made to mitigate the effects of nonequilibrium conditions on run times.

As previously noted in Sections 4.2.1 and 4.2.2, an unusual degree of oscillatory behavior occurred at the hot leg-steam generator interfaces after the pump suctions were cleared of liquid. A preliminary investigation indicates this calculated result may be a function of nodalization in the plenum regions. The hot leg was modeled as horizontal volume connected to the vertically-oriented steam generator inlet plenum. The sudden change in cell orientation (horizontal to vertical) may cause computational discontinuities in the momentum solution scheme sufficient to induce flow oscillations which may not be physical. One possible solution to the above difficulties is a finer cell-to-cell nodalization scheme in this region with small changes in cell angular orientation.

All TRAC simulations were characterized by rapid liquid convection from the core region to the steam generator inlet plenums after the pump seals were cleared. The most likely cause was concluded to be over calculation of interfacial shear in the TRAC simulation. One recommendation is that sensitivity studies with code updates and modeling changes be performed to confirm this suspicion or identify some other cause for the large convection rates.

In the course of performing the steady-state initialization, the potential was discovered for calculating unrealistically large pressure drops across either a PLENUM or TEE component if the fluid velocities are large and if there are internal sign changes in the velocity fields. As an example, liquid entering the secondary cell of a TEE component, internally splits and mixes with liquid flowing out both ends of the primary side. This problem did not manifest itself in the transient simulations because of relatively low velocities. However, these problems were observed during the steady-state initialization calculation and were mitigated by increasing the flow areas at the junctions with large velocities. These modifications did not significantly affect the final steady-state results.

Relative to improving code user convenience, one recommendation is that future TRAC-PF1 versions have the capability to model stored energy in PLENUM components. An additional suggestion is that the capability to connect multiple one-dimensional components to the same VESSEL cell also be added to the code.

4.3 Comparison of RELAP5 and TRAC Results

In Sections 4.3.1 and 4.3.2, comparisons will be made between the 2-, 3-, and 4-in.-diameter-break simulations performed with TRAC and RELAP5. Section 4.3.1 will detail differences between the 3-in.-diameter-break calculations using TRAC and RELAP5 simulations. Section 4.3.2 presents additional details of how varying break size affects relative differences in the TRAC and RELAP5 simulations.

4.3.1 Representative Comparison. This section details comparisons between the TRAC and RELAP5 3-in.-diameter-break simulations. Both simulations showed a number of similar responses. In particular, the calculated primary system pressures, break flows, and event timings were generally in good agreement. The principal difference between the TRAC and RELAP5 simulations was the absence of a core level depression in the TRAC calculation that was sufficient to induce fuel cladding temperature excursions.

Figure 47 presents a comparison of the calculated pressure responses. Both simulations show the following similar trends during the three key phases of the transient:

1. Break initiation to loss of natural circulation.
2. Loss of natural circulation to loop seal clearing.
3. Loop seal clearing to time at which ECC injection exceeded the break mass flow rate.

Explanations for the controlling phenomena leading to the above-mentioned phases have been previously detailed in Sections 4.1.2 and 4.2.2, respectively. During period 1, the TRAC

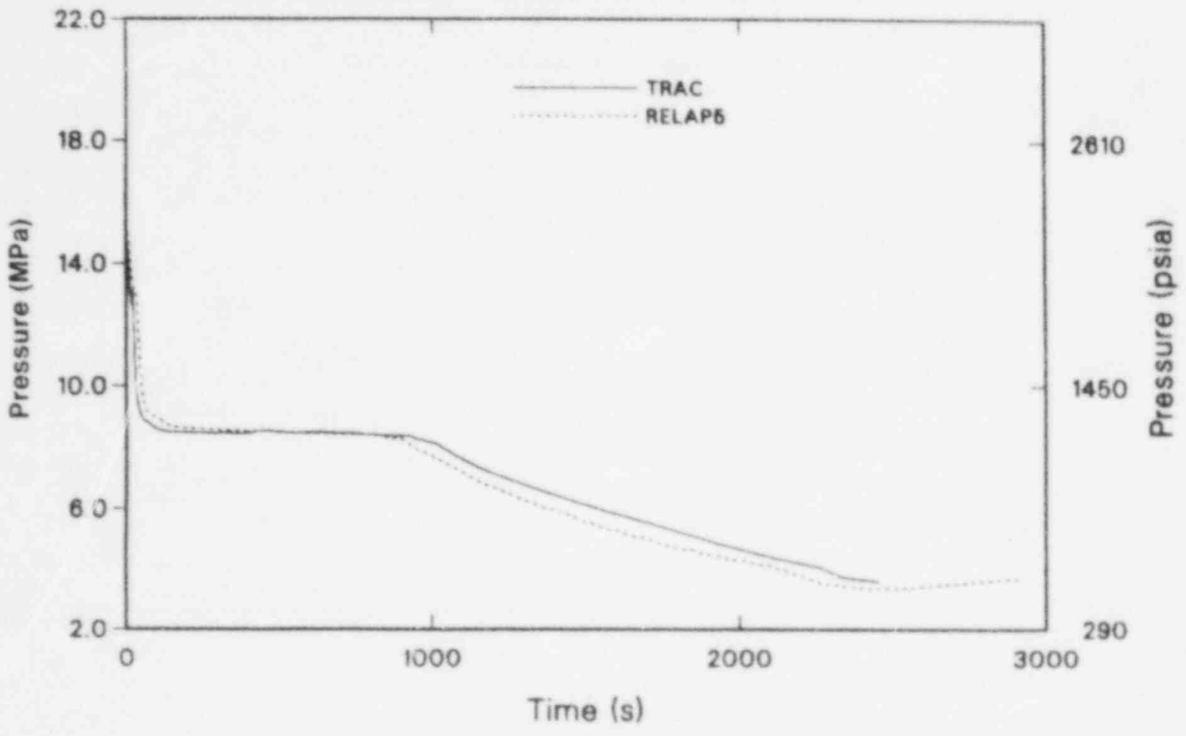

Figure 47. Comparison of RELAP5 and TRAC pressurizer pressures.

simulation produced a slightly faster depressurization than RELAP5. The principal cause of this difference during the initial 60 s was related to initial differences in the pressurizer liquid levels. The initial liquid level in the TRAC model was less than the initial liquid level in the RELAP5 simulation. As a consequence, the pressurizer emptying occurred sooner in the TRAC simulation. The loss of all pressurizer liquid inventory resulted in a temporary increase in the primary system depressurization rate. Once the pressurizer is empty, additional liquid is not immediately available to flash into steam. A further reduction in the depressurization rate will not occur until flashing occurs in some other region of the primary system. The RELAP5 pressurizer initial level is consistent with that of the plant.

The larger initial pressurizer liquid inventory in the RELAP5 steady-state initialization calculation is probably not responsible for any significant differences between the TRAC and RELAP5 simulations. The principal reason for the larger pressurizer liquid inventory in the RELAP5 model is a consequence of slightly different total loop primary system volumes in the two models. The larger overall loop volume in the TRAC model, relative to RELAP5, is suspected of causing less liquid to be distributed to the pressurizer. The two models had pressurizers with the same total volumes.

After natural circulation was established in both simulations, the primary system pressures stabilized at approximately the same values. After loop seal clearing, a slower depressurization rate was calculated in the TRAC simulation. This was the consequence of a slightly larger break volumetric flow rate being calculated in the RELAP5 simulation. The principal phenomena controlling primary system pressure in both simulations was the calculated break flows. Figure 48 presents a comparison of the calculated break mass flow rates for the TRAC and RELAP5 simulations.

In general, the two simulations yielded break flow responses which were similar, with the exception of the initial period when the primary coolant loop flows transitioned from natural circulation to stagnant conditions. During this period prior to loop-seal clearing, the TRAC-calculated break flow remained relatively constant; the RELAP5-calculated break flow underwent a temporary transition to a much higher value during this period. The transition to a larger mass flow rate was coincident with flow reversal in the broken loop. In both simulations, the broken-loop flow reversal was

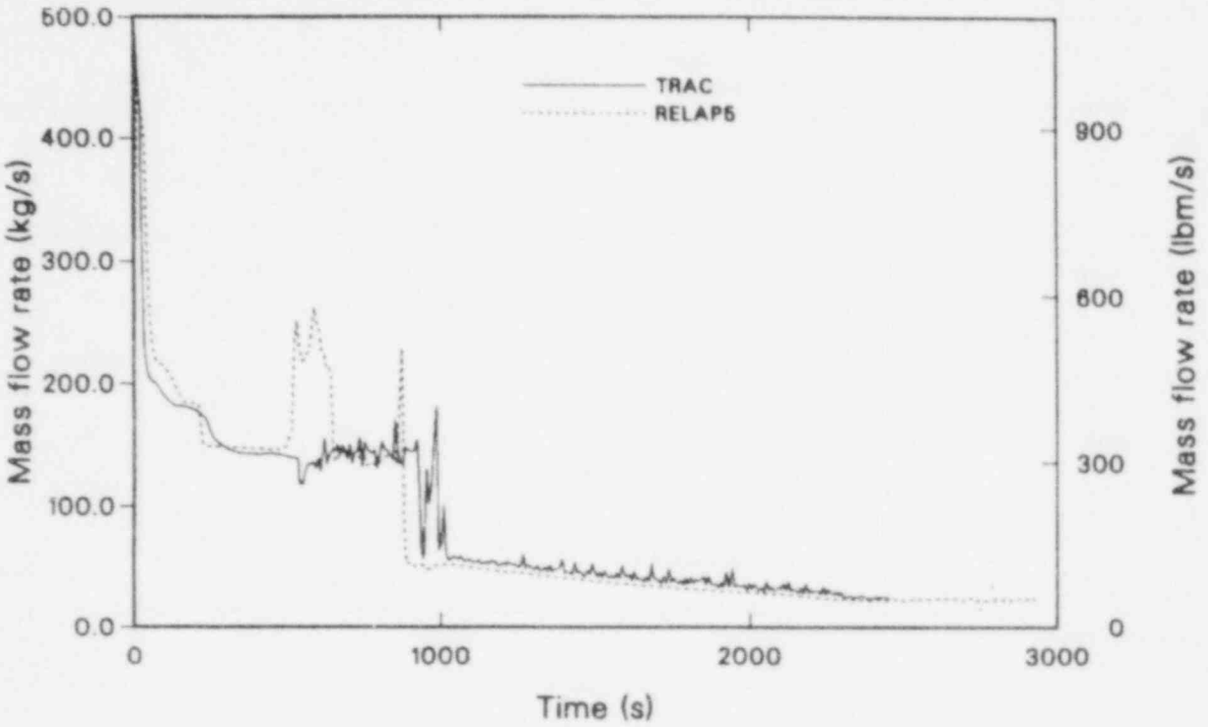

Figure 48. Comparison of RELAP5 and TRAC break mass flow rates.

coincident with loss of natural circulation. Figure 49 presents a comparison between the integrated break flows. After 500 s, a significant divergence occurred between the integrated flows, with the RELAP5 integrated flow exceeding the TRAC integrated break flow. In the RELAP5 calculation, the liquid convected to the break plane came from both directions: from the pump and from the reactor vessel. By 1200 s, both the integrated break flows were again in close agreement. The integrated break flows converged again because in the TRAC simulation the transition from two-phase liquid to predominantly single-phase steam flow conditions took approximately 100 s longer.

One conclusion is that the differences between the calculated break flows were not a direct cause explaining the differences between TRAC- and RELAP5-calculated core level-depression responses. A further conclusion is that the differences in calculated vessel flow rates at the vessel inlet and outlets were the main cause in the differences between the TRAC and RELAP5 core level responses. In other words, differences between how the gravity head distributions in the primary system were calculated caused the differences in core level response, not the break flow.

During the period after loss of natural circulation and before loop-seal clearing, the fluid volume draining back into the reactor vessel was less than the mass flow rate of fluid exiting through the downcomer to the broken loop cold leg in the RELAP5 calculation (Figure 50). In contrast, during the same period in the TRAC simulation, the net mass flow into and out of the reactor vessel were approximately equal (Figure 51). A comparison of the collapsed liquid levels spanning the top of the reactor vessel upper plenum to the bottom of the reactor vessel is shown in Figure 52. After loss of natural circulation, the core level in the TRAC simulation stabilized. This is consistent with the reactor vessel mass flow behavior shown in Figure 51. Approximately as much mass was entering the vessel due to draining from the hot legs as was exiting the vessel cold leg outlet. In the RELAP5 simulation, the mass exiting the downcomer to the cold legs exceeded the mass draining from the hot legs into the vessel. Thus, in the RELAP5 simulation, the reactor vessel level dropped at an accelerated rate, beginning at 750 s.

In the RELAP5 simulation, the accelerated rate of core level depression was coincident with the time when the downside pump suction level dropped below the upside pump suction level. As

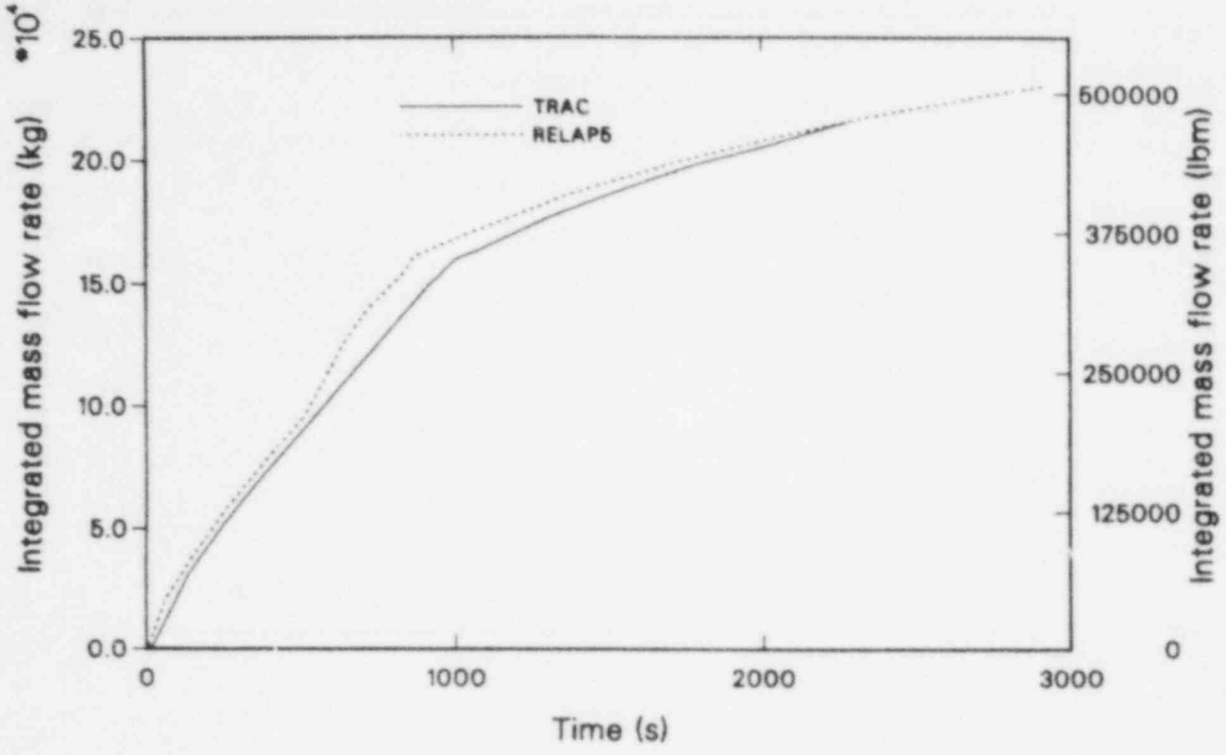

Figure 49. Comparison of RELAP5 and TRAC integrated break mass flow rates.

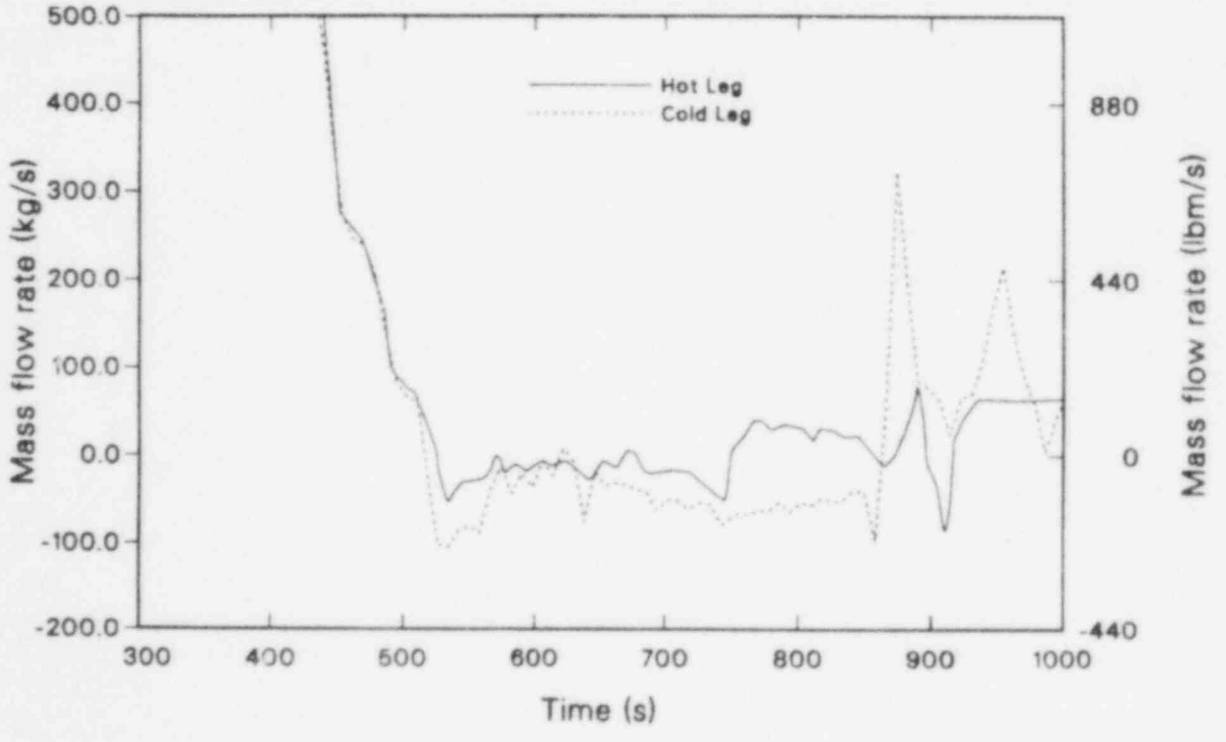

Figure 50. RELAP5 calculated vessel total cold and hot leg mass flow rates.

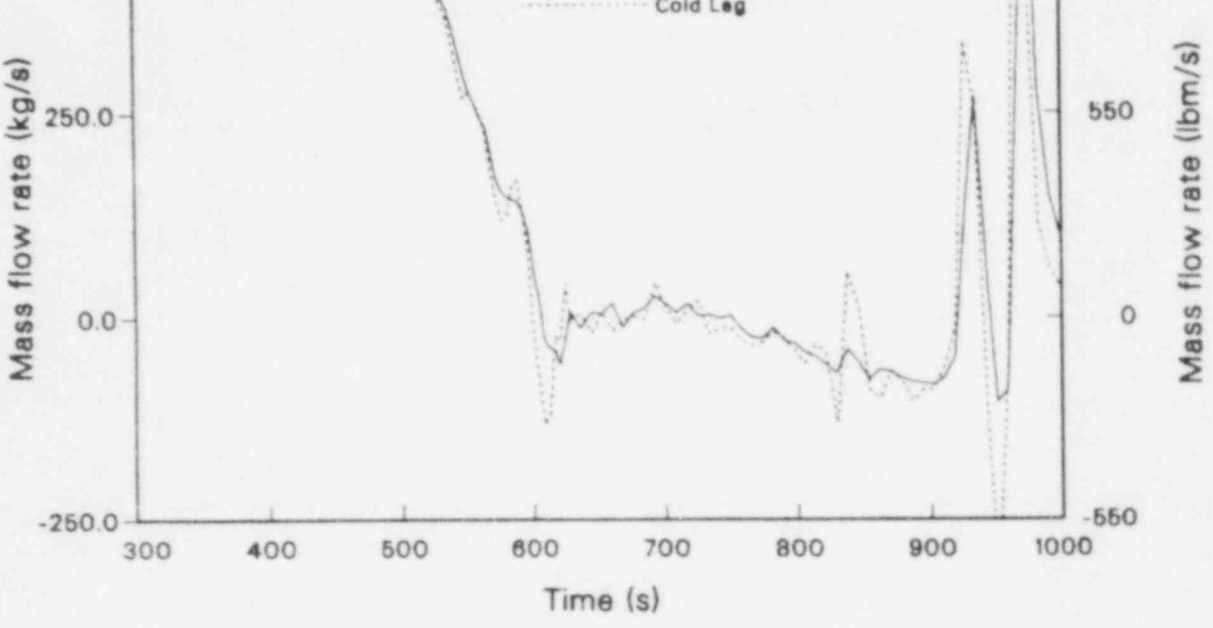

Figure 51. TRAC calculated vessel total cold and hot leg mass flow rates.

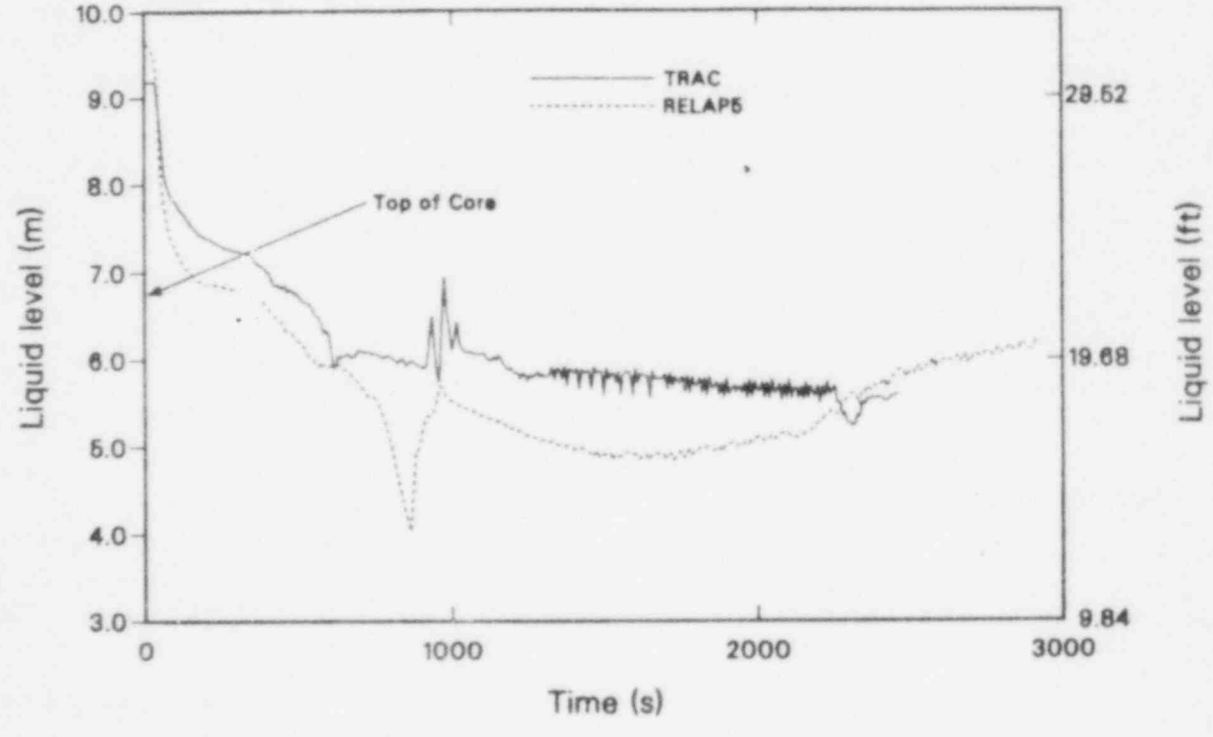

Figure 52. Comparison of RELAP5 and TRAC collapsed core levels.

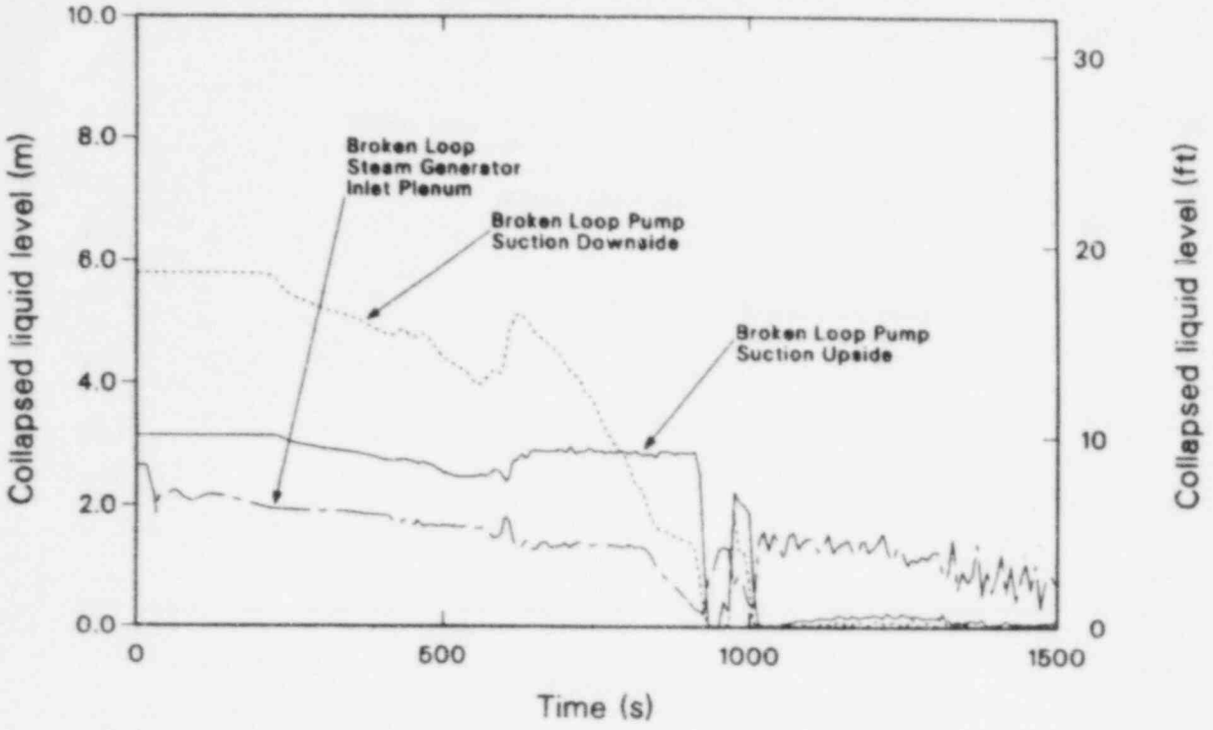

Figure 53. TRAC calculated broken loop U-tube and pump suction levels.

the downside level dropped below the upside, an additional gravity head was generated to depress the core in the RELAP5 simulation (Figure 53). The same process occurred in the TRAC simulation, with one major difference: the liquid in the steam generator inlet plenum region dropped down into the hot legs (Figure 54) coincident with the above changes in the pump suction levels. Thus, in the TRAC simulation, the net gravity head change was not sufficient to induce a core level depression of the magnitude calculated with RELAP5. As a result, a core heatup was calculated with RELAP5, but not with TRAC.

In conclusion, most calculated trends from the RELAP5 and TRAC simulations were in close agreement. The major exception was TRAC did not calculate a core level depression sufficient to induce temperature excursions whereas the RELAP5 simulation did. Possible causes as to why these differences exist are pursued in Section 4.3.2.

4.3.2 Break Size Effect. This section details the effect of break size on the differences between the TRAC and RELAP5 simulations. The RELAP5 and TRAC 2- and 4-in.-diameter break simulations are described, and similarities and differences in these simulations are identified. Differences and similarities between all three break-size simulations are also summarized.

In general, the trends and timing of events between the two sets of simulations using TRAC and RELAP5 were in good agreement. Table 13 presents a summary of key events between the two sets of simulations. The smaller break size tended to enhance the differences in event timing. A progressively larger difference in break flow response occurred as the break size decreased. Comparisons are presented in Figures 55 and 56 for the 2- and 4-in.-diameter-integrated-break flows. For the 4-in. break, the integrated break flows are in excellent agreement, but for the 2-in. break, the integrated break flows show significant differences between 1000 and 2000 s. The larger integrated break flow in the RELAP5 simulation is believed to be responsible for the earlier times to loop stagnation and loop-seal clearing in the 2-in. and 3-in. simulations. The best agreement in integrated break flow and timing events was for the 4-in.-diameter-break simulation.

Differences in integrated break flows did not significantly enhance the differences in the calculated depressurization responses. Comparisons of calculated pressurizer pressures for the RELAP5 and

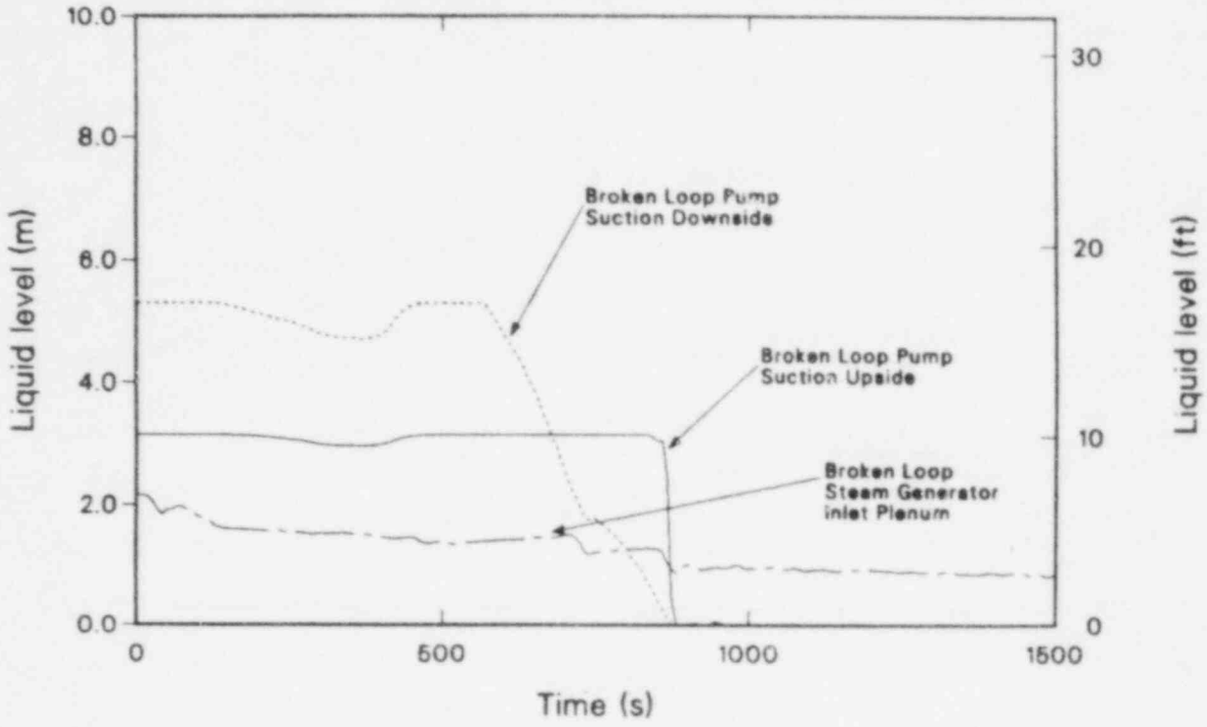

Figure 54. RELAP5 calculated broken loop U-tube and pump suction levels.

TRAC simulations are presented in Figures 57 and 58. The pressure responses are in good agreement. Differences between the RELAP5 and TRAC simulations are similar to those noted in Section 4.3.1.

The most significant differences between calculated break flow responses occurred after loop stagnation. Figures 59 and 60 present the calculated RELAP5 and TRAC break flow comparisons for 2- and 4-in.-diameter-break scenarios, respectively. The RELAP5 simulation consistently showed transitions in break flow magnitude after loop stagnation. The biggest difference was between the 2-in.-diameter-break simulations when flow reversal in the broken-loop cold leg caused a significant increase in break flow in the RELAP5 simulation. No discernable break flow increases or decreases occurred in the TRAC simulations immediately following loop stagnation conditions. Because of the greater rate of primary system mass reduction in the RELAP5 simulation, events occurred sooner. In particular, loop stagnation was calculated to occur sooner in the RELAP5 simulations. Differences in event timings became progressively larger as the break size became smaller. Two reasons account for the above differences. First, differences in initial conditions in the pressurizer mass inventories were responsible for the differences in integrated mass flows before loop stagnation. Second, differences in the mass-donoring schemes for the cell immediately upstream of the break plane were responsible for the differences after loop stagnation.

With respect to initial pressurizer conditions, the larger pressurizer mass inventory in the RELAP5 simulation maintained the primary pressure at a higher value than in the TRAC simulation. This is due to more liquid being available for flashing in the RELAP5 pressurizer. The higher pressure in the RELAP5 simulations produced integrated break flows which initially exceeded those in the corresponding TRAC simulations. These differences resulted in earlier drainage and loss of natural circulation in the RELAP5 simulations.

After loop flow reversal, the break flow in the RELAP5 simulation increased because of mass donoring from the regions where ECCS was being injected. The coarser cold leg noding in the RELAP5 model probably allowed more subcooled liquid from the intact cold leg to be convected directly to the cell upstream of the break plane. The finer noding in the TRAC model allowed more cell-to-cell mixing of ECC liquid before it reached the break plane. The warmer upstream conditions

Table 13. Comparison of TRAC and RELAP5 event sequence timing

Event	Break Diameter (in.)	Event Time (s) TRAC	Event Time (s) RELAP5
Break opens	2	0.0	0.0
	3	0.0	0.0
	4	0.0	0.0
Reactor trip, RCP trip, shut stop valves and main feedwater (MFW) valves	2	36	72
	3	16	35
	4	8	22
Initiate high pressure injection (HPI) and makeup flow	2	68	103
	3	52	65
	4	41	51
Initiate auxiliary feedwater (AFW)	2	97	133
	3	77	96
	4	69	83
Natural circulation ends, loops stagnate	2	1400	1000
	3	600	490
	4	220	220
Broken loop pump suction clears	2	2500	1930
	3	900	873
	4	480	529
Intact loop pump suction clears	2	—	—
	3	950	—
	4	520	—
Accumulator injection begins	2	—	—
	3	2200	2104
	4	1200	980
End of calculation	2	2826	4518
	3	2557	2928
	4	1300	1152

relative to the RELAP5 simulation prevented any substantial increase in TRAC break flow.

Although differences in break flow affected event timing between the TRAC and RELAP5 simulations, these differences were concluded not to be the principal reason for the differences in core level responses. Vessel collapsed liquid level comparisons for the 2- and 4-in.-diameter-break simulations are presented in Figures 61 and 62. In the 4-in.-diameter-break simulation, the net integrated break flows are in excellent agreement during the period when the TRAC and RELAP5 core level responses differ. In the 2- and 3-in.-diameter break simulations, the RELAP5 integrated mass flows

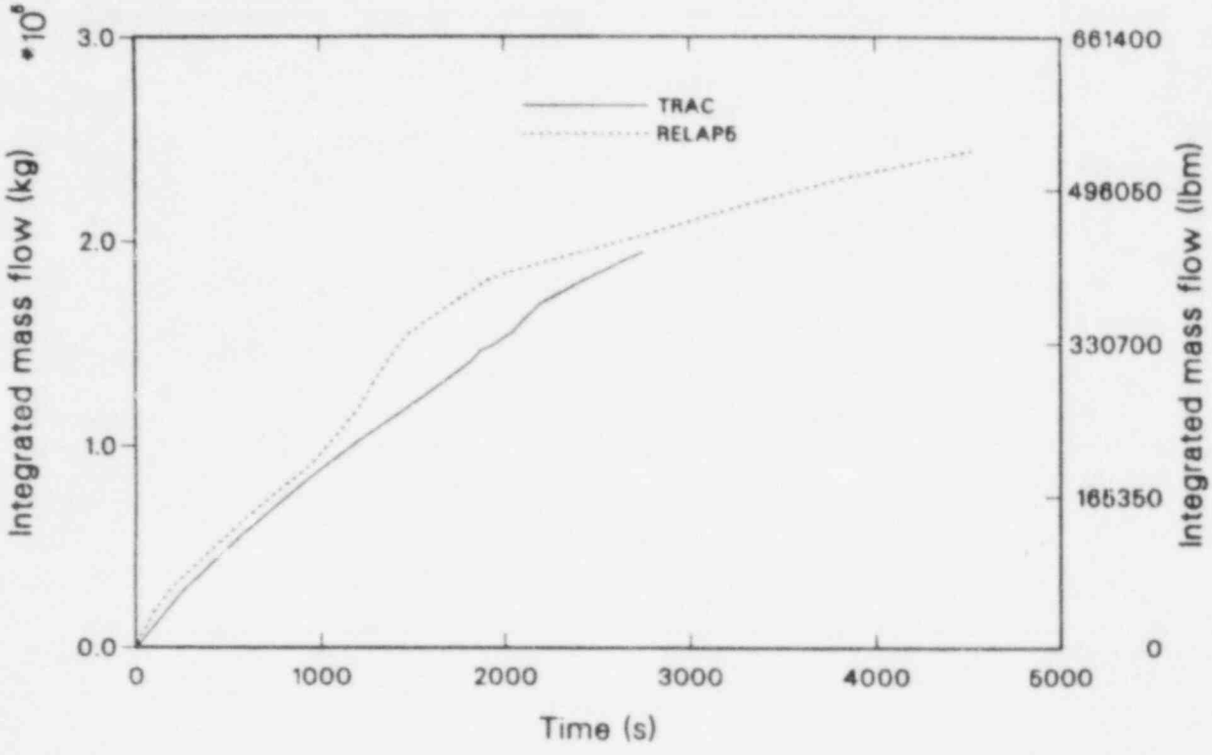

Figure 55. Comparison of TRAC and RELAP5 integrated break flows, 2-in.-diameter break.

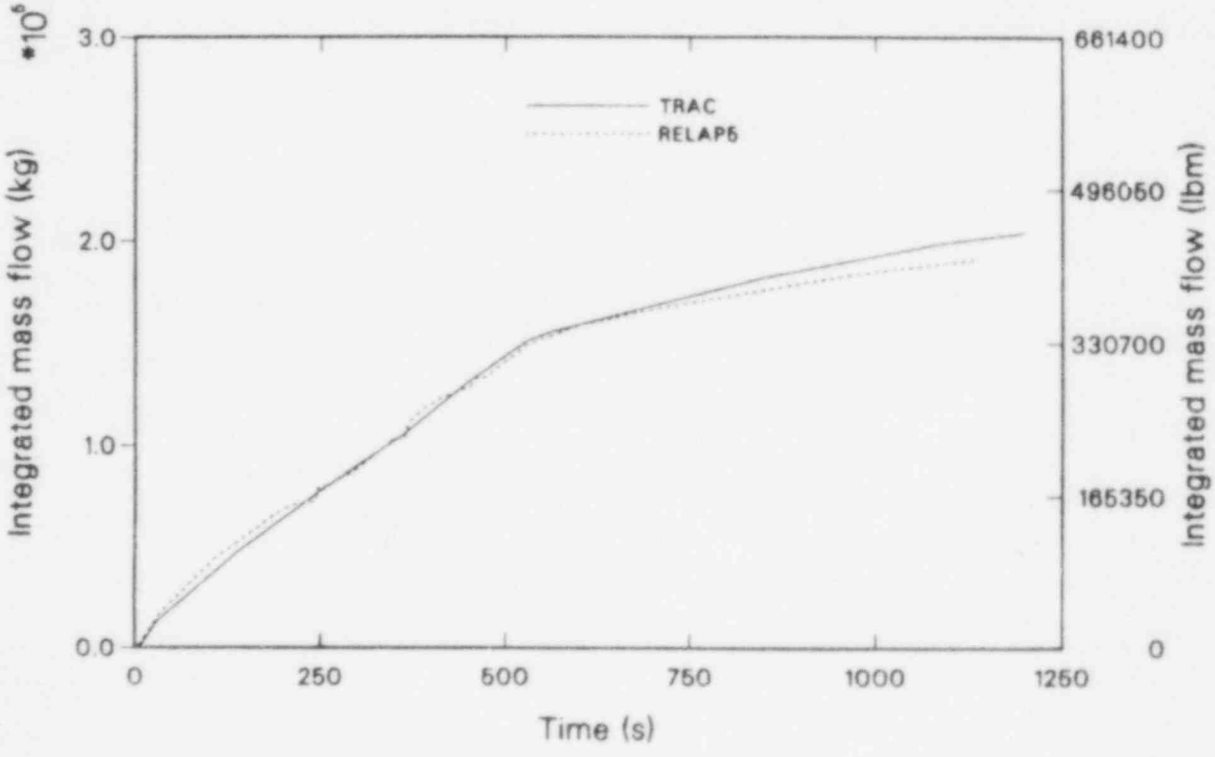

Figure 56. Comparison of TRAC and RELAP5 integrated break flows, 4-in.-diameter break.

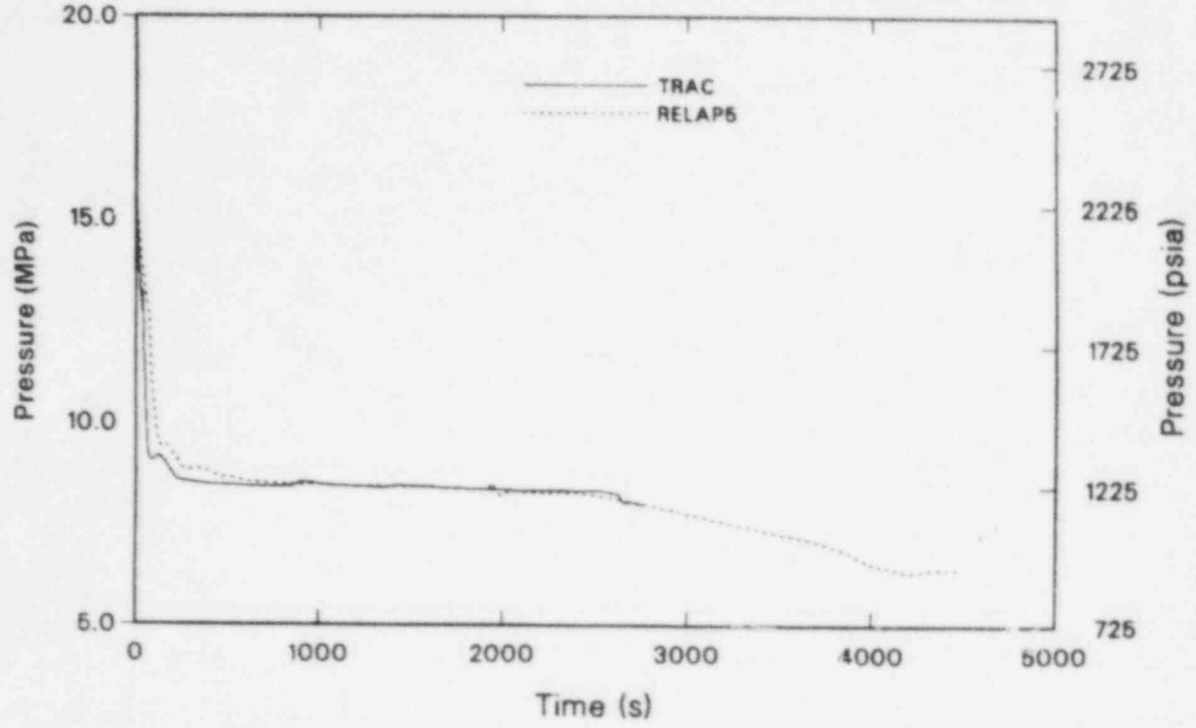

Figure 57. Comparison of TRAC and RELAP5 pressurizer pressures, 2-in.-diameter break.

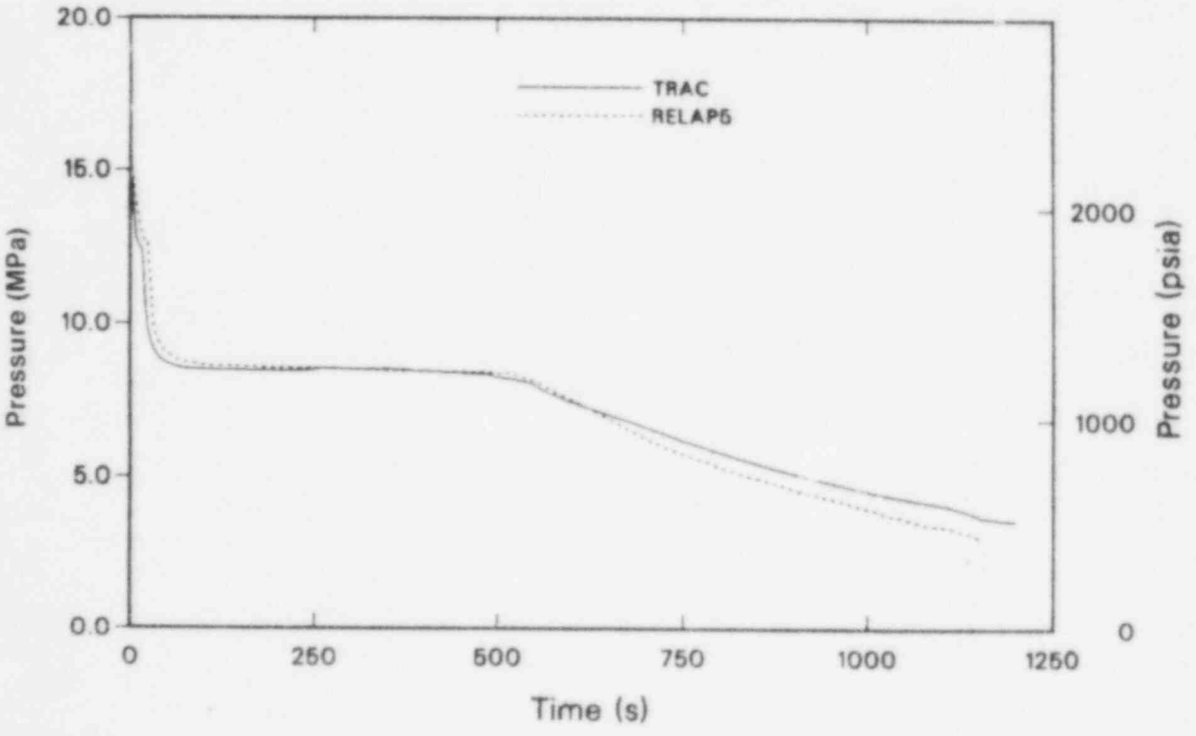

Figure 58. Comparison of TRAC and RELAP5 pressurizer pressures, 4-in.-diameter break.

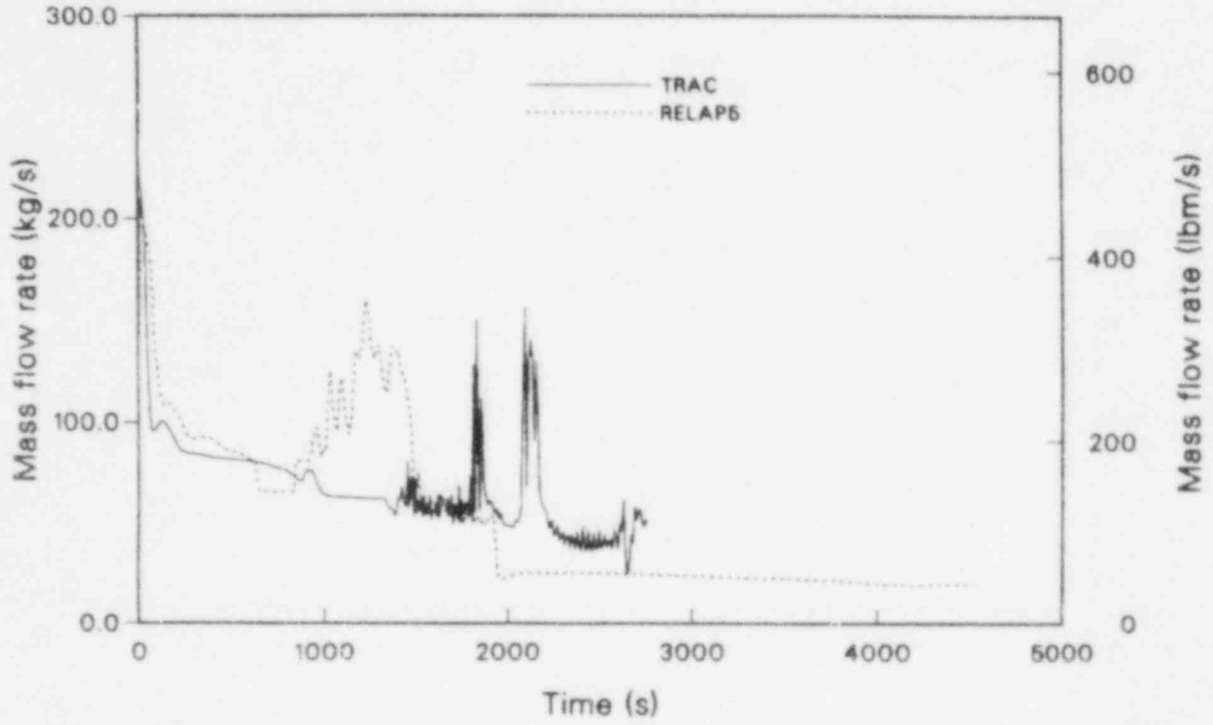

Figure 59. Comparison of TRAC and RELAP5 break mass flow rates, 2-in.-diameter break.

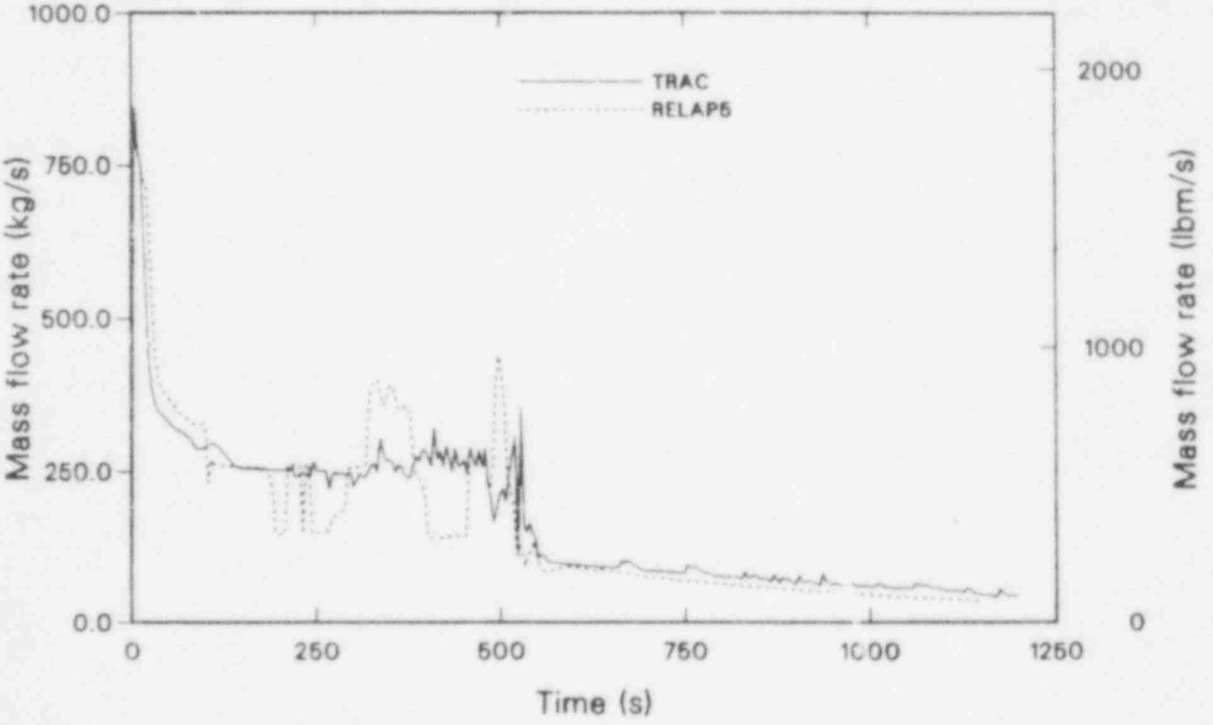

Figure 60. Comparison of TRAC and RELAP5 break flows, 4-in.-diameter break.

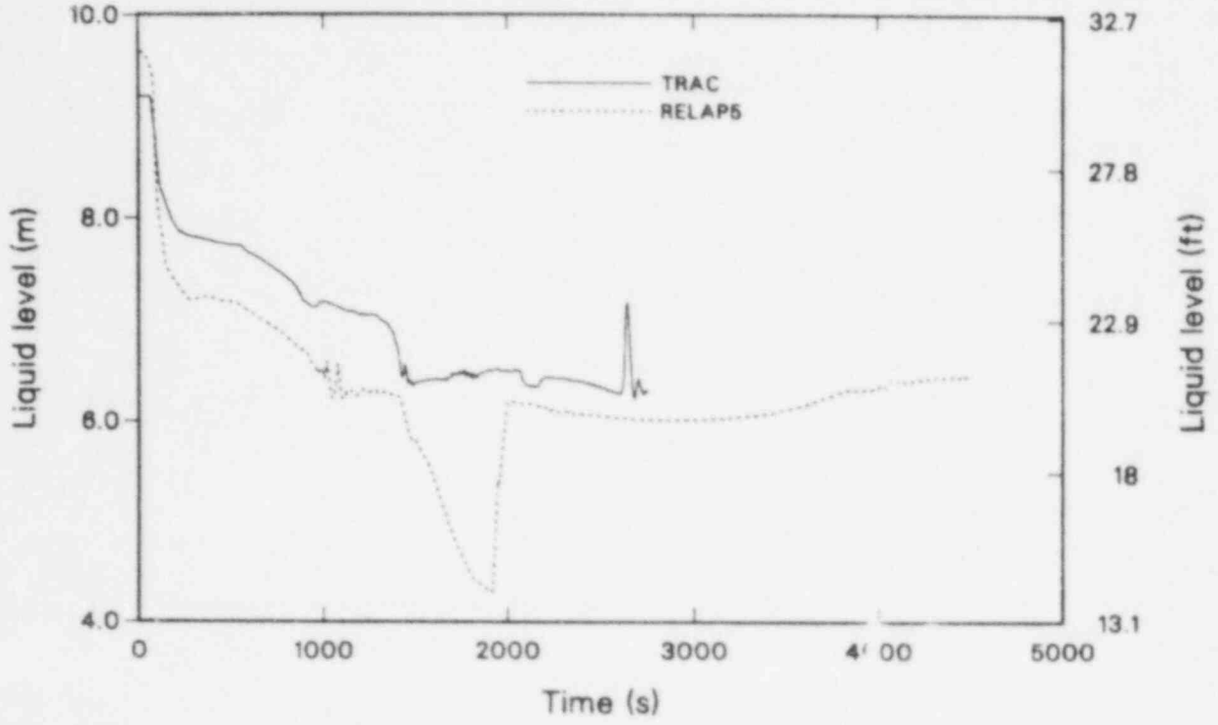

Figure 61. Comparison of TRAC and RELAP5 collapsed vessel levels, 2-in.-diameter break.

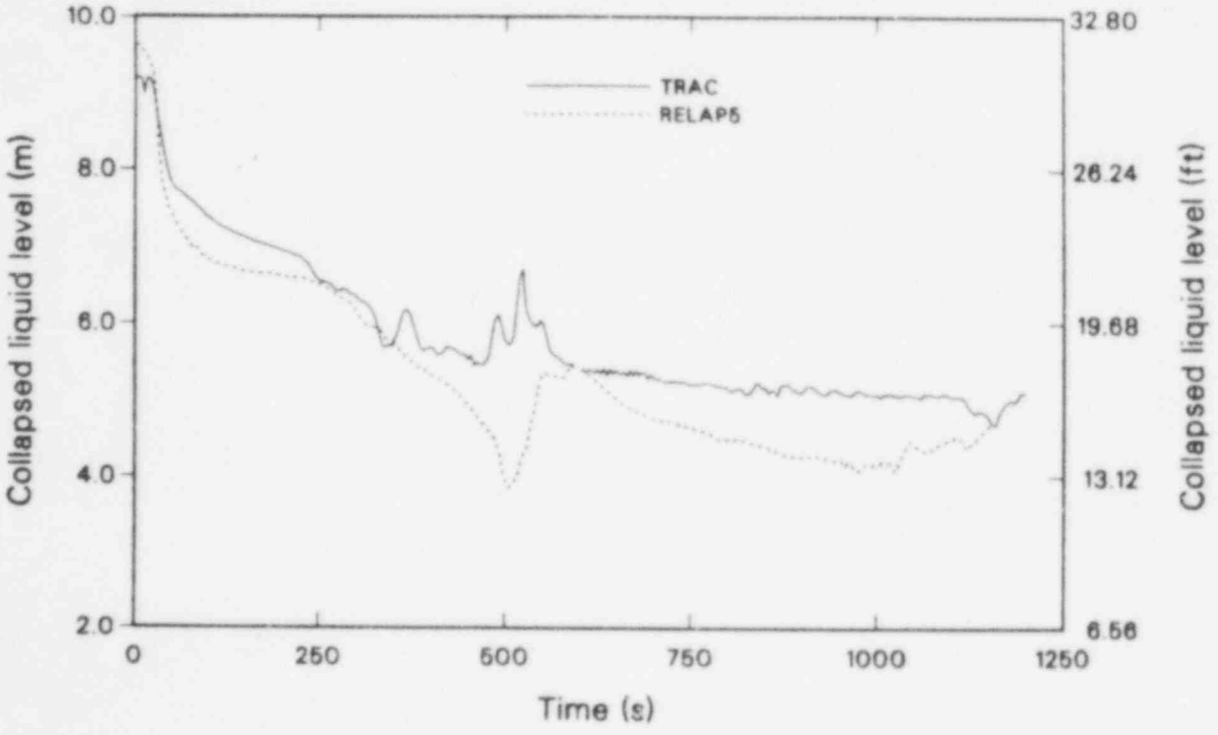

Figure 62. Comparison of TRAC and RELAP5 collapsed vessel levels, 4-in.-diameter break.

are significantly greater than with TRAC, but the differences in core level responses are unchanged.

One conclusion was that no core heatup was calculated to occur in the 2-, 3-, and 4-in.-diameter-break TRAC simulations because of how the TRAC code simulated the dynamic response of liquid in the steam generator inlet plenum and pump suction regions as compared to the RELAP5 simulation. In the RELAP5 simulations, the liquid suspended in the steam generator inlet plenum remained in the plenum until pump suction loop-seal clearing began. The combined static heads from the upsides of the pump suctions and steam generator inlet plenum were sufficient to depress the core level so clad dryout and cladding temperature excursions occurred with RELAP5. In the 2- and 3-in.-diameter-break TRAC simulations, the liquid in the steam generator inlet plenum dropped into the hot legs as levels in the downsides of the pump suctions dropped below those in the pump suction upsides. In the 4-in.-diameter-break TRAC simulation, a depletion of liquid in the pump suction upside regions occurred prior to loop-seal clearing. Unlike the 2- and 3-in.-diameter-break TRAC simulations, the 4-in.-diameter TRAC simulation did not exhibit significant depletion of liquid in the steam generator inlet plenum. The TRAC simulation included a decrease in the pump suction upside levels relative to the 4-in.-diameter-break RELAP5 simulation. This decrease was sufficient to prevent a core level depression large enough to cause a core heatup in the TRAC simulation. Thus, the net gravity head available to depress the core in the TRAC simulations was always smaller than in the RELAP5 simulations (Figures 61 and 62).

Several probable causes exist as to why the two codes simulated inventory responses in the steam generator inlet plenum differently. Moreover, these same causes are suspected to be responsible for clearing both loop seals in all the TRAC simulations, but not in the corresponding RELAP5 simulations. One possible reason deals with differences in how the plenums were nodalized in the two models. In the TRAC model, the plenums were nodalized with two volumes, while in the RELAP5 model the plenums were nodalized with only one volume. Other possible reasons include intrinsic differences in how the two codes generate solutions. A discussion of differences between algorithms in the two codes is beyond the scope of this report, but future work is recommended to be done in this area to clarify how differences in code solution schemes may affect final calculated results in systems dominated by gravity head forces.

In conclusion, the RELAP5 and TRAC simulations were generally in close agreement. Overall pressure, break flow, and mass distribution trends were in close agreement. The main exception was RELAP5 consistently calculated temporary core level depressions that were sufficient to induce clad temperature excursions, while TRAC did not. Also, each TRAC simulation calculated rapid convection of liquid from the core region to the steam generator inlet plenum after loop-seal clearing. To resolve these differences, several areas for investigation were identified which include:

1. Identifying how differences between TRAC and RELAP5 model nodalization may affect calculational results.

2. Identifying differences between TRAC and RELAP5 solution schemes which may affect calculational results.

3. Identifying needed improvements in coding algorithms to improve computational accuracy.

5. CONCLUSIONS AND RECOMMENDATIONS

A series of calculations were performed, using the TRAC-PF1 and RELAP5/MOD2 computer codes, to investigate RESAR-3S plant response to small break loss-of-coolant-accident sequences. The peak cladding temperatures experienced in each calculation are summarized in Table 14. In all cases, the peak cladding temperatures shown were experienced in the hot pin, and a temperature entry is shown only if an excursion from saturation temperature was calculated.

As indicated in Section 2, both the RELAP5/MOD2 and TRAC-PF1 codes have been shown to be capable of predicting the liquid holdup and related core level depression and core heatup phenomena for Semiscale Test S-UT-8. The calculations presented in this report represent an extension of code application for different break sizes and facility scale than those used in Test S-UT-8. This extension involves considerable uncertainty as evidenced by the significantly different cladding temperature responses calculated with RELAP5/MOD2 and TRAC-PF1 for the RESAR Model F steam generator 2-, 3-, and 4-in.-diameter-break sequences. Further assessment of both codes in predicting this phenomena appears to be warranted.

Both RELAP5/MOD2 and TRAC-PF1 predicted liquid drainback from steam generator U-tubes to plenums in a manner consistent with the Wallis flooding correlation. Similarly, the codes predicted drainback from steam generator inlet plenums to hot legs in a manner consistent with the Kutateladze correlation. However, considerable uncertainty exists in the applicable constants to be used in these correlations for the geometries present in a pressurized water reactor (PWR). Further experimental investigation into flooding correlation constants applicable at these locations appears warranted.

Only minor differences were observed in plant behavior due to differing steam generator configuration. Results of calculations using Models D and F steam generators were comparable.

The RELAP5-calculated collapsed core level at which core heatup begins was found to be strongly affected by break size. This level ranged from 7.28 ft (above bottom of heated length) for the 1.5-in.-diameter break to 0.89 ft for the 7-in.-diameter break. These levels are inconsistent with Semiscale S-UT test series data which showed core heatup beginning at mid-core level for both 6.7- and 9.5-in.-equivalent-diameter breaks. Further investigation of this discrepancy, including assessment of the codes against experimental core boiloff data, is recommended.

Results of calculations comparing coarse and fine steam generator nodalization were consistent with those previously reported by Argonne.[2] Peak cladding temperatures were found to be higher when using a finely-noded steam generator. These calculations also showed significant previously-unreported sensitivities of peak cladding temperature to initial steam generator secondary mass and separator modeling. We recommend a thorough sensitivity study be performed to evaluate steam generator nodalization, initial secondary mass, and separator modeling effects.

Clad temperatures excursions were encountered in RELAP5 simulations, but not in TRAC simulations for 2-, 3-, and 4-in.-diameter breaks. Complete explanations for these differences have not been found. Pertinent differences in code behavior were observed, however, in the following areas:

(1) Voiding characteristics in the pump suction upflow sides.

(2) Convection of liquid from the reactor vessel to the steam generator inlet plenums following clearing of the loop seal.

(3) Sensitivities to nodalization in the pump suction, reactor coolant pump, and steam generator plenum regions.

(4) Minor differences in calculating countercurrent flow limiting flooding phenomena within the hot legs and steam generators which had a major impact on core level and rod temperature responses.

Table 14. Summary of cladding temperature excursion results

Code	SG Configuration	Break Diameter (in.)	Clad Temperature Excursions Loop Seal Clearing		Peak Cladding Temperature (°F)	Notes
			Pre-	Post-		
RELAP5	F	1.5	Yes	No	744	—
RELAP5	D	2	Yes	No	1199	—
RELAP5	D (coarse node)	2	Yes	No	840	—
TRAC	F	2	No	No	—	—
RELAP5	F	2	Yes	No	959	—
RELAP5	D	3	Yes	No	768	—
TRAC	F	3	No	No	—	—
RELAP5	F	3	Yes	No	790	—
RELAP5	D	4	Yes	Yes	912	B
TRAC	F	4	No	No	—	—
RELAP5	F	4	Yes	Yes	860	B
RELAP5	D	5	Yes	Yes	969	B
RELAP5	F	5	Yes	No	760	—
RELAP5	D	6	Yes	Yes	1026	C
RELAP5	F	6	Yes	Yes	1148	C
RELAP5	D	7	Yes	Yes	678	A
RELAP5	F	7	Yes	Yes	962	C

NOTES: A = Peak occurs prior to loop-seal clearing.
B = Peak occurs following loop-seal clearing.
C = Rewet does not occur when loop seal clears, pre- and post-loop-seal-clearing excursions merge.

6. REFERENCES

1. M. T. Leonard, *Vessel Coolant Mass Depletion During a Small Break LOCA*, EG&G Idaho, Inc., EGG-SEMI-6010, September 1982.

2. C. Lee et al., *Sensitivity of SBLOCA Computations to Steam Generator Nodalization Selection*, Argonne National Laboratory, ANL/LWR/NRC 83-4, February 1983.

3. W. W. Tingle, *Experimental Operating Specification for Semiscale-Mod-2A 5.0% Break Experiment S-UT-8*, EGG-SEMI-5685, EG&G Idaho, Inc., December 1981.

4. P. D. Wheatley et al., *RELAP5/MOD2 Code Assessment at the Idaho National Engineering Laboratory*, EG&G Idaho, Inc., NUREG/CR-4454 (Draft), November 1985.

5. R. Fujita, *TRAC-PF1/MOD1 Posttest Analysis of Semiscale Small-Break Test S-UT-8*, LA-UR-84-2079, Los Alamos National Laboratory, 1984.

6. J. E. Blakeley and J. M. Cozzuol, *Best Estimate Analysis of a Small Break LOCA in a RESAR-3S Pressurized Water Reactor*, EGG-NTAP-6032, EG&G Idaho, Inc., September 1982.

7. G. B. Wallis, *One-Dimensional Two-Phase Flow*, McGraw-Hill Inc., 1969.

8. INEL TRAC-BWR Development Group, *TRAC-BD1/MOD1: An Advanced Best Estimate Computer Code for Boiling Water Reactor Analysis*, NUREG/CR-3633, April 1984.

9. M. T. Leonard, *Posttest RELAP5 Simulations of the Semiscale S-UT Series Experiments*, EG&G Idaho, Inc., EGG-SEMI-5622, October 1981.

10. J. R. Wolf et al., *Analysis of the Semiscale Mod-2B Power Loss Experiment S-PL-3*, EGG-SEMI-6429, EG&G Idaho, Inc., October 1983.

NRC FORM 335 (2.84) NRCM 1102 3201, 3202

U.S. NUCLEAR REGULATORY COMMISSION

BIBLIOGRAPHIC DATA SHEET

SEE INSTRUCTIONS ON THE REVERSE

1. REPORT NUMBER (Assigned by TIDC add Vol. No., if any)

NUREG/CR-4384
EGG-2416

2. TITLE AND SUBTITLE

Break Spectrum Analysis for Small Break Loss-of-Coolant Accidents in a RESAR-35 Plant

3. LEAVE BLANK

4. DATE REPORT COMPLETED

MONTH	YEAR
March	1986

5. AUTHOR(S)

C. Don Fletcher
Craig M. Kullberg

6. DATE REPORT ISSUED

MONTH	YEAR
March	1986

7. PERFORMING ORGANIZATION NAME AND MAILING ADDRESS (Include Zip Code)

Idaho National Engineering Laboratory
EG&G Idaho, Inc.
Idaho Falls, ID 83415

8. PROJECT/TASK/WORK UNIT NUMBER

9. FIN OR GRANT NUMBER

A6047

10. SPONSORING ORGANIZATION NAME AND MAILING ADDRESS (Include Zip Code)

U.S. Nuclear Regulatory Commission
Office of Nuclear Regulatory Research
Washington, DC 20555

11a. TYPE OF REPORT

Technical

b. PERIOD COVERED (Inclusive dates)

12. SUPPLEMENTARY NOTES

13. ABSTRACT (200 words or less)

A series of thermal-hydraulic analyses were performed to investigate phenomena occurring during small break loss-of-coolant-accident (LOCA) sequences in a RESAR-3S pressurized water reactor. The analysis included simulations of plant behavior using the TRAC-PF1 and RELAP5/MOD2 computer codes. Series of calculations were performed using both codes for different break sizes. The analyses presented here also served an audit function in that the results shown here were used by the U.S. Nuclear Regulatory Commission (NRC) as an independent confirmation of similar analyses performed by Westinghouse Electric Company using another computer code.

14. DOCUMENT ANALYSIS - a. KEYWORDS/DESCRIPTORS

b. IDENTIFIERS/OPEN-ENDED TERMS

15. AVAILABILITY STATEMENT

Unlimited

16. SECURITY CLASSIFICATION

(This page)
Unclassified
(This report)
Unclassified

17. NUMBER OF PAGES

18. PRICE

120555078877 1 1AS1R4
US NRC
ADM-DIV OF TIDC
POLICY & PUB MGT BR-PDR NUREG
A-901
WASHINGTON DC 20555

EG&G Idaho
P.O. Box 1625
Idaho Falls, Idaho
83415